Development and Optimization of a Preservable Three-Dimensional Bio-Construct

by

Lukas A. Underwood

A dissertation submitted in partial fulfillment
of the requirements for the degree of
Doctor of Philosophy
(Mechanical Sciences and Engineering)
in the University of Michigan-Dearborn
2022

Doctoral Committee:

       Nilay Chakraborty, Co-Chair, American Type Culture Collection
       Associate Professor Joe Lo, Co-Chair
       Professor Krisanu Bandyopadhyay
       Associate Professor Gargi Ghosh
       Associate Professor Mathumai Kanapathipillai

Lukas Underwood

launderw@umich.edu

ORCID iD: 0000-0001-6132-7742

Dedication

This dissertation is dedicated to my parents and Rebecca for supporting me through this long academic journey.

Table of Contents

List of Figures

Abstract

Many cellular culture and assay models are still considered in "two dimensions (2D)", despite the obvious need for biologically relevant, three dimensional (3D) systems. Forcing cells to adapt to a pseudo 2D environment causes phenotypic changes in growth, metabolism, and functionality, leading to poor clinical translation. In recent years, the need for more biologically relevant 3D systems have become a major focus of research (i.e. lab on chip, organoids) to attempt to resolve these geometric issues. With the creation of these increasingly complex cell and tissue systems requires a parallel need for transportation and storage solutions via preservation techniques. The preservation of these culture and assay products must allow ample viability and functionality afterwards.

The material of this dissertation can be divided into two major components. Early focus was towards cryoprotective solution (CPA) formulation and characterization of suspension freezing to improve upon post-thaw outcome. As the shift in industrial focus was gleaned towards more complex, 3D cellular systems, focus shifted towards the translation of knowledge in suspension cryobiology to creating a cryopreservation methodology for simple 3D constructs. Thermodynamic studies (using differential scanning calorimetry (DSC)) and a Raman spectroscopic based analysis of hydrogen bonding network were used to study mechanisms of non-penetrating cryoprotectants.

Alginate hydrogel suspension is one method of creating a 3D pseudo extra cellular matrix for cells to be housed in. Alginate's biocompatibility and easily tunable properties make it an

ideal candidate for biological mimicking tissue systems which have the potential to be cryopreserved. Optimization studies on liver carcinoma cells were performed to develop a comprehensive system for cryopreserving cell-laden alginate hydrogels.

Optimization studies were separated into 3 major components: alginate precursor formulation, protocol modulation, and CPA formulation; however, the final two received bulk focus due to previous expertise. Studies found that liver carcinoma (HepG2) cells could be cryopreserved in alginate hydrogels with substantial post-thaw cell viability and metabolic recovery. Subtle changes were made to slow suspension freezing protocol to adapt to 3D preservation. In addition, osmotic pressure was found to be an important factor in post-thaw outcome. Cells of differing origins (neurological and immunological) were also evaluated using the same cryopreservation and encapsulation techniques. It was found that although the HepG2 optimized technique was viable for other cell types, an optimization study is recommended for all cell types to enhance post thaw outcome.

This research provides a framework for the development of 3D culture systems and their cryopreservation outcome characterization. This methodology can be applied for future work to create more complex and biologically relevant constructs with long-term storage implications.

Chapter 1 An Introduction to the Biopreservation Landscape

The advancement of research and development of innovative biological technologies depends on both short- and long-term preservation techniques. International collaboration and sharing of cellular and tissue samples is particularly important for studying rare diseases where the cellular models are not as readily available and the ability to preserve and transport cells and tissue in stable conditions that allow ample viability and functional recovery upon delivery is critical for this collaboration.

1.1 Normothermic and Hypothermic Preservation

Cell culture is not often considered a type of preservation, as there is often some end goal or product to be achieved from the process. In research cell culture is a means to an end for studying some phenotypic or biochemical change because of experimental processing. On a larger scale, bioreactor culture is used to produce a variety of pharmaceutical (i.e. vaccines, monoclonal antibodies, recombinant proteins). With respect to short-term preservation protocol, it could be arguable that normothermic preservation is the optimal technique to prevent any kind of low temperature-based injuries; however, there are still several limitations. Most of the limitations are related to the economics using normothermic preservation for extended periods of time. Normothermic preservation of cell lines are susceptible to contamination and genetic drift over high passage numbers, which would require expensive quality control measures to ensure the reproducibility of cell phenotype from both the supplier and buyer. In addition, over

production and subsequent loss of product would be a major issue for the supplier to maintain an ample supply to meet variable demand.

Hypothermic storage is a short-term technique that utilizes the suppression of biochemical events by reducing the temperature to levels slightly above the melting temperature water (~4°C). Currently, hypothermic preservation is employed for transfusion and transplant medicine. Interestingly, it has even been shown that hypothermic storage of red blood cells for longer than 21 days can inactivate T lymphocytes and reduce chance of transfusion associated graft-vs-host disease [1]. In addition, hypothermic storage and transport is the best option for organ transplant. The primary limitation of hypothermic storage is called "cooling injury". Cooling injury describes the disruption to the overall cell homeostasis as the temperature is reduced below physiological temperatures. Some of the major changes which lead to cell injury include membrane pump deactivation, disruption of calcium homeostasis, and the build of free radicals that can induce apoptosis. The combination of these changes does not allow survival of the most cells in these conditions for more than a few days.

A heavy burden of the research has been directed towards developing solutions to put the cells and tissues in mitigating cellular response to these low temperatures. The solutions are a cocktail mixture the has elements to maintain ion gradients, calcium homeostasis, pH buffers, and antioxidants. Later techniques focused on the continuous circulation of these oxygenated preservation solutions to further increase time of survival at these temperatures. Despite the still high clinical use of the hypothermic technique, it is typically agreed that the advancement of this science has reached a limit and that exploration of new techniques will be required in the field of tissue and organ preservation to further enhance preservation times [2].

1.2 Classic Cryopreservation and Vitrification

Cryopreservation involves reducing the temperature of a biological sample to temperatures significantly below the melting point of water. The most used cryopreservation procedure for 2D cell culture is described in figure 1-1.

| Harvest cells from culture | Centrifuge suspension | Remove supernatent | Resuspend in CPA | Aliquot into cryovials | Place in freezing container overnight to -80C | Transfer vials to liquid nitrogen tank for long-term storage |
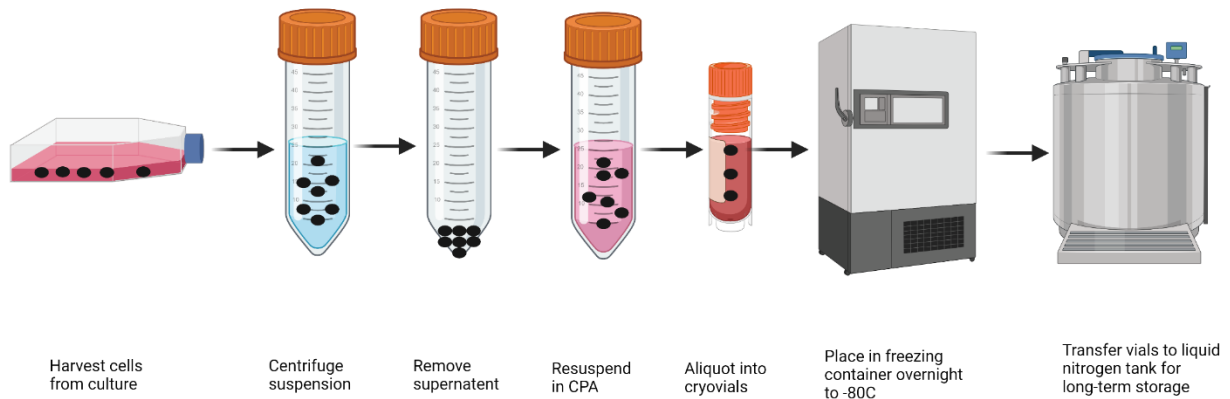
Figure 1-1 Standard Operating Procedure for Suspension Cryopreservation

Cryopreservation is the "gold standard" and most used procedure for the long-term storage of biological material. Despite its frequent use, there are many cellular injury mechanisms that must be addressed to get post-thaw viability following preservation.

1.2.1 Freezing Injury

Over the past several decades an enormous amount of progress has been made tot determine the underlying mechanisms of cell injury during cryopreservation. As the temperature of the sample is reduced below the melting point, ice will first form in the extracellular environment. Ice crystal formation excludes non-water solutes, including cells, to the spaces between the ice crystals. This space is called the unfrozen fraction, while the actual ice crystals are called the frozen fraction. Because of the water volume lost during crystallization, there is a massive increase in solute concentration in the unfrozen fraction space where the cells reside. The solute concentration gradient between the intracellular space and extracellular space is the

driving force for the efflux of water across the cell membrane. If the cooling rates during cryopreservation are sufficiently slow, ice will continue to form, and water will be able to diffuse across the membrane with at a rate fast enough to maintain chemical equilibrium. However, too low of a cooling rate has been implicated injury stemming from excessive water and prolonged membrane exposure to high concentrations of solutes. On the other hand, because membrane permeability is correlated to temperature, too high a rate of cooling leads to supercooling of the extracellular solution with reduced water efflux from the cell. This situation can lead to the formation of intracellular ice, which is considered deadly to cells, despite the exact mechanism having yet to be resolved.

Empirical evidence has proven this ideal range of cooling rates for freezing the prevent excessive solute based injuries at low rates and excessive intracellular ice formation at high rates. Despite the presence of this fundamental "ideal" zone being realized, the exact mechanisms are difficult to resolve. A wide range of physical and chemical phenomena ranging from ice nucleation and crystal morphology, osmotic stresses, and thermal gradients. Because all these different aspects of cryoinjury are interrelated, it is difficult to resolve the magnitude of injury corresponding to each. However, a significant portion of the injury appears to be related to ice formation both extracellular and intracellularly.

1.2.2 Vitrification

Vitrification is the solidification of a liquid into an amorphous solid (glass state). The significance of this phenomena has been well understood for many years with respect to the manufacturing of familiar items such as porcelain or windows; however, its biological significance started with the vitrification of pure water about 30 years ago [3]. Essentially, vitrification-based cryopreservation allows us to reduce the sample temperature to these desired

cryogenic temperature without the crystallization of ice. We achieve this by using cooling rates several orders of magnitude higher than that of slow freezing and essential "outrun" the thermodynamic kinetics which result in the formation of ice.

The use of the vitrification technique allows the avoidance of ice formation all together, which associated with many injury mechanisms during slow-cooling preservation. However, other forms of injury arise with this new technique. There is a direct injury associated with the extreme rates of temperature change often termed "cold shock". In addition, it has been shown that the thawing rate following vitrification becomes extremely important due to devitrification and recrystallization. Recrystallization is the growth of innocuous small ice crystals that began to form during the cooling process into larger more damaging crystals. Once again, the solution is to employ high warming rates to "outrun" the kinetics of ice formation as we are warming the sample. There also exists a critical cooling rate and warming rate which can be employed where appreciable (damaging) ice formation is not observed.

Interestingly, these critical rates of cooling and warming during vitrification are strongly related to the nature and concentration of the solutes present in the CPA. Generally, the solutes used for vitrification are the same ones used to protect against freezing injury during slow-cooling preservation. We can reduce the critical cooling and warming rates of vitrification by increasing the concentrations of certain CPAs; these rates are typically more manageable, controllable, and result in less "cold shock" than rates required with less CPA concentration. It is theorized that advanced vitrification techniques are the most promising solutions to solve long-term preservation of larger cell structures such as tissues and full organs as detrimental injury due to ice crystal formation appear to be detrimental.

1.3 Lyopreservation

Long-term preservation is based on the idea of chemical and molecular suspension. This can be achieved in two main ways: temperature reduction and water reduction. Kinetic motion suppression using temperature reduction is the basis for all the previously mentioned preservation techniques. However, lyopreservation attempts to reduce molecular motion by drastically reducing water content and increasing the viscosity of the environment. A reassuring aspect of this mechanism of preservation is that it can be found in nature (even small animals) for long-term preservation of the entire organism. Tardigrades for example can enter a tun state where they reduce their water content to 2-3% of what was present in their active state. While in this tun state oxygen consumption is reduced to nearly zero indicating a complete suppression of metabolism. More research indicates tardigrades also have desiccation mitigation mechanisms to improve post-desiccation recovery [4].

1.3.1 Lyopreservation Techniques

The most employed technique for lyopreservation is called freeze-drying. Freeze drying removes water by following a 3-step process. First, the temperature of the sample is reduced and frozen in a solid state. Second, pressure is reduced to ensure the temperature and pressure are well below the triple point pictured in figure 1-2. Finally, the sample is warmed while under vacuum and the water sublimates out of the sample. The result is a sample of the same volume with almost no residual water in a "desiccated state".
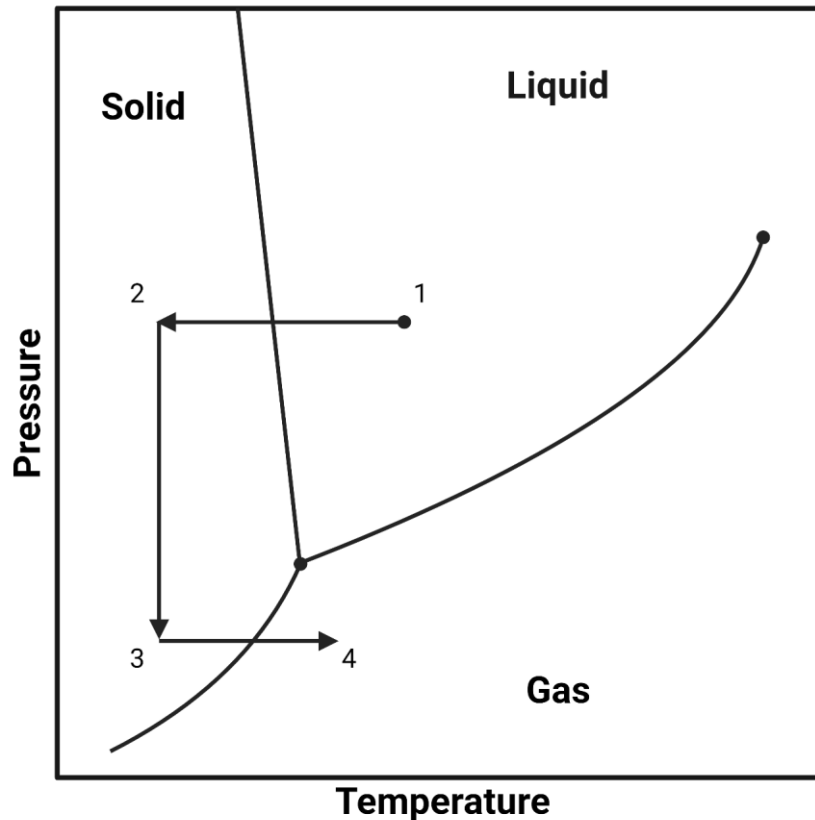
Figure 1-2 Representative Phase Diagram for Freeze Drying: Process 1-2 freezing the sample. Process 2-3 applies a vacuum and reduces the pressure. Process 3-4 gradually warms the sample and sublimation of water out of sample begins

Currently freeze drying is heavily employed for food products and non-living biochemical compounds. Freeze drying is a difficult technique to employ on complex cells because it involves two-fold injury with first freezing, removal of water, and rehydration. Other lyopreservation techniques look to desiccate cellular material without the requirement of freezing. One methodology called "dip coating" is described in figure 1-3 [5]. Dip coating lyopreservation dry's a sample using surface tension of highly viscous trehalose solutions which "coat" and dry the sample.
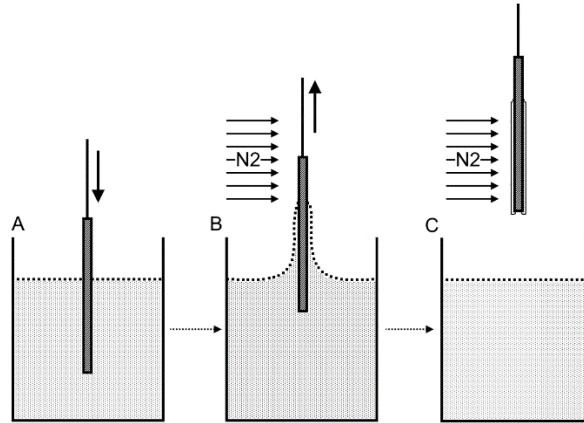
Figure 1-3 Dip-coating schematic

The rehydration viability of the cells preserved using this technique was found to be sensitive of the rate that the sample was removed from the coating reservoir (figure 4). Optimal viability and growth kinetics were observed by the samples that were coated at a rate of 200 mm/min.

1.4 Transitioning from 2D to 3D Cell Preservation

Preservation protocols and technologies play a fundamental role in the roll-out of new culture and assays products. Currently, 2D systems are still primarily utilized because of their ease-of-use and scalability. In parallel, suspension-based techniques for the long-term preservation of been heavily developed to allow ample supply to be banked for research demand. In the last decade there has been a call for the improvement of biological modelling in preference of more biologically relevant systems. Forcing cells to attach in a near 2D monolayer can cause changes to metabolism and phenotypic expression. This lack of relevance to an in vivo human condition results in a high failure rate of drug discovery studies that transition to clinical trials after successfully passing in vitro testing. Spheroids [6], organ-on-chips [7], and organoids [8] are a few of the exciting technologies undergoing major research.

Despite the pace of advancement into these engineered 3D cell systems, there is still a lack of a preservation protocol to allow immediate use of these products immediately following preservation. Organoid preservation for product banking and transportation is a primary example of the lacking preservation systems for these ingenious new technologies. Figure 1-4 describes the flow of steps from the collection of primary cell tissue and 2 phase process of preservation.
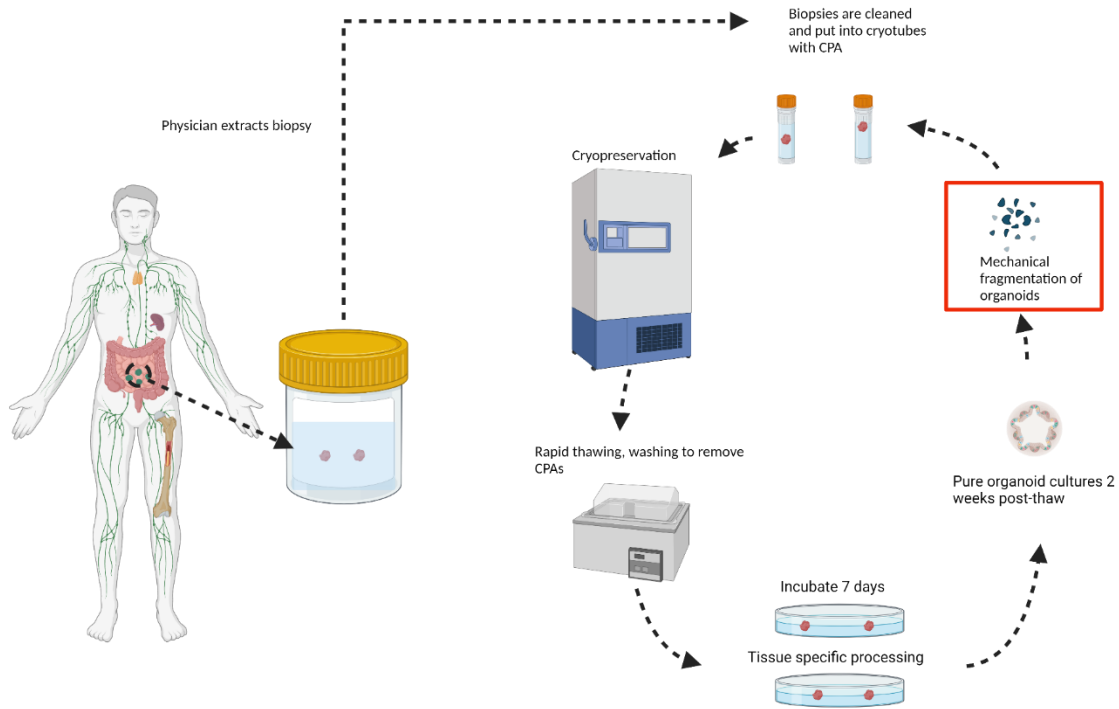
Figure 1-4 Cryopreservation of Organoids

Preservation steps that are related to organoids occur in two phases. The first preservation steps occur a direct extraction of a tissue biopsy which is cleaned, and small samples are divided into cryotubes containing CPA. Tissue specific organoid culture can be created by implementing the cells into the organoid culture system. After undergoing several tissue specific steps over several weeks, pure organoid cultures are obtained. A second phase of cryopreservation follows the direct preservation of those cultured organoids. However, the main rate limiting step involves fragmenting these organoids. Following this process, organoid fragments are essential suspended

in the CPA formula and undergo preservation protocols. This process is not ideal because new organoid cultures will still have to be grown using similar techniques undergone with the small sample of extracting tissue. There exists an opportunity for the development of a repeatable preservation system so that these pure organoids can be preserved without fragmentation and removing the post-preservation re-thaw steps.

1.5 Long-Term Organ and Tissue Preservation

To flesh out the issues with long-term preservation of larger tissue and organ structures, we must determine the major differences compared to suspension freezing of cells. With respect to the cells themselves there are several factors which complicate preservation. Tissues contain a variety of different cell types, each with different optimal cooling/thawing rates based on cytosol and membrane compositions. In addition, there are heterogeneous tissue compositions at different regions of tissue that make up organs. In addition, there are cell-cell and cell-matrix interactions which are present during tissue preservation, which will also likely change the freezing kinetics.

The other major difference and hurdle to overcome stems for the increase in overall volume of the sample. In suspensions, the sample size is essentially one cell and therefore heat and mass transfer kinetics are not often a concern. In large tissues, there a major heat and mass transfer phenomena resulting in significantly different preservation outcomes throughout the tissue. Even if the tissue was homogenous from the center to the outer surface, there are difficulties achieving the optimal cooling/warming rates throughout the entire sample. In addition, mass transfer hurdles result in non-uniform distribution of CPAs.

The final difference relates the extra cellular matrix structure itself. Uncontrolled ice formation due to the heat and mass transfer considerations already mentioned can lead to

significant mechanical distortion of the tissue matrix containing the cells. Even under the healthiest ice formation conditions, it is potentially possible that ice crystallization damage to the matrix will be extensive enough to cause irreversible injury to the overall tissue or organ structure before even considering the cellular implications. For this reason, it is generally agreed that avoiding ice crystal formation during larger tissue and organ preservation should be avoided altogether. Vitrification cryopreservation allows the cryopreservation of samples without the formation of ice and the resulting injury; however, the aforementioned heat and mass transfer hurdles may be an even larger issue for vitrification which requires more extreme cooling/heating conditions and higher CPA concentrations.

1.6 Relevance of Research to the Current Preservation Landscape

The bulk of this dissertation can be separated into two major themes. The first is the thermodynamic and molecular characterization of CPA components (Chapter 2 and 3). There is a generally agreed upon protocol for the cryopreservation of 2D cultured cell lines via suspension freezing. However, the specific mechanisms of injury and the subsequent mitigation of that injury are still largely unresolved. Therefore, it is important to develop and explore new methods and analysis techniques to discern these mechanisms in relationship to the CPA composition. Thermodynamic evaluation using DSC provides descriptive properties which elucidate the freezing and thawing behaviors of freezing. Raman spectroscopy allows us to study minute changes to the hydrogen bonding interactions of water molecules through the process of cooling, freezing, and subsequent thawing. The analysis of these two independent methods will help to further develop the mechanistic framework behind freezing injury and CPA mitigation.

Chapter two focuses on the bioprotective properties of disaccharide sugars. These molecules have already been implicated in desiccation tolerance (especially trehalose, refer

section 1.3). In addition these molecules have been extensively studied for use in cryoprotective formulations [9]. DSC is employed to study freezing point and protein stability in the presence if disaccharides, while Raman spectroscopy provides in-depth analysis of hydrogen bonding characteristics. Results of this study elucidate that all disaccharides possess bioprotective abilities; however, trehalose is a significantly more effective cryoprotectant. The Raman analysis suggests these abilities are due to a more organized water network.

Chapter three focuses on the study of a less studied cryoprotective additive: sericin. Like disaccharides, polymeric proteins have been extensively studied as non-penetrating CPAs; however, sericin is relatively new on the cryoprotective radar despite its common use in cosmetics. Sericin's extensive hydrogen bonding interaction, which provide the glue-like mechanism in silk, along with its antioxidant properties make it an interesting cryoprotective candidate. One goal of the study was to compare the freezing/thawing thermodynamic properties between the penetrating CPA (DMSO) and sericin. The results indicate DMSO is able to drastically modulate the melting point and heat of fusion properties compared to sericin and trehalose, which could explain why significant DMSO replacement cannot be reconciled using non-penetrating protectants. Like trehalose, sericin interacts heavily with the hydrogen bonding network resulting in major differences in enthalpy and entropy of reaction between symmetric and asymmetric water molecules. Overall sericin is an effective cryoprotectant. Collaborative enhancement using multiple additives (trehalose and sericin) of post-thaw growth kinetics were observed on HepG2 cells, despite viability loss at excessive concentrations.

The second theme of this dissertation shifts the focus from mechanistic characterization of suspension freezing to developing and optimizing a preservable cell-laden hydrogel (chapter 4). This research fits into the preservation landscape by focusing on the transition from 2D to 3D

cell preservation technologies. There is still a major lack of research describing cellular outcome in simple 3D cryopreserved structures. Alginate hydrogels are arguably one of the simplest scaffolds for 3D cell interaction and therefore are a perfect foundational starting point for deep study of cellular recovery following cryopreservation protocols. The primary goal of this study was to optimize viability and metabolic recovery of encapsulated HepG2 cells cryopreserved in an alginate-based matrix. Primary focus was on improving the protocol and determining whether significant changes would need to be made to the CPA. Additionally, this preservation system was tested on cell-lines of neurological and immunological origin with acceptable success. This research provides a framework for the optimization of cellular outcome of 3D cell constructs. The simple alginate matrix used serves as the first foundational step to introducing further complexity and addressing the injury that coincides. As complexity progresses closer to the level of organoid structures, we can begin to consider future viable and repeatable use of these preservation protocols for these important in vitro culture systems and hopefully beyond.

1.7 Bibliography

[1]   O. Mykhailova *et al.*, "Hypothermic storage of leukoreduced red blood cells for greater than 21 days is a safe alternative to irradiation," *Transfusion*, vol. 61, no. 4, pp. 1247–1257, Apr. 2021, doi: 10.1111/TRF.16273.

[2]   M. J. Taylor, B. P. Weegman, S. C. Baicu, and S. E. Giwa, "New Approaches to Cryopreservation of Cells, Tissues, and Organs," *Transfus. Med. Hemotherapy*, vol. 46, no. 3, pp. 197–215, Jun. 2019, doi: 10.1159/000499453.

[3]   P. Brüggeller, E. Mayer, P. Brüggeller, and E. Mayer, "Complete vitrification in pure liquid water and dilute aqueous solutions," *Natur*, vol. 288, no. 5791, pp. 569–571, 1980, doi: 10.1038/288569A0.

[4]   J. D. Hibshman, J. S. Clegg, and B. Goldstein, "Mechanisms of Desiccation Tolerance: Themes and Variations in Brine Shrimp, Roundworms, and Tardigrades," *Front. Physiol.*, vol. 11, Oct. 2020, doi: 10.3389/FPHYS.2020.592016.

[5]   J. Solocinski, Q. A. Osgood, E. Rosiek, L. Underwood, O. Zikanov, and N. Chakraborty, "Development of a surface tension mediated technique for dry stabilization of mammalian cells," *PLoS One*, vol. 13, no. 3, Mar. 2018, doi: 10.1371/journal.pone.0193160.

[6]   M. Zanoni *et al.*, "3D tumor spheroid models for in vitro therapeutic screening: a systematic approach to enhance the biological relevance of data obtained," *Sci. Reports 2016 61*, vol. 6, no. 1, pp. 1–11, Jan. 2016, doi: 10.1038/srep19103.

[7]   L. A. Low, C. Mummery, B. R. Berridge, C. P. Austin, and D. A. Tagle, "Organs-on-chips: into the next decade," *Nat. Rev. Drug Discov. 2020 205*, vol. 20, no. 5, pp. 345–361, Sep. 2020, doi: 10.1038/s41573-020-0079-3.

[8]   J. Kim, B. K. Koo, and J. A. Knoblich, "Human organoids: model systems for human biology and medicine," *Nat. Rev. Mol. Cell Biol. 2020 2110*, vol. 21, no. 10, pp. 571–584, Jul. 2020, doi: 10.1038/s41580-020-0259-3.

[9]   K. W. Yong, L. Laouar, J. A. W. Elliott, and N. M. Jomha, "Review of non-permeating cryoprotectants as supplements for vitrification of mammalian tissues," *Cryobiology*, vol. 96, pp. 1–11, Oct. 2020, doi: 10.1016/J.CRYOBIOL.2020.08.012.

Chapter 2 Estimating Preservation Potential of Disaccharides

2.1 Introduction

Reliable structural and functional preservation of complex biological material is an enduring challenge in biotechnology. There are two principal approaches to biopreservation – one involving use of low temperature involving cryopreservation technologies [1,2] and the other includes use of a low water activity desiccated state at ambient temperatures (lyopreservation) [3,4]. Both strategies have been theorized to rely upon formation of a chemically non-reactive state having very low-molecular mobility [5].

Homologous disaccharides are known to play an important role in creating low molecular mobility environment that offer protection to the biomolecules during processing for preservation. However, there is no consensus on the actual mechanism of protection offered by these disaccharides. Sugar-water binary systems have been studied using various spectroscopic techniques [6-10] and molecular dynamics simulations [11,12] to elucidate the protective effect exerted by the disaccharides. These studies have led to development of several complementary hypotheses. Water replacement hypothesis theorizes that formation of the dense network of hydrogen bonds between the biomolecule and the disaccharides as water is removed from the matrix due to ice formation or desiccation to offer structural stability to the biomolecules [10,13]. The glass formation hypothesis focuses on the ability of the disaccharides to create a high viscosity environment when water molecules are removed from the matrix. Reduced molecular mobility at glassy state is believed to arrest dynamic processes responsible for denaturation of

biomolecules [14,15]. A third hypothesis, known as preferential hydration hypothesis, proposes the ability of the disaccharides to entrap residual water at the interface of the biomolecule during glass formation to impart stability [16-19]. Finally, a fourth hypothesis suggests that the protective effect of the homologous disaccharides, especially trehalose, arise from its ability to switch between the anhydrous and hydrated form leading to a reversible and gentler dehydration-hydration mechanism [20]. Most of these hypotheses indicate the nature of interaction between disaccharides and water molecules to be one of the most important reasons for biomolecular stability. Hence, developing a deeper understanding of the nature of water-disaccharide relationship and preservation potential of the disaccharides.

In a water-disaccharide system, the fraction of water molecules that do not form any fully developed hydrogen bonds is regarded as "free water" [21]. These 'free water' molecules are thought highly reactive in nature [22,24] and can increase the availability of biomolecules to participate in chemical reactions. On the other hand, the fraction of water molecules that are hydrogen-bonded is known as 'cluster water', that form small tetrahedral clusters or even larger octamer network through hydrogen bonding. Cluster water is more stable [25] than free water and can easily make a transition to ice at lower temperatures [26,27]. With the increase in temperature of the water-disaccharide system, the increased molecular vibration increases the portion of 'free water' in the system, which in turn increases the chances of molecular denaturation. On the other hand, at lower temperatures the concentration of free water molecules is reduced drastically and are replaced by cluster water [28].

In this study we sought to understand the effect of presence of disaccharides in an aqueous system. A highly sensitive Raman microspectroscopic system was used to investigate the nature of disaccharide-water interaction to both free and cluster water systems. Raman

16

microspectroscopy is a highly sensitive molecular spectroscopy technique that can detect spatially correlated molecular vibration from samples when excited with laser irradiation. Since the vibrational information is specific to the chemical bonds and symmetry of molecules, the technique provides 'molecular fingerprints' by which the molecule can be identified even for the same substance with different state. Therefore, this can also be used to study the state of hydrogen bonding for a solution of water molecules.

Here intermolecular OH stretching modes of water in Raman spectra was investigated in presence of different homologous disaccharides (trehalose, sucrose, and maltose). How the presence of disaccharide at varying concentrations influences the existence of symmetric, asymmetric, and free water proportions was quantified and efforts were made to relate the results obtained to the preservation efficiency extended to the biomolecules relevant to cryopreservation and lyopreservation. The sugar which has the strongest decreasing effect on the reactive, free water on OH symmetric stretching peak may have a better ability to prevent ice nucleation at low temperatures and thermal denaturation at high temperatures. On the other hand, the sugar which creates the most ordered hydrogen bonding network at low temperatures may have the greatest chance at preventing cold denaturation. To verify our hypothesis, a detailed dynamic scanning calorimetry (DSC) study was undertaken to investigate the extent of bioprotective abilities offered by the different disaccharides studied here at both low and high temperatures. In addition, cold denaturation was evaluating using a novel Raman spectroscopic analysis of the amide I band.

Our results indicate that all disaccharide sugars are effective bioprotectants at both low and high temperatures. However, trehalose is uniquely effective at low temperatures, indicated by the lowest lysozyme solution freezing temperature (~-25.1°C) and the largest decrease in cold

denaturation temperature of β-lactoglobulin. At high temperature, the addition of all sugars into lysozyme solutions resulted in similar stability trends, which suggests neither sugar possesses unique bioprotective characteristics at relative high temperatures. Molecular analysis of the hydrogen bonding suggests the addition of any of the three disaccharides results in a less reactive aqueous environment at all temperatures. Although, trehalose replaces more of these unbound water molecules with a higher ratio of symmetric water to asymmetric water. The results of bioprotective studies agree well with the hypothesis based on Raman spectroscopy measurements.

2.2 Materials and Methods

2.2.1 Sample Preparation and Data Analysis

Maltose, sucrose, chicken egg white lysozyme, urea, and Beta-lactoglobulin (BLG) were procured from Sigma Aldrich (St. Louis, MO) while trehalose (α-trehalose, dihydrate) was procured from Pfanstieh (Waukegan, IL). Each solution was prepared by gravimetric measurement of solid components using an analytical balance (Mettler Toledo, Columbus, OH) followed by dissolving in deionized and distilled 18 MΩ water. Each water-based mixture was stirred using a vortex mixer (Fisher Scientific, Pittsburgh, PA) for at least 15 min until a transparent and homogeneous solution was obtained.

2.2.2 Raman Microspectroscopy

Experiments were conducted using Confocal Raman Microspectroscopy (WITec, alpha 300M). A liquid nitrogen-cooled low temperature stage (FDCS 196, Linkam Scientific Instruments, UK) was used to control sample temperatures during time series experiments. The temperature-controlled stage was integrated with the Raman microspectrometer using a custom-

designed adaptor. An EMCCD camera (Andor Technology, Belfest NIR) stabilized at - 60°C was used as a detector, a 532nm solid state laser operated at 20 mW power was used for excitation, and recorded with a 10X objective (Carl Zeiss, Jena Germany). All Raman data was collected as a time series set to integrate for a specified time as sample temperature was changing. To reduce spectral interference, cosmic rays were removed and a background subtraction technique from WITec was applied to all the spectra recorded.

2.2.3 Cold Denaturation Analysis

Solutions for this analysis contained 100 mg/mL of β-lactoglobulin, 4M urea, and 0 mM,125 mM, or 250 mM of disaccharide sugar (trehalose, maltose, sucrose). Raman spectra were collected in a time series at 30 second intervals while the temperature of the sample was reduced at 1°C/min from 40°C to 0°C. After 5 minutes of stabilization, the same spectra were collected while ramping the temperature back up to 40°C. These experiments were performed in triplicates for each sugar concentration tested. Sigmoidal plot fitting was performed on each set of data. The denaturation/renaturation temperature was determined using the inflection point of the sigmoidal fit (see results section for further analysis). All data analysis was performed in Origin2018.

2.2.4 OH Stretching Analysis

Sugar solutions (trehalose, sucrose, and maltose) of different concentrations (5%, 15%, 25%, 35%, 45% w/w) were prepared by diluting the stock solution in deionized water. 300 µL of solution was pipetted into a quartz crucible located inside of the temperature control stage and a quartz slide place over the crucible to prevent evaporation of the solution. Raman spectra were

collected in continuous 10 second intervals as the temperature cooled from 80°C to -10°C at a rate of 1°C/min resulting to 540 data points for each sugar solution tested.

2.2.5 Dynamic Scanning Calorimetry

DSC measurements were conducted using the Linkam DSC 600 stage (Linkam Scientific Instrument, UK). A 100mg/mL lysozyme solution for DSC measurements was made by dissolving lysozyme powder in solutions of 15%, 25%, 35%, and 45% w/w of each sugar. The concentration of sugars selected for this study was expected to provide lysozyme its maximal structural stabilization while retaining its solubility in solution. Before each experiment lysozyme solutions with or without sugar were loaded into alumina pans and sealed with press separately. For low temperatures study, the temperature was decreased from 25°C to -80°C with a cooling rate of 10°C/min; for high temperatures study, the temperature was increased from 25°C to 95°C also at 10°C/min. DSC peaks were measured by the DSC peak tool from Linksys 32 software, and Origin2018 software was used to perform baseline subtraction from thermograms and DSC peak data plotting.

2.3 Results

In this study, DSC was used to observe two energetic phenomena: crystallization of an aqueous solution and the thermal denaturation of the lysozyme protein at high temperatures. Figure 2-1 contains the data that was collected using the DSC technique. Figure 2-1A plots freezing points of aqueous solutions containing lysozyme protein at differing concentrations of disaccharide sugars. Lysozyme solution that contains no added sugars had a freezing point of -15.73°C. The addition of increasing concentrations of disaccharide to these solutions results in continuous freezing point depression. When comparing equal concentrations of the different

disaccharides, trehalose significantly depresses the freezing point of lysozyme solutions in the

concentration ranges between 15-35%. Figure 2-1B plots the thermal denaturation temperatures

of lysozyme protein in the presence of the disaccharides. The addition of increasing amounts of

disaccharide results in a continual increase in the thermal denaturation temperature of lysozyme.

Nearly identical spline fits are observed for all three sets of data, indicating that all sugars are

able to protect lysozyme protein from thermal denaturation, giving a slight advantage to sucrose

in this specific protection factor.
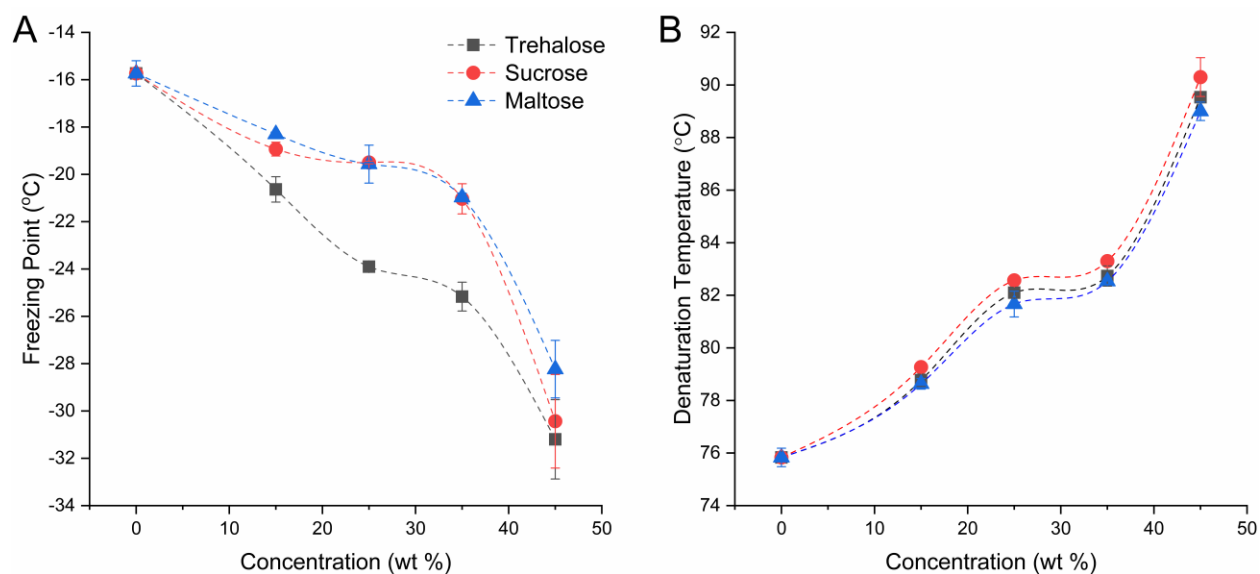
Figure 2-1 DSC Collected Parameters: A) Freezing point of sugar-lysozyme solutions were collected at sugar
concentrations ranging from 0-45% (w/w). Trehalose depresses freezing point significantly compared to the other
sugars in the 15-35% range. B) Thermal denaturation temperature was recorded as the temperature located at the
peak of the DSC thermogram for the event. Same sugar concentrations were used as A. Dashed lines represent
spline fits and Error bars represent ±SEM, n=3.

The DSC technique was also attempted to observe the temperatures at which cold

denaturation of protein was observed. Unfortunately, the energetic fingerprint of cold

denaturation is significantly lower than that of thermal denaturation and was not observable

using the DSC technique. However, a novel technique using time series Raman spectroscopy of

aqueous protein solutions was utilized to observe the structural changes of protein secondary structure due to cold denaturation.

Figure 2-2 displays the Raman spectral signature of an aqueous protein solution with an enhanced look at the amide I band related to protein structure. As the temperatures of these solutions is decreased, conformations to the secondary structure are indicated by a change in the amide peak ratio, primarily in the peak 2.
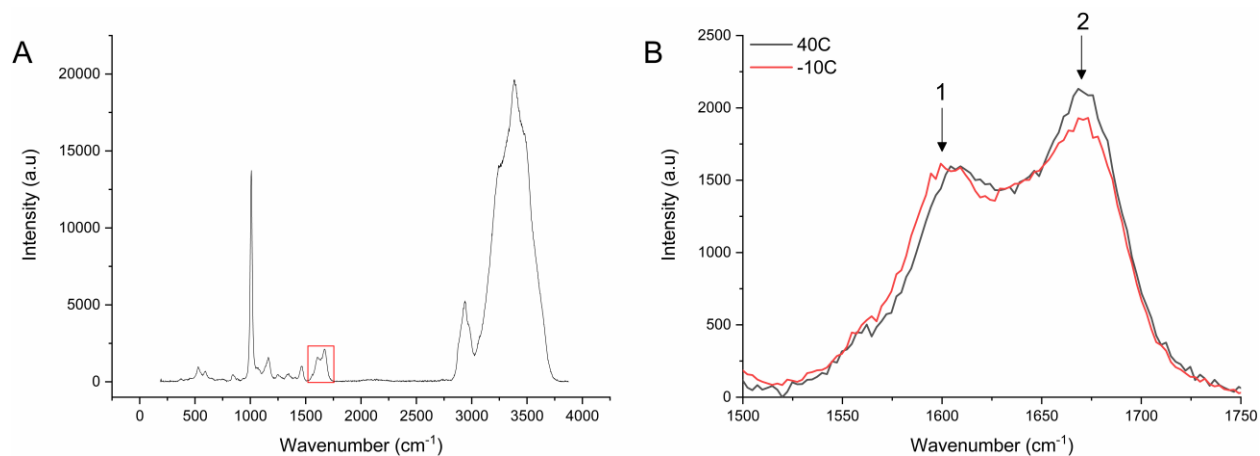
Figure 2-2 Raman Spectroscopy of the Amide I Band: A) Zoomed out view of Raman spectra for a solution containing disaccharide sugar and BLG protein. The red box outlines the spectra of interest located in B. B) Amide I spectra for BLG at -10°C (red) and 40°C (black). The two major peaks of interest are located at approximately 1600 cm^{-1} and 1670 cm^{-1}. Intensity differences are related to secondary protein structure changes resulting from cold denaturation.

Figure 2-3 contains a time series plot of spectral peak ratios of the beta sheet peak over the alpha helix peak for a lysozyme solution with no additional sugar. As the temperature of solution is ramped down, this ratio begins to decrease and plateau back out following a Boltzmann sigmoidal model. This model is fitted using the following equation:

$$A2 + \frac{A1 - A2}{1 + e^{\frac{x - x_0}{dt}}} \tag{1}$$

where,

A1 and A2 are the equilibrium values of the beta/alpha peak ratio before and after the cold denaturation transition occurs.

x_0 is the inflection point value of the stimulus where we assume the cold

denaturation/renaturation temperature to be.

dt is the coefficient that describes the slope behavior of the process during the transition and

identifies the continuity and discontinuity of the process [29].
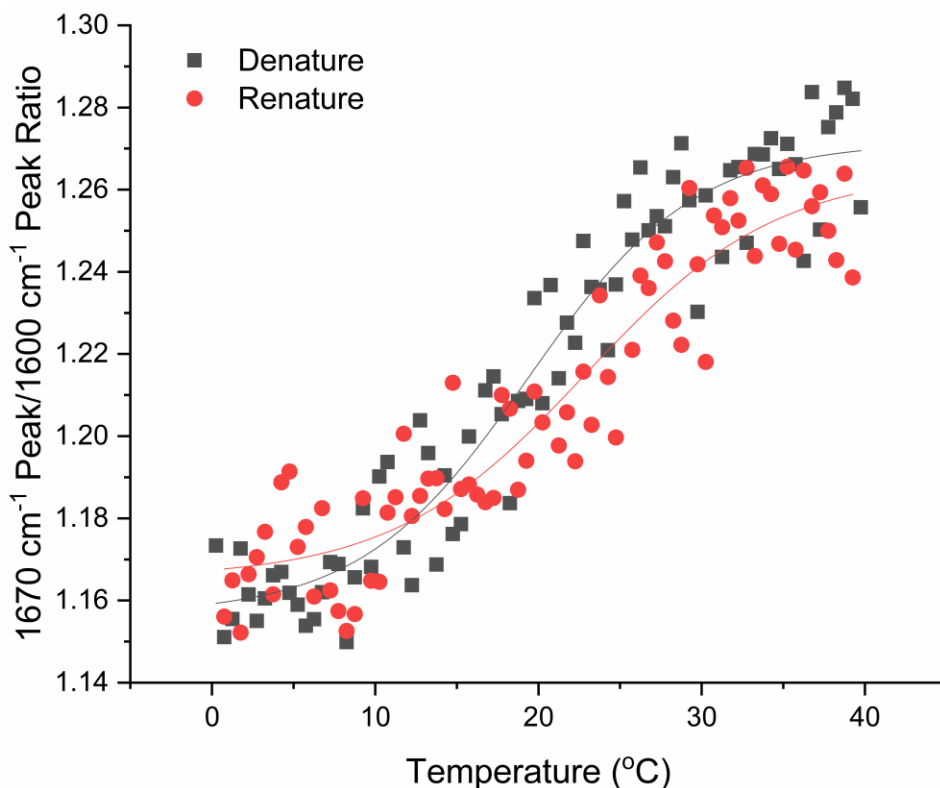
Figure 2-3 Raman Spectroscopic Analysis of BLG Cold Denaturation: Data points represent peak ratio of amide I peak 2 and amide I peak 2 at temperatures between 0°C and 40°C. As the temperature is ramped down, the ratio between the peaks decreases, indicating a shift in BLG secondary structure. This ratio returns to similar value after increasing th temperature, indicating renaturation of protein structure. Data fitted with Boltzmann sigmoidal model where the inflection point is considered the denature/renature temperature.

Figure 2-4A and 2-4B plot the denaturation and renaturation temperatures calculated

respectively for the solutions containing protein and disaccharide sugars. When adding 150 mM

of disaccharide sugar to the protein solutions, there was a significant decrease in the protein

denaturation temperature, although there was no significant difference between the three sugars.

Trehalose separated itself from the other two sugars at the 250 mM concentration as it was the

only sugar able to decrease the protein cold denaturation temperature below 0°C. Interestingly,

renaturation temperature, indicated by an increase in the amide I ratio, was recorded at higher

temperatures than denaturation and follows a different trend as sugar concentration is increased.

While the lowest denaturation temperature recorded was -0.86°C for the 250 mM trehalose

solution, the lowest renaturation temperature recorded was 10.5°C for the 250 mM sucrose

solution.
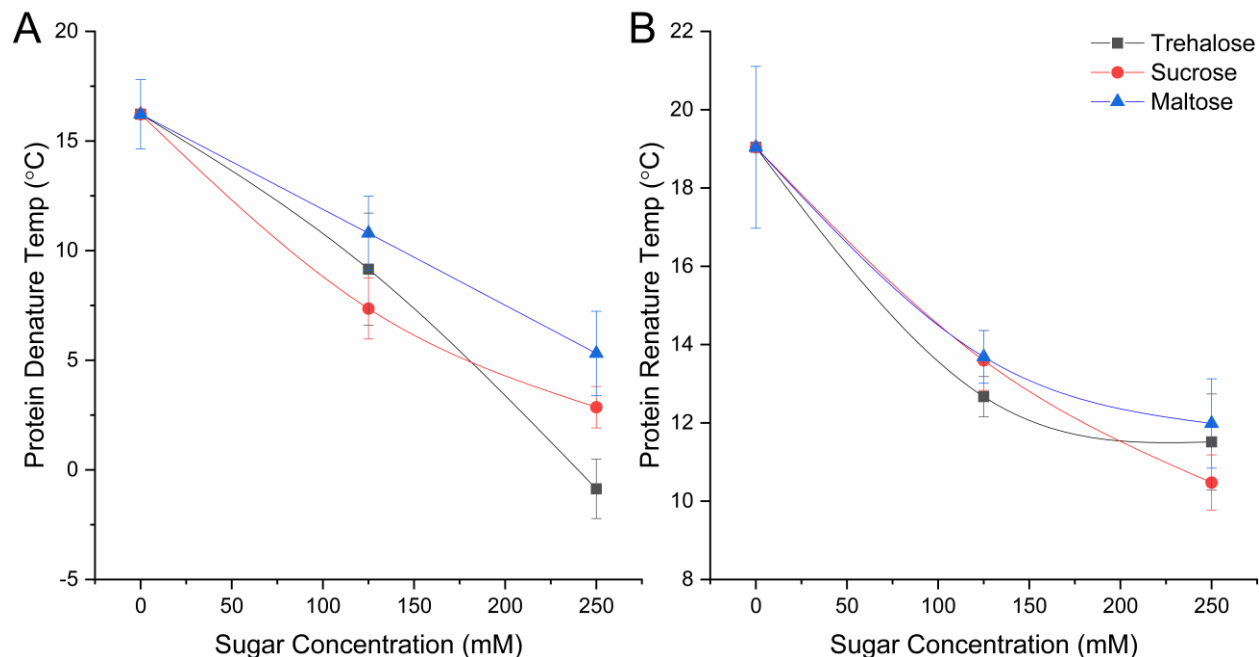
Figure 2-4 Modulation of Cold Denaturation via Disaccharide Sugars: A) Cold denaturation temperature of BLG in the presence of disaccharides. All sugars reduce denaturation temperature significantly. At higher concentrations, trehalose significantly depresses cold denaturation temperature compared to other sugars. B) Renaturation temperature of BLG occurs at significantly higher temperature than denaturation temperature. There is no significant difference in sugar effects on renaturation temperature. Error bars represent ±SEM, n=3.

The remaining data represents the Raman Spectroscopic analysis of the OH stretching

region. Figure 2-5 shows waterfall spectral plots for pure water and aqueous solutions containing

45% w/w of the 3 disaccharides tested. These plots are normalized to the asymmetric peak

intensity to achieve equal spectral heights. This normalization also emphasizes the overall shift

in the OH stretching region to higher wave numbers and the reduction of the symmetric spectral

peak as the temperature increases. Notice that each sugar has its own specific CH stretching

spectral fingerprint located between 2800 cm^{-1} and 3000 cm^{-1}. There is also no shift in CH and

minimal change in intensity to this peak with respect to temperature. The minor increases in CH stretching intensity observed at lower temperatures is primarily due to the overlap from the shift of the OH stretching region to lower wavenumbers.
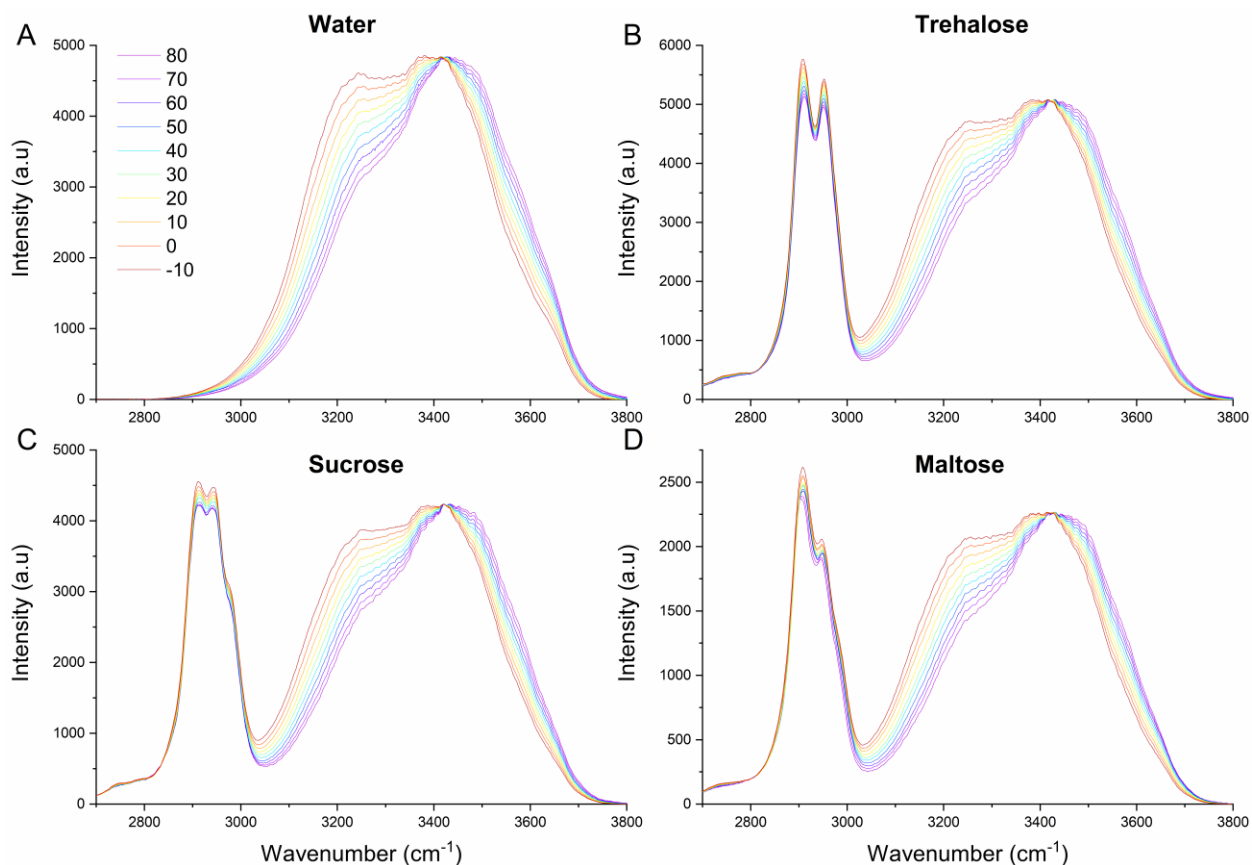
Figure 2-5 Waterfall Raman Spectra of Aqueous Sugar Solutions: Each plot contains 10 spectral graphs ranging between -10°C and 80°C for A) Water B) Trehalose C) Sucrose D) Maltose. Each sugar has a unique CH stretching band between 2800 cm^{-1} and 3000 cm^{-1}. As temperature is increased there is an observable shift in the OH stretching region to higher wavenumbers and a noticeable decrease in the symmetric OH stretching shoulder (~3200 cm^{-1}). Each waterfall plot is normalized to maximum OH stretching intensity.

To quantify the changes in the OH stretching region, spectral analysis is performed. Figure 2-6 illustrates three commonly used techniques for quantifying spectral peaks. The first and most basic of the techniques is to record point intensities of the spectral data where a peak is expected to be located. This technique is simple when there is only one spectral peak located at a point with little peak overlap. Temperature causing peak shift is also another factor that can add complexity to this analysis technique. For this study, point intensities were recorded at 3246.6

cm^{-1}, 3424.84 cm^{-1}, and 3616.03 cm^{-1} for the symmetric, asymmetric, and unbound OH regions

respectively. The second analysis technique is to calculate an area under the curve for a finite

region of the spectral data. Like the point intensity method, this integral needs to be selected for

where the desired peak is expected to be across a wide range of temperatures. The symmetric

area ranges from 3099.45 cm^{-1} – 3301.62 cm^{-1}, the asymmetric area ranges from 3389.86 cm^{-1} –

3549.72 cm^{-1}, and the unbound area ranges from 3616.03 cm^{-1} – 3783.62 cm^{-1}. The final

analysis technique is to using peak deconvolution to identify and parameterize the 3 peaks of

interest for this study. Origin 2018 contains a deconvolution algorithm which inputs spectral data

and estimated location/intensity of the peaks of interest to decompose the gaussian formulas for

each respective peak.
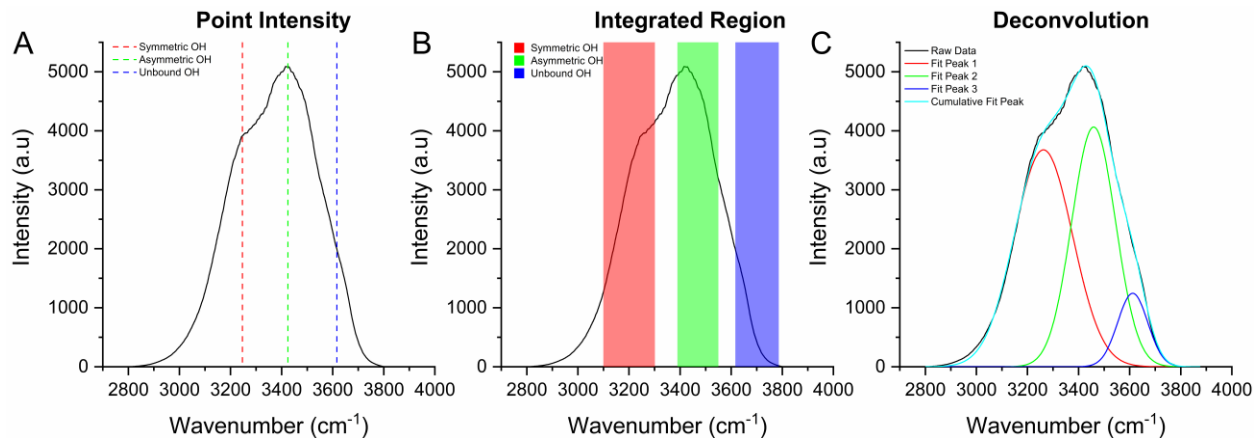
Figure 2-6 Spectral Analysis Techniques: 3 wavenumbers of interest were selected to represent the symmetric, asymmetric, and unbound regions of the OH stretching band. The wavenumbers selected are at 3246.6 cm^{-1}, 3424.84 cm^{-1}, and 3616.03 cm^{-1} B) Area under curve is calculated for a finite region of the spectral data. The symmetric area ranges from 3099.45 cm^{-1} - 3301.62 cm^{-1}, the asymmetric area ranges from 3389.86 cm^{-1} – 3549.72 cm^{-1}, and the unbound area ranges from 3616.03 cm^{-1} - 3783.62 cm^{-1}. C) Deconvolution method attempts to parameterize the three gaussian peaks of interest making up the OH-stretching region. A cumulative fit is shown adding up the 3 calculated peaks.

Figure 2-7 plots the Raman spectroscopic data that was analyzed via the point intensity

technique. Each row of plots contains the point intensity data for three different temperature

points (80°C, 40°C, and 0°C) from the top respectively. Each column of plots shows the point

intensities for the three OH stretching regions of interest (symmetric, asymmetric, and unbound)

from the left respectively. All data was fitted using a linear regression model with r value greater than 0.7. Notice that the slope trend for each sugar is similar, independent of the temperature for each OH stretching region. For the three temperature points of focus, trehalose has the highest slope in the symmetric region, followed by sucrose and maltose being the lowest. Interestingly, at lower temperatures the increase of sugar has less of an impact on the symmetric region and the maltose plot has a negative slope under the 0°C condition (Fig. 2-7G). The second column of plots, containing the asymmetric region data, displays a positive slope for all three sugars at all three temperature points. However, trehalose clearly has a reduced slope value compared to the other two sugars across all temperatures. The slope for all sugars is the highest at lower temperatures, which is the reverse trend noted for the symmetric region. The furthest right column containing the data for the unbound region shows negative slopes for all three sugars across all temperature points. At higher temperatures (Fig. 2-7C) there is a separation of the slopes with trehalose having the highest negative slope followed by sucrose and maltose. As temperature is reduced, this gap shrinks for the maltose and sucrose data, while trehalose continues to maintain a stronger negative trend.
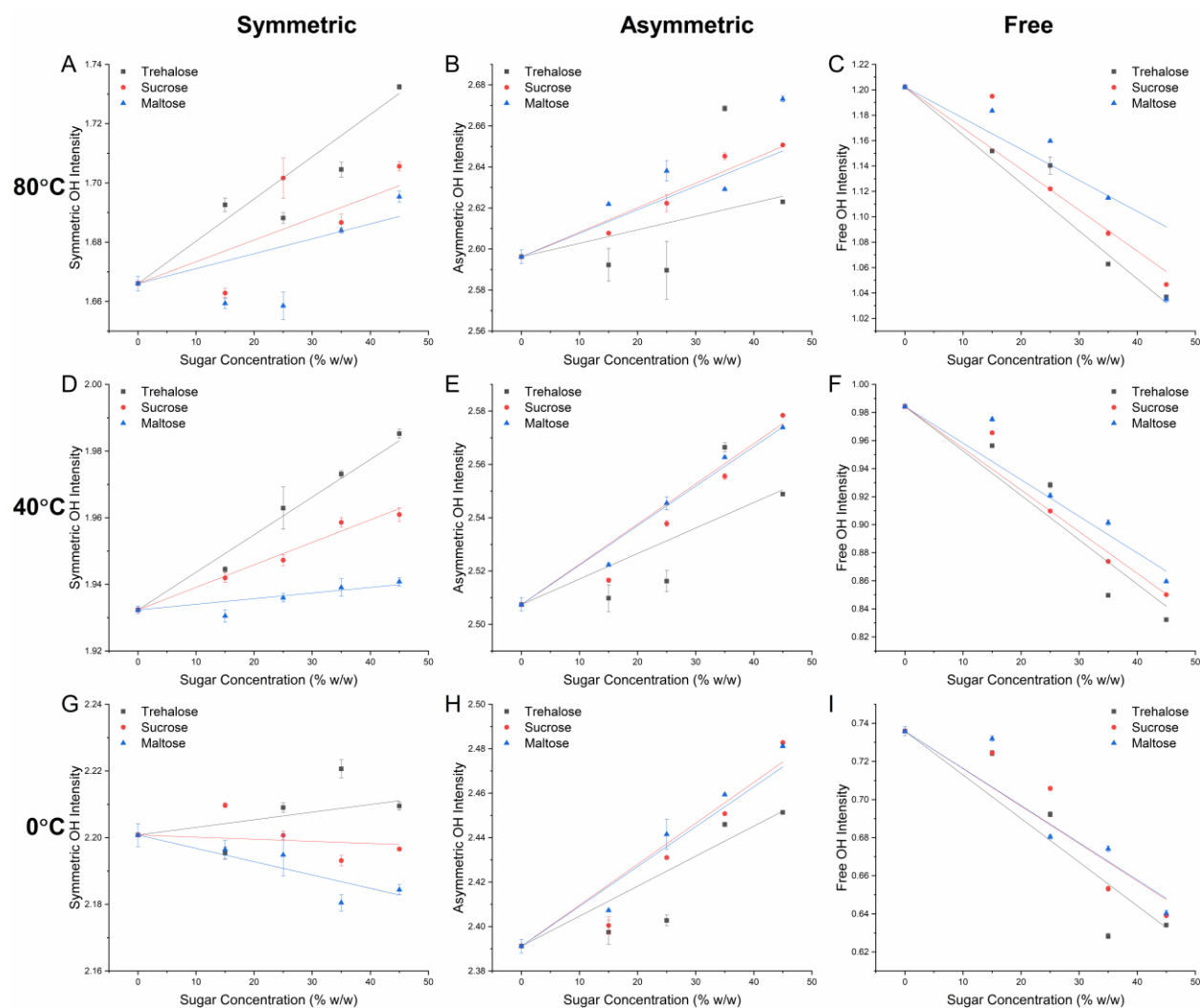
Figure 2-7 Point Intensity Analysis of OH Stretching Region: The plots can be separated by row and column. The first row (A-C), second row (D-F), and third row (G-I) contain the recorded data at three different temperature points (80, 40, and 0°C). The first (A, D, G), second (B, E, H), and third (C, F, I) columns contains the data for the three different regions of interest of the OH stretching band (symmetric, asymmetric, unbound OH). Plots show trehalose enhanced ability to create a more organized OH bonding structure by reducing the total amount of unbound OH, increasing the amount of symmetric OH, and having the smallest increase in asymmetric OH compared to the other two sugars.

Figures 2-8 and 2-9 contain the same data values as figure 2-7 for the other two analysis methods. Figure 8 plots the analysis data the was performed using the integrated area technique. The slopes of all the 9 plots follow similar trends to that of figure 2-6 with some minor differences. In the symmetric region, all sugar plots follow the similar trends, although there is a negative slope for the sucrose solution at 0°C. This slope was approximately 0 when using the

28

point intensity analysis. In the asymmetric region, similar trends are observed again, however the major difference is the separation of the maltose and sucrose slopes at all temperature values. In the unbound region, major negative slopes are observed again. However, the significantly higher slope value for the trehalose sugar is not observed at all temperature points. At 80°C (Fig. 2-8C), the slope values for all three sugars are equal. At 40°C, there is a moderately larger negative slope for the maltose solution. Finally at 0°C, trehalose and maltose have significantly larger negative slops than the sucrose solution.
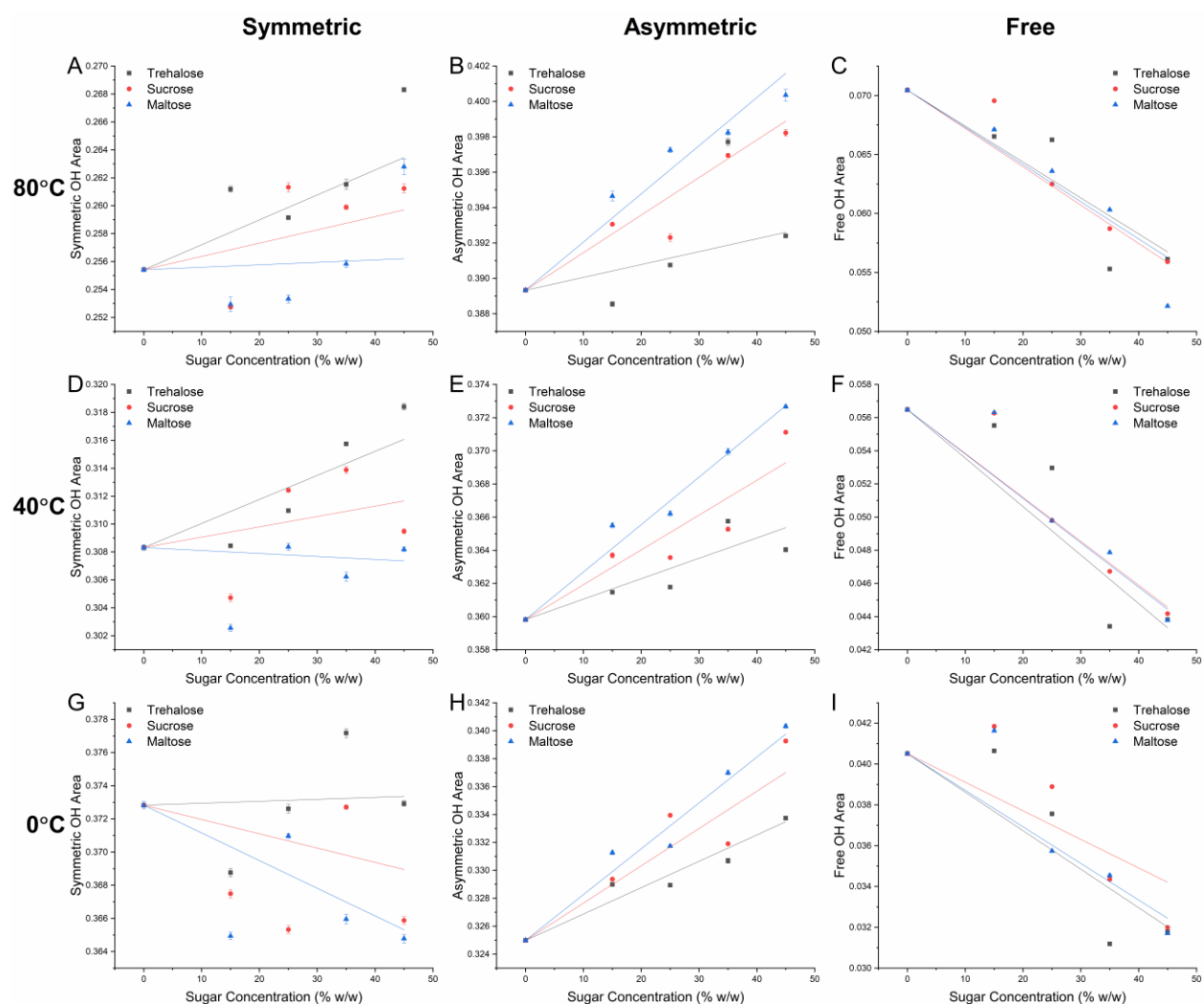
Figure 2-8 Integrated Region Analysis of OH Stretching Region

Figure 2-9 contains identical data calculated using the peak deconvolution algorithm. Once again, all 9 plots contain similar trends as the previous two analysis techniques despite significantly higher error values in some of the plots. The symmetric region plots maintain a consistent slope trend for all sugars, noticing a negative slope for all three sugars at the 0°C temperature.
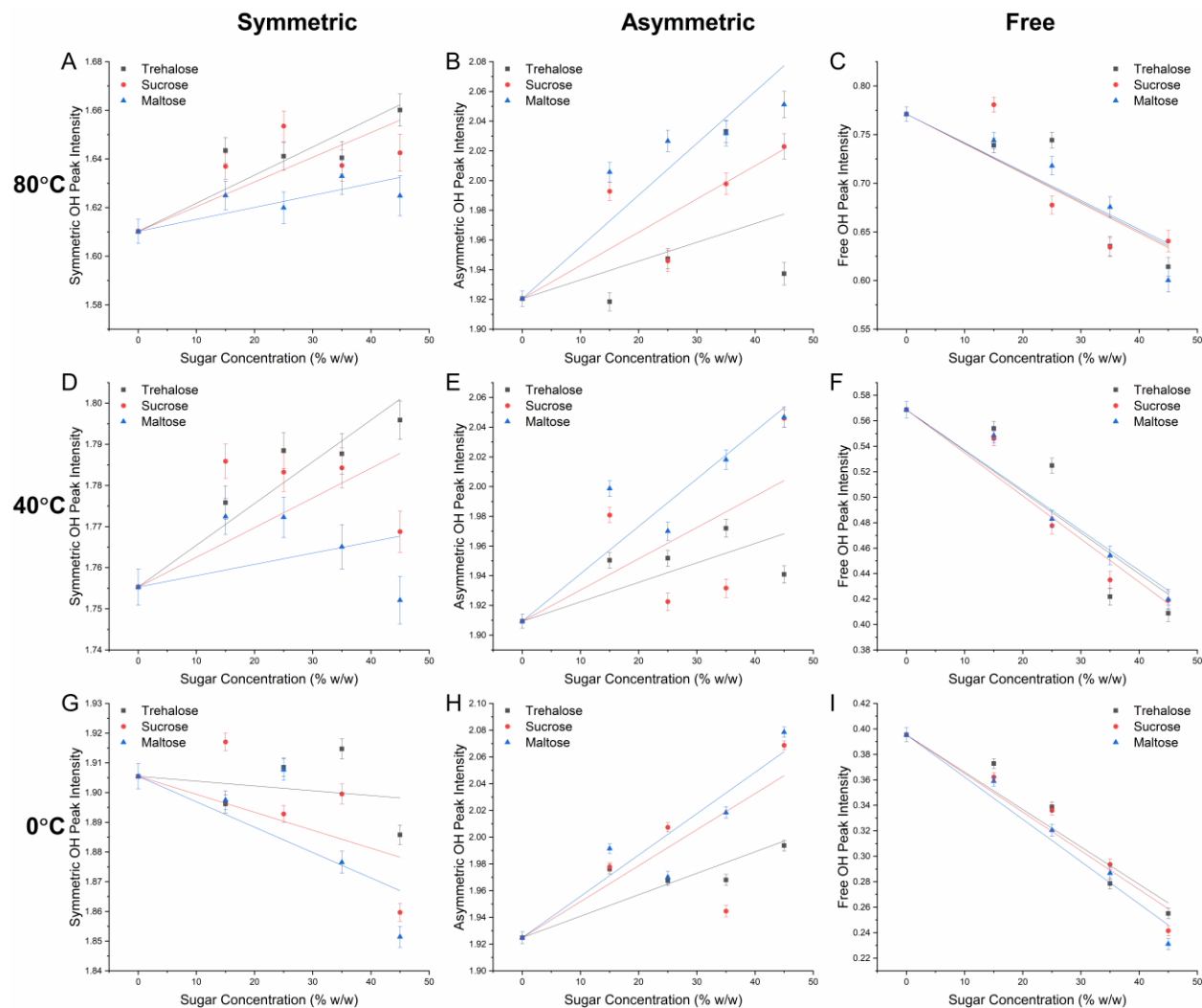
Figure 2-9 Peak Deconvolution Analysis of OH Stretching Region

Figure 2-10 condenses the slope data from the previous 3 figures to compare trends observed from each analysis method. Each column contains the slope intensity data for the three different OH stretching regions of interest, while each row has compared the three different

analysis techniques stacked from top to bottom. The point intensity technique has noticeably

smaller error values overall, while the deconvolution method has the largest. While the linear

regression fit was effective for the point analysis method, there were data sets collected using the

other two methods that did not appear to fit a linear regression model. For comparison of the

three methods, a linear regression was used for all analysis, however it is possible other models

may be more effective. Due to the apparent random nature of these non-linear data sets, we

theorize these poor fits could be an artifact of the analysis method itself, especially in the case of

deconvolution. This result further confirms that the point analysis method is most effective for

detecting minor spectral differences in the OH stretching region.
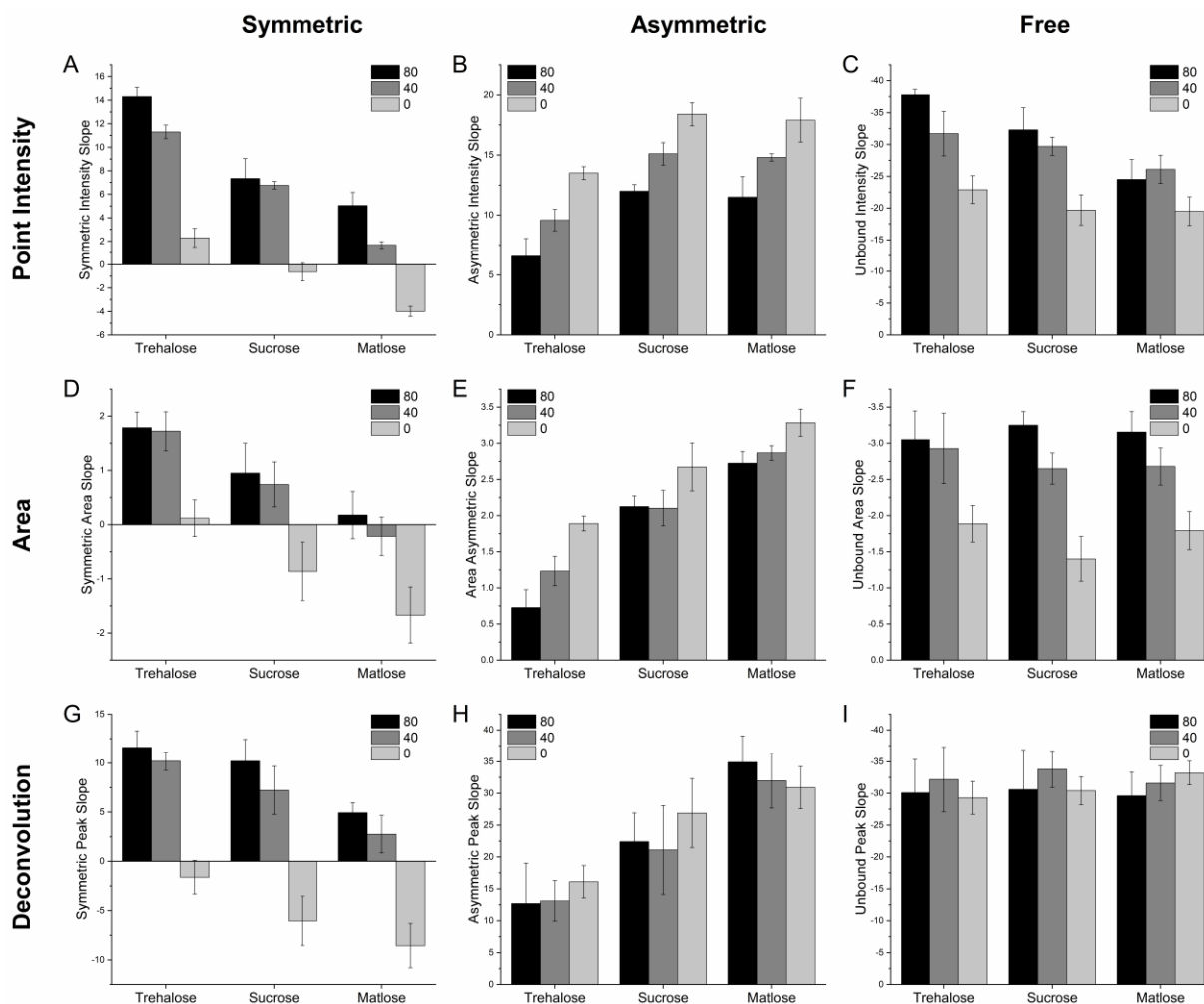
Figure 2-10 OH Stretching Analysis Method Comparison: The intensity of the bar graphs represents slope of linear regression fits for the represented data. The type of OH stretching data is separated by the vertical columns, while the rows separate the type of analysis method

2.4 Discussion

The results of this study further establish that disaccharide sugars have a positive impact on several relevant preservation properties. All three sugars were equally effective at higher temperatures; however, trehalose significantly improves the parameters relevant to cryopreservation (freezing point depression and cold denaturation stability). Therefore, it is important to consider what makes trehalose more effective at lower temperatures.

The OH stretching data suggests all three disaccharides mesh significantly into the hydrogen bonding network, indicated by significant reductions in the amount of free OH present at all temperatures. In addition, the hydrogen bonding interactions caused by the addition of trehalose result in a larger increase of symmetrically bonded water and a smaller increase in asymmetrically bonded water compared to the other two sugars. This result seems to contradict other spectroscopy-based studies that only consider two OH stretching bands when performing analysis [30]. However, the total increase in number of hydrogen bonds observed in trehalose (followed by sucrose and then maltose) solutions should result in a total slowing of water dynamics [6], which could be one explanation for trehalose's more pronounced bioprotective properties. In addition, we attempt to correlate the changes in hydrogen bonding characteristics to the freezing point depression and protein stability characteristics.

2.4.1 Freezing Point Depression

Freezing point depression has been heavily studied in the characterization of cryopreservation. Reducing the temperature at which a solution freezes allows efficient dehydration to occur, resulting in a more viscous environment and less crystallization [31]. High amounts of crystallization during freezing and recrystallization during thawing has been shown to be a primary cause of protein and membrane damage during the cryopreservation process [32]. Therefore, it is important to note trehalose's unique ability to depress freezing point significantly at moderate concentrations compared to the other two disaccharides. Wang et. al. reached a similar conclusion and additionally found that trehalose also reduced the heat of freezing compared to the sucrose and other monosaccharides. In addition, free water present in solution has been implicated as the portion of water that nucleates to form primary ice [33], therefore increasing the concentration of sugar is expected to decrease the freezing point. However, this

does not reconcile trehalose has significantly greater depression compared to sucrose and maltose. There is a strong correlation between the freezing point depression data and asymmetric OH spectral data. While all three sugars increase asymmetric OH binding with increasing concentration, trehalose has a significantly lower effect. Asymmetrically bound water is less reactive than symmetric water and can potentially form a nucleation site more readily. This difference could explain why solutions containing trehalose have a lower freezing point.

2.4.2 Thermal Denaturation Stability

This study indicates that trehalose, sucrose, and maltose all provide lysozyme stability in an aqueous environment. This is indicated by a significant increase in the thermal denaturation temperature for all sugars, however, there is no indication that either sugar boasts a stronger stability at these temperatures. There have been several studies highlighting disaccharide's ability to stabilize proteins from thermal denaturation. However, the exact mechanism of stabilization is up for debate [34-36]. Most studies offer a theory for the molecular process but emphasize the necessity for a detailed molecular study of the water-sugar-protein interactions. This study focuses on hydrogen bonding environment of binary water-sugar solutions. At temperatures where thermal denaturation is likely, all three sugars greatly reduce the amount of free water present in the solution. This is important because even at optimal temperatures there are several processes that are mediated by water that can act to break down proteins [37], so decreasing the amount of reactive water in solution should be vital to improving protein stability at high temperatures. The OH stretching data suggests that trehalose can reduce concentration of free water even more significantly than the other two sugars, which could be an explanation for improved protein stability observed by other studies. Further study involving tertiary protein-

sugar-water solutions is necessary to reach further conclusions about specific sugar-protein interactions in this environment.

2.4.3 Cold Denaturation Stability and Renaturation

A novel time series collection of Raman spectra across a range of temperatures was used to determine the denaturation temperature and renaturation temperature of beta-lactoglobulin. A similar study was performed by Seo et.al. for determining the thermal denaturation temperature characteristics of beta-lactoglobulin [38]; however, to the best of our knowledge Raman spectroscopic evaluation of cold-denaturation has not been studied. The principal area of focus was the amide I spectral band; 80% of this region is due to the carbon-oxygen double bond present in the protein structure [39]. Within this larger spectral region, there are smaller bands that correspond to the conformational differences in the secondary structure of the protein [40]. Our data indicates that cold denaturation is characterized by a reduction in intensity of the 1670 cm^{-1} peak and an increase in the peak at 1600 cm^{-1}, resulting in an overall reduction of the intensity ratio of these two peaks as temperature is reduced. It is difficult to pinpoint the exact conformational changes taking place in the secondary structure due to some overlap in the bands. Typically, the higher wave numbers of the amide I band (1655-1700 cm^{-1}) are associated with turn structures present in the protein [41]; however, there is also a weak band corresponding to anti-parallel beta sheets in this region. In addition, parallel beta sheets are typically found between 1613-1637 cm^{-1} and alpha helices are found around 1650 cm^{-1} [42]. Therefore, cold misfolding being observed is most likely due to a reduction in turn structures corresponding to straightening of the peptide chain and a possible minor increase in alpha helix/beta sheet structure. In contrast, the previously aforementioned study suggests a similar shift is due to a misfolding the beta sheet structure in favor of alpha helices at high temperatures because of an

overall high concentration of beta sheets present in beta-lactoglobulin (53%) in the native state [38]. A more detailed analysis of the amide I band is necessary to determine the exact changes in secondary structure characterizing cold denaturation of BLG.

One focus of this study was to determine the cold denaturation temperature of BLG in an aqueous solution and how adding sugars into the environment changes the stability of the protein. All sugar environments were able to increase the stabilization window of BLG with a 250 mM concentration of trehalose creating the most stable environment. In addition, renaturation of BLG was observed as the temperature was ramped back to 40°C. This renaturation is typical for cold denaturation [43], however it is unclear what percentage of denaturation does not recover and whether renaturation is further inhibited by a frozen solution state. A more precise and detailed study of the amide I band could provide further insights in this area.

Finally, we attempt to predict a molecules ability to protect proteins from cold denaturation. Perhaps counter-intuitively exposure of the non-polar groups of a protein to water results in a more ordered hydrogen bonding network [44,45]. Therefore, an aqueous hydrogen bonding system which is already more ordered with the addition of disaccharides will have a smaller enthalpic change from denaturation. Because cold denaturation is enthalpy driven, a lower temperature is required to reduce the entropic term to the point where enthalpy can again outweigh entropy and protein denaturation can occur. Trehalose based solutions display the most ordered hydrogen bonding environment characterized by significantly lower unbound OH and a stronger ratio of symmetric/asymmetric replacement. In addition, sucrose solutions are more ordered than maltose-based solutions. This result agrees with the cold denaturation data recorded using Raman spectroscopy.

2.5 Thermodynamic Derivation of Cold Denaturation

A thermodynamic explanation for the existence of the non-intuitive cold denaturation event can be derived using basic equations for Gibbs free energy (G), entropy (S), and enthalpy (H). Assume we consider the reaction of protein denaturation a 1 step process going from a state of folded (F) to unfolded (U). (See figure 2-11)

Folded   **Unfolded**
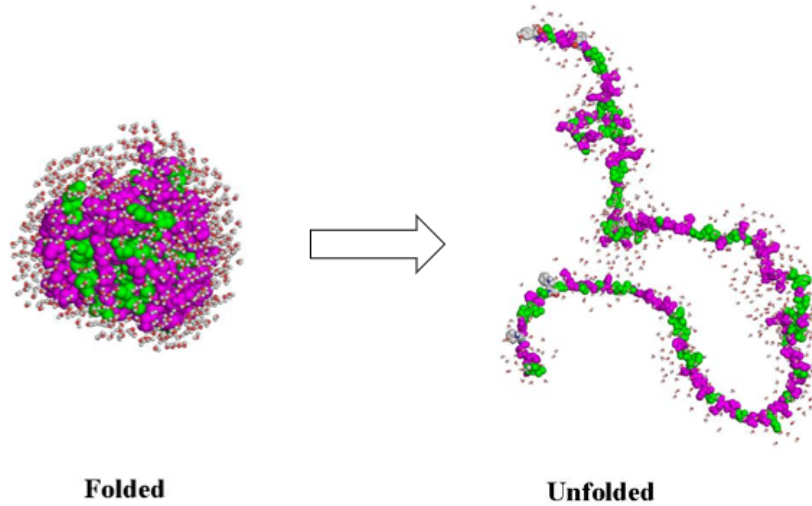
Figure 2-11 Simple single step reaction for denaturation of a protein

The Gibbs free energy can be described by equations 1 and 2.

$$\Delta G = G^u - G^f \tag{2}$$

$$\Delta G(T) = \Delta H(T) - T\Delta S(T) \tag{3}$$

We assume to know one of the equilibrium points where the Gibbs free energy equals zero. This assumption can be made due to the relative ease of determining the thermal denaturation temperature. These values can typically be found in thermodynamic protein tables. The constant thermal denaturation temperature will be labeled T_C.

$$\Delta G(T_c) = \Delta H(T_c) - T_c\Delta S(T_c) = 0 \tag{4}$$

Eq. 3 can be used to solve for the change in entropy at T_C. This value is not as easily determined experimentally.

$$\Delta H(T) = \Delta H(T_c) + (T - T_c)\Delta C_p \tag{5}$$

$$\Delta S(T) = \Delta S(T_c) + \Delta C_p \ln\left(\frac{T}{T_c}\right) \tag{6}$$

Equations 4 and 5 are simplified by assuming the heat capacity is unchanged by the denaturation reaction. Finally, we can plug equations 3, 4, and 5 into equation 1 to solve for change in Gibb's free energy.

$$\Delta G(T) = \frac{(T_c - T)}{T_c}\Delta H(T_c) + (T - T_c)\Delta C_p - T\Delta C_p \ln\left(\frac{T}{T_c}\right) \tag{7}$$

Where T_c, $\Delta H(T_C)$, and ΔC_p are experimentally determinable values. To solve this system, we can assume values for all 3. $T_c = 60°C$, $\Delta H(T_C) = 500$ kJ/mol, $\Delta C_p = 10$ kj/mol*K. The inverse parabola is plotted in figure 2-12. The parabola crosses the x-intercept at our thermal denaturation temp (T_C) and at a second lower temperature where the cold denaturation temperature is located (~3°C in this case). What is interesting is the presence of stabilizing agents shifts this parabola up and increases the stability window of the protein, while the opposite is the case for denaturants.
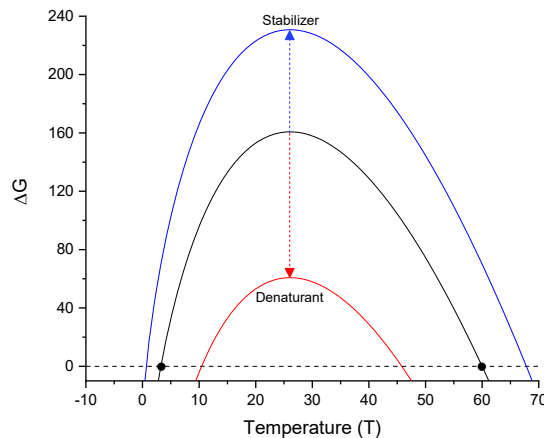
Figure 2-12 Thermodynamic representation of the Existence of Cold Denaturation Temperature

2.6 Bibliography

[1]   D. E. Pegg, "Principles of Cryopreservation," *Methods Mol. Biol.*, 2007, doi: 10.1007/978-1-59745-362-2_3.

[2]   W. F. Rall and G. M. Fahy, "Ice-free cryopreservation of mouse embryos at -196 degrees C by vitrification," *Nature*, vol. 313, no. 6003, pp. 573–575, 1985, doi: 10.1038/313573A0.

[3]   N. Chakraborty, A. Chang, H. Elmoazzen, M. A. Menze, S. C. Hand, and M. Toner, "A spin-drying technique for lyopreservation of mammalian cells," *Ann. Biomed. Eng.*, vol. 39, no. 5, pp. 1582–1591, May 2011, doi: 10.1007/S10439-011-0253-1.

[4]   L. K. McGinnis, L. Zhu, J. A. Lawitts, S. Bhowmick, M. Toner, and J. D. Biggers, "Mouse sperm desiccated and stored in trehalose medium without freezing," *Biol. Reprod.*, vol. 73, no. 4, pp. 627–633, Oct. 2005, doi: 10.1095/BIOLREPROD.105.042291.

[5]   X. He, A. Fowler, and M. Toner, "Water activity and mobility in solutions of glycerol and small molecular weight sugars: Implication for cryo- and lyopreservation," *J. Appl. Phys.*, vol. 100, no. 7, p. 074702, Oct. 2006, doi: 10.1063/1.2336304.

[6]   A. Lerbret, F. Affouard, P. Bordat, A. Hedoux, Y. Guinet, and M. Descamps, "Slowing down of water dynamics in disaccharide aqueous solutions," *J. Non. Cryst. Solids*, vol. 357, no. 2, pp. 695–699, May 2010, doi: 10.1016/j.jnoncrysol.2010.05.092.

[7]   A. Hédoux *et al.*, "Analysis of sugar bioprotective mechanisms on the thermal denaturation of lysozyme from Raman scattering and differential scanning calorimetry investigations," *J. Phys. Chem. B*, vol. 110, no. 45, pp. 22886–22893, Nov. 2006, doi: 10.1021/JP061568I.

[8]   S. Perticaroli, P. Sassi, A. Morresi, and M. Paolantoni, "Low-wavenumber Raman scattering from aqueous solutions of carbohydrates," *J. Raman Spectrosc.*, vol. 39, no. 2, pp. 227–232, Feb. 2008, doi: 10.1002/JRS.1910.

[9]   K. I. Murata and H. Tanaka, "Liquid–liquid transition without macroscopic phase separation in a water–glycerol mixture," *Nat. Mater. 2012 115*, vol. 11, no. 5, pp. 436–443, Mar. 2012, doi: 10.1038/nmat3271.

[10]   C. Branca, S. Magazù, F. Migliardo, and P. Migliardo, "Destructuring effect of trehalose on the tetrahedral network of water: A Raman and neutron diffraction comparison," *Phys. A Stat. Mech. its Appl.*, vol. 304, no. 1–2, pp. 314–318, Feb. 2002, doi: 10.1016/S0378-4371(01)00517-9.

[11]   A. Lerbret, P. Bordat, F. Affouard, M. Descamps, and F. Migliardo, "How Homogeneous Are the Trehalose, Maltose, and Sucrose Water Solutions? An Insight from Molecular Dynamics Simulations," *J. Phys. Chem. B*, vol. 109, no. 21, pp. 11046–11057, Jun. 2005,

doi: 10.1021/JP0468657.

[12] C. J. Roberts and P. G. Debenedetti, "Structure and Dynamics in Concentrated, Amorphous Carbohydrate−Water Systems by Molecular Dynamics Simulation," *J. Phys. Chem. B*, vol. 103, no. 34, pp. 7308–7318, Aug. 1999, doi: 10.1021/JP9911548.

[13] J. H. Crowe, J. S. Clegg, and L. M. Crowe, "Anhydrobiosis: the water replacement hypothesis," *Prop. Water Foods ISOPOW 6*, pp. 440–455, 1998, doi: 10.1007/978-1-4613-0311-4_20.

[14] J. H. Crowe, J. F. Carpenter, and L. M. Crowe, "The role of vitrification in anhydrobiosis," *Annu. Rev. Physiol.*, vol. 60, pp. 73–103, 1998, doi: 10.1146/ANNUREV.PHYSIOL.60.1.73.

[15] J. L. Green and C. A. Angell, "Phase relations and vitrification in saccharide-water solutions and the trehalose anomaly," *J. Phys. Chem.*, vol. 93, no. 8, pp. 2880–2882, 2002, doi: 10.1021/J100345A006.

[16] M. Sola-Penna and J. R. Meyer-Fernandes, "Stabilization against thermal inactivation promoted by sugars on enzyme structure and function: Why is trehalose more effective than other sugars?," *Arch. Biochem. Biophys.*, vol. 360, no. 1, pp. 10–14, Dec. 1998, doi: 10.1006/ABBI.1998.0906.

[17] R. D. Lins, C. S. Pereira, and P. H. Hünenberger, "Trehalose-protein interaction in aqueous solution," *Proteins*, vol. 55, no. 1, pp. 177–186, Apr. 2004, doi: 10.1002/PROT.10632.

[18] S. N. Timasheff, "Protein Hydration, Thermodynamic Binding, and Preferential Hydration," *Biochemistry*, vol. 41, no. 46, pp. 13473–13482, Nov. 2002, doi: 10.1021/BI020316E.

[19] K. Gekko and S. Koga, "Increased thermal stability of collagen in the presence of sugars and polyols," *J. Biochem.*, vol. 94, no. 1, pp. 199–205, 1983, doi: 10.1093/OXFORDJOURNALS.JBCHEM.A134330.

[20] F. Sussich, C. Skopec, J. Brady, and A. Cesàro, "Reversible dehydration of trehalose and anhydrobiosis: from solution state to an exotic crystal?," *Carbohydr. Res.*, vol. 334, no. 3, pp. 165–176, Aug. 2001, doi: 10.1016/S0008-6215(01)00189-6.

[21] Q. Hu, H. Zhao, and S. Ouyang, "Understanding water structure from Raman spectra of isotopic substitution H2O/D2O up to 573 K," *Phys. Chem. Chem. Phys.*, vol. 19, no. 32, pp. 21540–21547, Aug. 2017, doi: 10.1039/C7CP02065A.

[22] P. M. Wiggins, "Role of water in some biological processes.," *Microbiol. Rev.*, vol. 54, no. 4, p. 432, 1990, doi: 10.1128/mmbr.54.4.432-449.1990.

[23]   M. Chaplin, "Do we underestimate the importance of water in cell biology?," *Nat. Rev. Mol. Cell Biol. 2006 711*, vol. 7, no. 11, pp. 861–866, Sep. 2006, doi: 10.1038/nrm2021.

[24]   P. M. Wiggins, "High and low density water and resting, active and transformed cells," *Cell Biol. Int.*, vol. 20, no. 6, pp. 429–435, 1996, doi: 10.1006/CBIR.1996.0054.

[25]   M. F. Chaplin, "Water: its importance to life," *Biochem. Mol. Biol. Educ.*, vol. 29, no. 2, pp. 54–59, Mar. 2001, doi: 10.1111/J.1539-3429.2001.TB00070.X.

[26]   G. D'Arrigo, G. Maisano, F. Mallamace, P. Migliardo, and F. Wanderlingh, "Raman scattering and structure of normal and supercooled water," *J. Chem. Phys.*, vol. 75, no. 9, p. 4264, Aug. 1998, doi: 10.1063/1.442629.

[27]   G. E. Walrafen, "Raman Spectral Studies of the Effects of Temperature on Water Structure," *J. Chem. Phys.*, vol. 47, no. 1, p. 114, May 2004, doi: 10.1063/1.1711834.

[28]   N. Akiya and P. E. Savage, "Roles of Water for Chemical Reactions in High-Temperature Water," *Chem. Rev.*, vol. 102, no. 8, pp. 2725–2750, 2002, doi: 10.1021/CR000668W.

[29]   A. L. Navarro-Verdugo, F. M. Goycoolea, G. Romero-Meléndez, I. Higuera-Ciapara, and W. Argüelles-Monal, "A modified Boltzmann sigmoidal model for the phase transition of smart gels," *Soft Matter*, vol. 7, no. 12, pp. 5847–5853, Jun. 2011, doi: 10.1039/C1SM05252G.

[30]   C. Branca, S. MacCarrone, S. Magazu, G. Maisano, S. M. Bennington, and J. Taylor, "Tetrahedral order in homologous disaccharide-water mixtures," *J. Chem. Phys.*, vol. 122, no. 17, p. 174513, May 2005, doi: 10.1063/1.1887167.

[31]   D. Whaley, K. Damyar, R. P. Witek, A. Mendoza, M. Alexander, and J. R. T. Lakey, "Cryopreservation: An Overview of Principles and Cell-Specific Considerations," *Cell Transplant.*, vol. 30, 2021, doi: 10.1177/0963689721999617.

[32]   D. Gao and J. K. Critser, "Mechanisms of cryoinjury in living cells," *ILAR J.*, 2000, doi: 10.1093/ilar.41.4.187.

[33]   Q. Wang, L. Zhao, C. Li, and Z. Cao, "The decisive role of free water in determining homogenous ice nucleation behavior of aqueous solutions," *Sci. Reports 2016 61*, vol. 6, no. 1, pp. 1–8, May 2016, doi: 10.1038/srep26831.

[34]   M. A. Mensink, H. W. Frijlink, K. van der Voort Maarschalk, and W. L. J. Hinrichs, "How sugars protect proteins in the solid state and during drying (review): Mechanisms of stabilization in relation to stress conditions," *Eur. J. Pharm. Biopharm.*, vol. 114, pp. 288–295, May 2017, doi: 10.1016/J.EJPB.2017.01.024.

[35]   C. Olsson and J. Swenson, "The role of disaccharides for protein–protein interactions – a SANS study," *https://doi.org/10.1080/00268976.2019.1640400*, vol. 117, no. 22, pp.

3408–3416, Nov. 2019, doi: 10.1080/00268976.2019.1640400.

[36] C. Olsson, R. Zangana, and J. Swenson, "Stabilization of proteins embedded in sugars and water as studied by dielectric spectroscopy," *Phys. Chem. Chem. Phys.*, vol. 22, no. 37, pp. 21197–21207, Sep. 2020, doi: 10.1039/D0CP03281F.

[37] S. Magazù, G. Maisano, P. Migliardo, and V. Villari, "Experimental simulation of macromolecules in trehalose aqueous solutions: A photon correlation spectroscopy study," *undefined*, vol. 111, no. 19, pp. 9086–9092, Nov. 1999, doi: 10.1063/1.480250.

[38] J. A. Seo *et al.*, "Thermal Denaturation of Beta-Lactoglobulin and Stabilization Mechanism by Trehalose Analyzed from Raman Spectroscopy Investigations," *J. Phys. Chem. B*, vol. 114, no. 19, pp. 6675–6684, May 2010, doi: 10.1021/JP1006022.

[39] S. Krimm and J. Bandekar, "Vibrational spectroscopy and conformation of peptides, polypeptides, and proteins," *Adv. Protein Chem.*, vol. 38, no. C, pp. 181–364, 1986, doi: 10.1016/S0065-3233(08)60528-8.

[40] N. C. Maiti, M. M. Apetri, M. G. Zagorski, P. R. Carey, and V. E. Anderson, "Raman Spectroscopic Characterization of Secondary Structure in Natively Unfolded Proteins: r-Synuclein," 2004, doi: 10.1021/ja0356176.

[41] H. Ishizaki, P. Balaram, R. Nagaraj, Y. V. Venkatachalapathi, and A. T. Tu, "Determination of beta-turn conformation by laser Raman spectroscopy.," *Biophys. J.*, vol. 36, no. 3, p. 509, 1981, doi: 10.1016/S0006-3495(81)84749-2.

[42] N. Kuhar, S. Sil, and S. Umapathy, "Potential of Raman spectroscopic techniques to study proteins," *Spectrochim. Acta Part A Mol. Biomol. Spectrosc.*, vol. 258, p. 119712, Sep. 2021, doi: 10.1016/J.SAA.2021.119712.

[43] A. I. Azuaga, M. L. Galisteo, O. L. Mayorga, M. Cortijo, and P. L. Mateo, "Heat and cold denaturation of beta-lactoglobulin B," *FEBS Lett.*, vol. 309, no. 3, pp. 258–260, Sep. 1992, doi: 10.1016/0014-5793(92)80784-E.

[44] C. L. Dias, T. Ala-Nissila, J. Wong-Ekkabut, I. Vattulainen, M. Grant, and M. Karttunen, "The hydrophobic effect and its role in cold denaturation q," 2009, doi: 10.1016/j.cryobiol.2009.07.005.

[45] C. J. Tsai, J. V. Maizel, and R. Nussinov, "The Hydrophobic Effect: A New Insight from Cold Denaturation and a Two-State Water Structure," *http://dx.doi.org/10.1080/10409230290771456*, vol. 37, no. 2, pp. 55–69, 2008, doi: 10.1080/10409230290771456.

Chapter 3 Modulation of Solution Hydrogen Bonding Properties by Sericin

3.1 Introduction

Biopreservation technologies can play an extremely important role in transitioning cell-based techniques from laboratory to bedside. Such translation of cell-based technologies requires the development of highly optimized and efficient long-term preservation strategies. In general, long-term preservation of cells and cellular materials is achieved through formation of a glassy matrix[1-3] at low temperatures in presence of cryoprotective agents (CPAs). This glassy matrix has been hypothesized to reduce molecular mobility and prevent degradative intracellular reactions at low storage temperatures [4]. Dimethyl sulfoxide (DMSO) is one of the most used CPAs in slow cooling rate cryopreservation techniques. However, use of DMSO has been frequently and closely associated with cellular toxicity effects and poor post-thaw performance [5-7].

At high concentrations (>10%) DMSO has been shown to be toxic to cells due in part to the formation of lipid membranes pores [8] and other irreversible membrane damage. This has been well-studied in the context of the development of drug delivery strategies [9]. Even at low concentrations, exposure to DMSO (<4% v/v) has recently been linked to apoptosis initiation in retinal neuronal cells [7]. In another study, exposure to 1% v/v DMSO did not produce any evidence of cell death, but there was significant mitochondrial damage due to increased levels of reactive oxygen species (ROS) following 24-hour exposure [10], leading to mitochondrial swelling and significant membrane potential impairment [11]. Exposure to DMSO levels as low

as 0.1% v/v causes drastic changes to human intercellular processes and the overall epigenetic landscape by impacting DNA methylation and down regulating microRNAs [12]. These studies suggest the need to revisit the optimal use of DMSO in CPA formulations.

Use of additives that can actively modulate the cryopreservation outcome in CPA formulations is a commonly accepted strategy to reduce DMSO toxicity and potentially decrease the required concentration of DMSO. The two primary ways in which additives mitigate injury are by altering the physical environment and by providing biochemical protection. Physically they can alter the nature of the frozen environment by modulating ice crystal morphology and creating areas with higher glass transition temperatures. Biochemically they can provide protection from membrane damage and osmotic stress [13].

In this study, the effect of using the polymeric protein sericin as a non-penetrating CPA was investigated. Sericin is a protein used by bombyx mori (silkworms) in the production of silk, where it acts as an adhesive coating to the fibers and has anti-oxidant properties [14]. Multiple studies have reported sericin's ability to mitigate oxidative stress in various tissue types and proposed use of sericin as a replacement for animal origin serum in cell culture [15,16]. Furthermore, it has been used as a serum replacing agent in CPA formulations for several different types of mammalian cells including human adipose tissue-derived stem cells [17], myeloma cell lines, fibroblasts, keratinocytes, insect cell lines [18], rat insulinoma cell lines, mouse hybridoma cell lines and mesenchymal stem cells [19].

Due to the polymeric nature of the protein, sericin can form extensive hydrogen bonding (H-bonding) in the extracellular matrix [20] and thus can play an important role in creating low-molecular mobility environment at low temperatures [21]. H-bonding can be used to impact the nature of the glass formation by modulating the strength of H-bonds formed [22]. In this study an

investigation was undertaken to characterize the effect of sericin as an additive to DMSO based CPA formulation. Special emphasis was given to understanding the effect of sericin in aqueous environment on H-bonding strength using Raman microspectroscopy. Thermophysical properties of CPA formulations containing different concentrations of sericin were characterized using differential scanning calorimetry (DSC). These properties were likened to the cryopreservation outcome of human hepatocellular carcinoma cells (HepG2) in terms of survival and growth.

3.2 Materials and Methods

3.2.1 Raman Microspectroscopic Analysis of CPA Formulations

The effect of addition of sericin in the CPA formulation was investigated by quantifying change in Raman spectral signatures at different temperatures. Special emphasis was given to the OH stretching regions of the Raman spectra as they closely relate to the local H-bonded network of water molecule [23] . A customized confocal Raman microspectrometer was used to collect spectral data (UHTS 300, WITec Instruments Crop, Germany). A 532-nm continuous wave laser system was used for photonic excitation. Spectral signatures were collected using a 10X objective (Zeiss, Thornwood, NY) and an EMCCD camera (Andor Technology, UK). A liquid nitrogen-cooled low temperature stage (FDCS 196, Linkam Scientific Instruments, UK) was used to control sample temperatures at desired setpoints. The temperature-controlled stage was integrated with Raman microspectrometer using custom-designed adaptor mechanisms discussed elsewhere [13]. For each sample, 300 µL of solution was added to a low form-factor quartz crucible and placed inside the freezing stage. The stage was pre-cooled and equilibrated to -10°C and then warmed at a rate of 10°C/min to 20°C. Raman microspectroscopic data was collected using an integration time of 1 s, averaged over 60 accumulations. Following collection,

background spectra was subtracted, and cosmic ray interference was removed. Spectral peaks were deconvoluted and analyzed using Origin Pro 2018 (OriginLab, Northampton, MA).

A customized chemometric deconvolution algorithm based on Fast Fourier Transform (FFT) of Raman signal is used to decompose the OH stretching regions of the CPA formulations [24,25]. The deconvolution is computed using the formula

$$f = fft^{-1} \left[\frac{fft(y)}{fft(s)} \right] \tag{8}$$

where y is the known response of the signal s. While several different peaks can be identified in the OH stretching region (Fig. 2A) that are related to the physical state of the water and H-bonding, two principals peaks related to symmetric ($\sim$3200 cm^{-1}) and asymmetric ($\sim$3415 cm^{-1}) vibrations of OH stretching were considered here for the analysis related to H-bonding. The higher-frequency asymmetric spectral component is known to be related to the water molecules with an incompletely formed H-bonding clusters [26]. Whereas, the lower-frequency symmetric component corresponds to the molecules with complete tetrahedral H-bonded clusters [27,28].

The experimentally obtained spectral intensity of the symmetric and asymmetric OH stretching peaks were then used to estimate the enthalpy and entropy of the formation of H-bonds in aqueous CPA formulations using Van't Hoff equation[29,30].
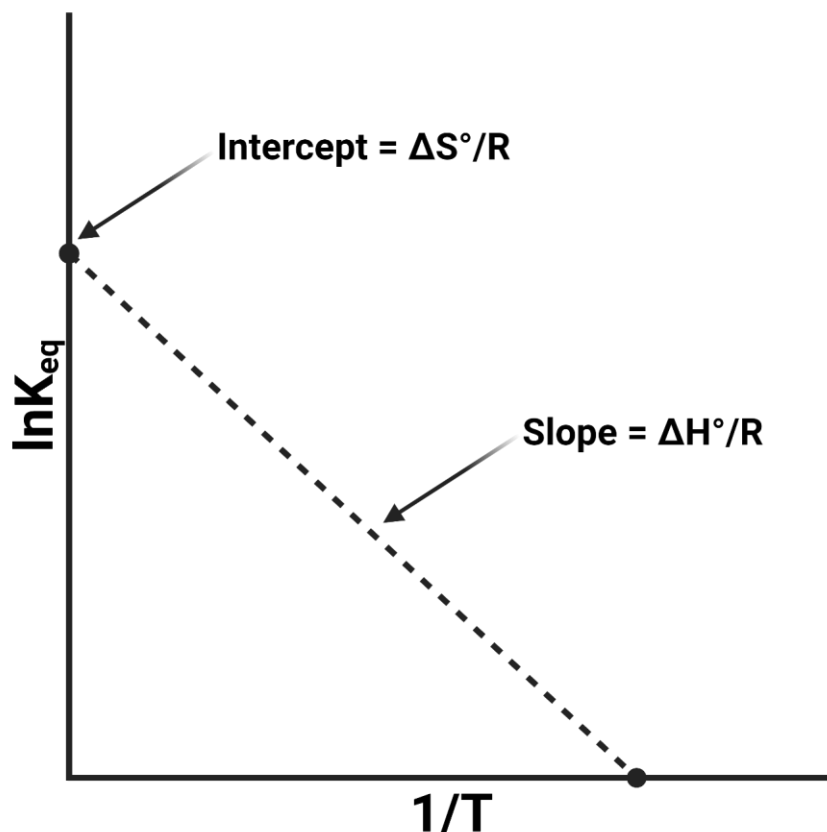
Figure 3-1 Graphical representation of a Van't Hoff Analysis: The inverse of temperature is graphed on the x-axis while the natural logarithm of the equilibrium constant (K_{eq}) is on the y axis. After fitting a linear regression model to the collected data, the slope can be used to quantify change in enthalpy and the y-intercept can be used to quantify the change in entropy of the reaction

A Van't Hoff plot (Figure 3-3A) was constructed as the linear dependence of ln(k) against the inverse of the temperature (T). The enthalpy (ΔH) of bonding was expressed as a product of the slope of the Van't Hoff plot and universal gas constant. The equilibrium constant (k) in this case is also equal to the ratio of the intensities of the individual OH stretching peaks Raman spectrum at different temperatures (T). Similar techniques have been used to estimate H-bonding energy and appearance of Clathrate-like Structures in aqueous solutions using Raman spectroscopy [31].

$$\ln(k) = \frac{-\Delta H^\circ}{R} \cdot \frac{1}{T} + const \tag{9}$$

Here R is the universal gas constant and $\Delta H°$ is the change in enthalpy during the formation of one mole of hydrogen bonded molecules from nonbonded ones under standard conditions of 298 K and 1 atm. The change in enthalpy (Figure 3-3B) and entropy (Figure 3-3C) was used to quantify the change in characteristics of H-bonding strength in aqueous solutions having varying concentrations of sericin.

In addition to the H-bonding characterization using intensities of the symmetric and asymmetric peaks in the OH stretching region of the Raman spectra, change of peak position (peak shift) was also used to analyze energetics related to H-bonding. The trend in peak-shift characteristics were quantified by comparing the shift in peak-center per unit temperature for both symmetric (n_1) and asymmetric peaks (n_2, as seen in Fig. 4A and B). This analysis indicates the variation in H-bonding energetics at different temperatures in presence of sericin.

3.2.2 Differential Scanning Calorimetry (DSC) for Determining Thermodynamic Properties

The effect of addition of an additive to the CPA formulation containing DMSO was analyzed using DSC. Properties including freezing point, melting point, and heat of fusion was quantified using DSC. DSC measurements were performed using a precise temperature-controlled microscopy stage and a temperature controller (FDCS 600, Linkam Scientific Instruments, Tadworth, UK). Calibration of the system was performed using indium as described in ASTM E968 ([32] - Data not shown). CPA formulations containing trehalose and sericin as additives were analyzed. Freezing/melting data was collected using a rate of 1°C/min until stabilized after freezing or thawing. The freezing and melting points were considered as the temperatures at which maximum heat flow occurred during the phase change process. Enthalpy of freezing was determined by measuring the area under the curve of the thermogram.

Thermogram data was normalized to the mass of the solution added to the DSC chamber. All thermogram data were plotted and analyzed using Origin Pro 2018.

3.2.3 Cell Culture, Cryopreservation, and Growth

Human hepatocellular carcinoma (HepG2) cells were obtained from the American Type Culture Collection (Manassas, VA), and grown in 75 cm^2 culture flasks (Corning Inc, Corning, NY). Opti-MEM (Gibco) culture media was supplemented with 5% fetal bovine serum (FBS) (Gibco) and penicillin-streptomycin to yield final 100 units/mL penicillin G and 100 μg/mL streptomycin sulfate (Hyclone-Thermo Scientific, Logan, UT). Cells were incubated in an atmosphere of 5% CO_2 and 95% air. The cells were collected using trypsinization followed by centrifugation and resuspended in 1 mL of cryoprotective solution in individual microtubes. A passive freezing container capable of controlling the cooling rate at 1°C/min (Cool Cell LX, 137 Biocision, Menlo Park, CA) was used to store samples in cryogenic conditions. After exposing the cells to cryogenic conditions for pre-determined duration, cells were thawed quickly in a 37°C water bath and re-suspended in fully complemented cell culture medium. Cell numbers were quantified using hemacytometer (Hausser Scientific, Horsham, PA) counts and membrane integrity was assessed using trypan blue exclusion.

3.3 Results

3.3.1 Raman Microscopy

The effect of the presence of sericin on H-bonding characteristics at different temperatures was investigated using Raman microspectroscopy. Figure 3-2A and 3-2B show the representative Raman spectrum at OH stretching regions of pure water at the temperatures 20°C and -10°C. The deconvoluted spectra in Figs. 3-2A and 3-2B show different vibrational peaks in

the OH stretching region including the symmetric and asymmetric OH stretching peaks (peaks 1

and 2) were used for analysis of H-bonding characteristics. The variation in intensity of the

symmetric and asymmetric OH stretching peaks with the change in temperature indicate relative

changes in the nature of H-bonding - with a relative increase in the symmetric peak indicating an

increase in the number of highly ordered H-bonded water clusters [27]. Figure 3-2C plots the

intensities of the symmetric and asymmetric OH stretching peaks from -10°C to 20°C in water

binary solutions. With increasing temperature symmetric OH stretching peak intensity decreases

linearly, while the asymmetric peak increases in intensity. As temperature decreases, the

symmetric peak intensities increase due to increase in number of water molecules completely

bound by its nearest neighbors. An opposite effect is observed for asymmetric OH stretching

peak which is associated with the incompletely H-bonded clusters of water molecules in solution.
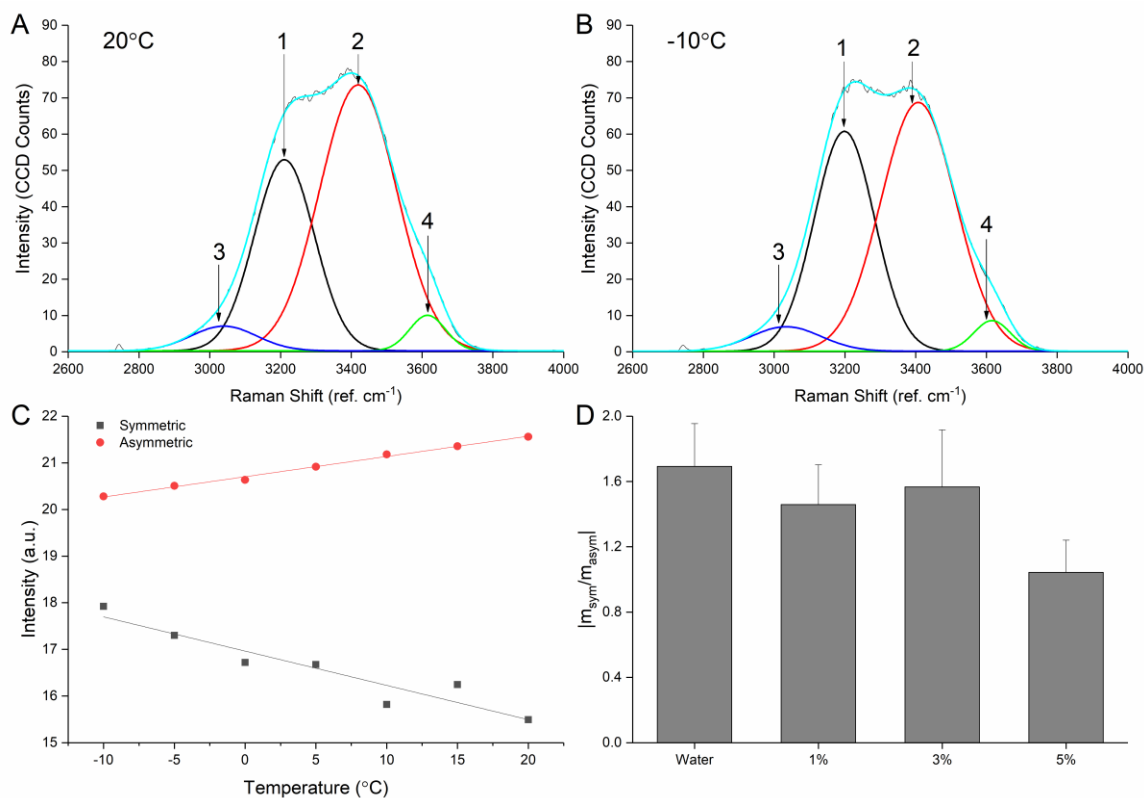
Figure 3-2 Raman spectroscopy of binary water-sericin solutions. (A) shows OH-stretching band (~2900-3700 cm⁻¹) of pure water at -10°C. Spectrum is deconvoluted into four primary bands and the reconstructed spectrum is superimposed on the original to show agreement of fit. Arrows 1 and 2 indicate symmetric and asymmetric peaks respectively. (B) shows OH-stretching band of pure water at 20°C. (C) shows symmetric and asymmetric peak intensities are plotted at the corresponding temperatures at which Raman scans were acquired for pure water. Linear fits are calculated for both sets of data with $R^2 \geq 0.9$ (sym) and 0.995 (asym) and slope m was calculated for each. (D) shows the ratio of slopes, m_{sym} to m_{asym}, was calculated for different sericin concentrations in water. Error bars represent SEM, n=3.

Presence of an additive to influence the H-bonding characteristics can thus be quantified by comparing the pattern of increase (or decrease) in peak intensities in OH stretching regions as shown in Fig. 3-2C. At lower temperature this variation in overall strength of H-bonding in water clusters can be represented by the slopes of the fitted trends (m_{sym} and m_{asym}). Figure 3-2D plots the ratio of m_1 and m_2 for different concentrations of sericin in water (0-5% w/v). Sericin in higher concentrations is shown to decrease the contribution of incomplete water clusters and increase the overall number of strongly H-bonded water clusters at lower temperatures (Fig 3-2D). In order to further investigate the thermodynamic effect of presence of sericin molecules in

51

water, a Van't Hoff analysis was performed (Fig. 3-3A). The change in enthalpy (Fig. 3-3B) and entropy (Fig. 3-3C) was used to quantify the change in the strength of H-bonded water clusters in aqueous solutions having varying concentrations of sericin.
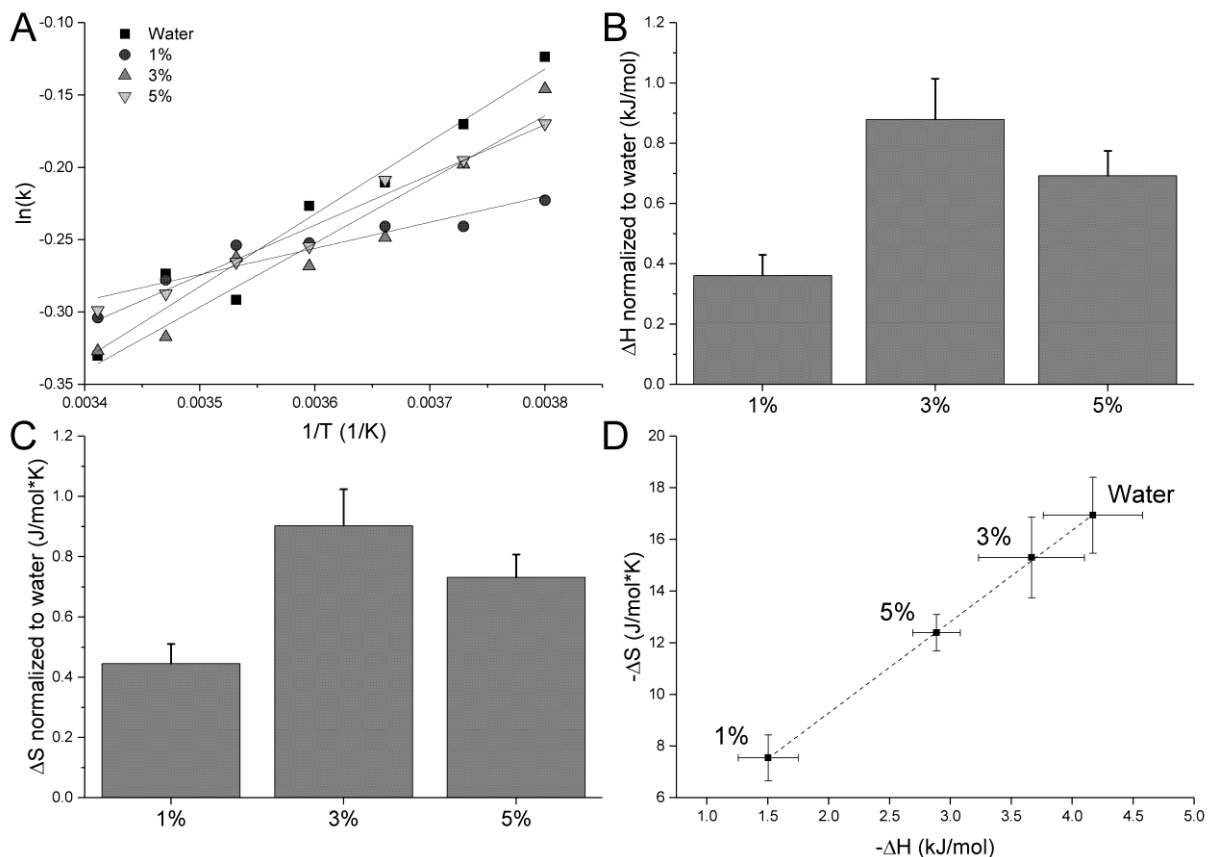
Figure 3-3 Raman microspectroscopic based thermodynamic analysis: (A) Van't Hoff plots for water-sericin solutions, k represents ratio between symmetric and asymmetric intensity of OH stretching region. (B) Change in the enthalpy of water-sericin binary solutions based on Van't Hoff plots, normalized to pure water. $p < 0.05$. (C) Change in the entropy of water-sericin binary solutions normalized to pure water. $p < 0.05$. (D) Linear fit of change in enthalpy against change in entropy for water-sericin binary solutions. Error bars indicate ±SEM, n=3.

Shift in the pattern of enthalpy change with temperature in presence of sericin can be attributed to alteration of H-bonded water clusters [33]. With the addition of 1% sericin, a 64% decrease in enthalpy related to H-bonding in aqueous solution was observed. However, such dramatic depression is not observed at higher concentrations. The entropy of the formation of H-bonds (ΔS) was calculated as a product of the y-intercept of the Van't Hoff plot and universal gas constant. When compared with the entropy of H-bond formation in comparison to water, a

similar trend in with the entropy values is observed (Fig. 3-3C). Fig. 3-3D indicates the isokinetic relationship obtained from the ratio of the entropy and enthalpy of the sericin solutions at different temperatures.

In addition to the spectral peak intensities in the OH stretching region, the shift in spectral wave number of the symmetric and asymmetric peaks were related to the energetics related with the in H-bonding characteristics [24,34]. Figure 3-4A and 3-4B indicate the peak-shift patterns related to symmetric and asymmetric peaks respectively at temperatures between $20^{\circ}C$ to $-10^{\circ}C$. Figures 3-4C and 3-4D highlight the difference in peak-shift characteristics at temperatures $20^{\circ}C$ and $-10^{\circ}C$ for both symmetric and asymmetric peaks. The solution containing 1% sericin presents a significantly different trend, indicating reduced peak-shift characteristics for both symmetric and asymmetric peaks. At higher temperatures the symmetric peaks shift towards lower wave numbers with increase in sericin concentration (Figure 3-4C). However, no such trend is observed for the asymmetric peak shift (Fig. 3-4D). At lower temperatures, addition of 1% sericin causes the symmetric peak to move towards higher wavenumbers, while with the increase in sericin concentration the trend is reversed. A similar trend is observed for the asymmetric peak at lower temperature indicating a unique trend in H-bonding strength at 1% sericin concentration.
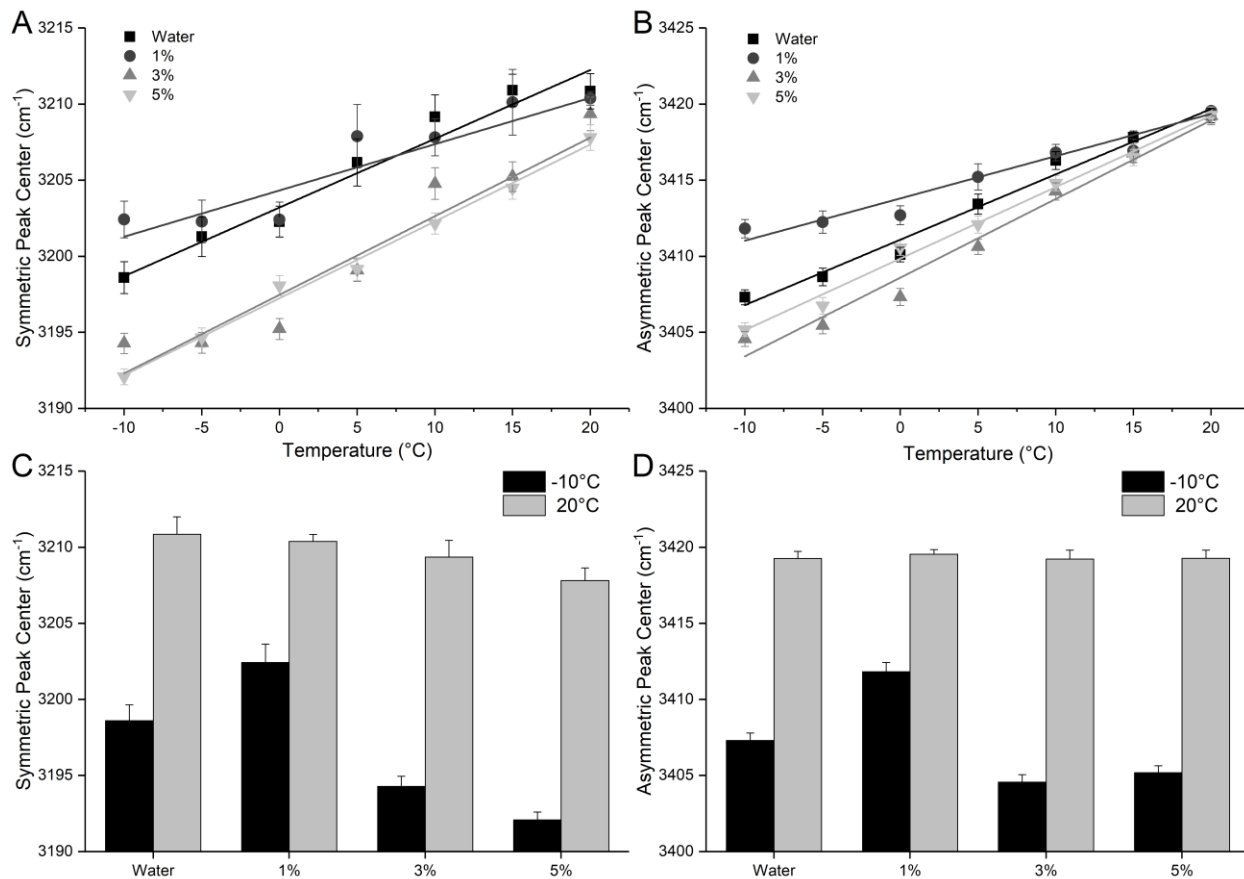
Figure 3-4 Peak center shift of OH stretching bands: (A) Symmetric peak center is plotted for water-sericin solutions at temperatures ranging from -10°C to 20°C. A noticeable difference in slope can be observed for the 1% sericin solution. (B) Asymmetric peak shift for the same solutions and temperatures as 3A. With the increase in temperature, the peak-center converges at wave number 3417 cm^{-1}. This indicates equal asymmetric H-bonding at higher temperature. (C) Symmetric peak center values for various water-sericin solutions at -10°C and 20°C. At low temperature, there are significant differences between the peak center values of the solutions. There is a slight trend towards lower frequency peak centers as sericin increases at higher temperature. (D) Asymmetric peak center values for water-sericin solutions. At low temperature, peak center shift follows a similar trend as the symmetric. At high temperature, there is no change between the peak center value. This shows sericin's ability to modulate hydrogen bonding (either stronger or weaker) as temperature is decreased toward freezing. Error bars indicate ±SEM, n=3.

When the peak-shift characteristics for both symmetric and asymmetric peaks are compared against each-other (n_1/n_2), there are no appreciable differences between any of the trends compared for any of the solutions including pure water (Figure 3-5A). When the slopes of the trend in peak shifts as observed in Figure 3-4A and 3-4B were normalized against the trend in peak shift exhibited by pure water, the peak shift characteristics of 1% sericin solution appear to be significantly different for both symmetric and asymmetric peaks (Figure 3-5B and 3-5C).
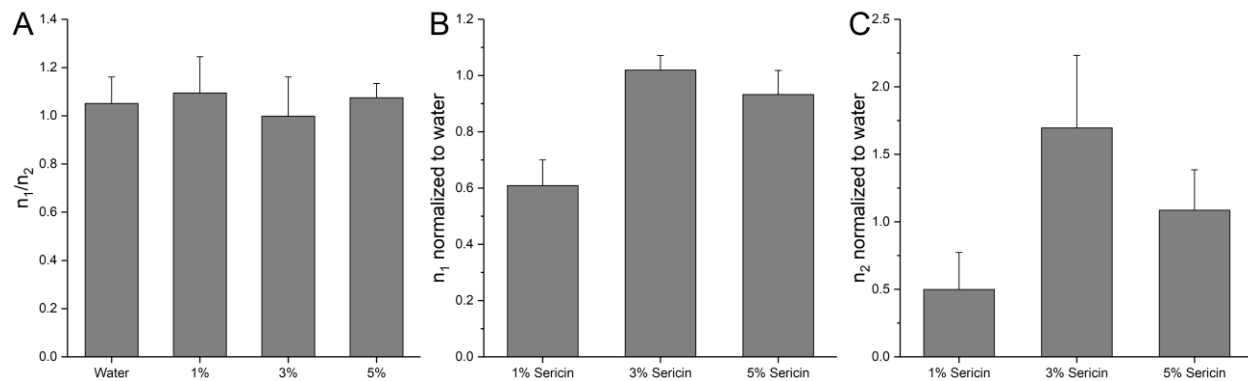
Figure 3-5 Raman OH stretching band shift hydrogen bonding analysis (A) The ratio of symmetric and asymmetric slopes for water-sericin solutions, n_1 and n_2, respectively. There is no statistically significant difference between the four solutions, indicating equal shift in both the symmetric and asymmetric peaks with respect to temperature for all solutions. (B) The ratio of sericin solution symmetric slope over pure water slope. The normalized slope is significantly lower for the 1% solution indicating less change in hydrogen bonding as temperature is decreased. $p < 0.05$. (C) Similar slope comparison as in (B), here for asymmetric slope. Significantly lower normalized slope for 1% sericin solution indicates reduced H-bonding at lower temperatures. Error bars indicate ±SEM, n=3.

3.3.2 DSC Studies

A comparative study was undertaken to evaluate thermodynamic responses of CPA formulations containing DMSO or sericin, and with or without trehalose using standard DSC techniques. Figure 3-6A indicates trends in freezing point depression in CPA formulations containing 100 mM trehalose in sericin and DMSO.

CPA solutions containing DMSO have significant freezing point depression as the concentration is increased. As expected, the DMSO solutions also containing 100 mM trehalose have stronger freezing point depression. Sericin also had a significant effect on freezing point depression with solutions containing 1% w/v sericin having the most profound change in freezing point depression while the depression plateaus with increasing concentrations. The addition of 100 mM trehalose to sericin based solutions leads to even further reduction in freezing point, indicating a potential synergistic effect of sericin and trehalose.
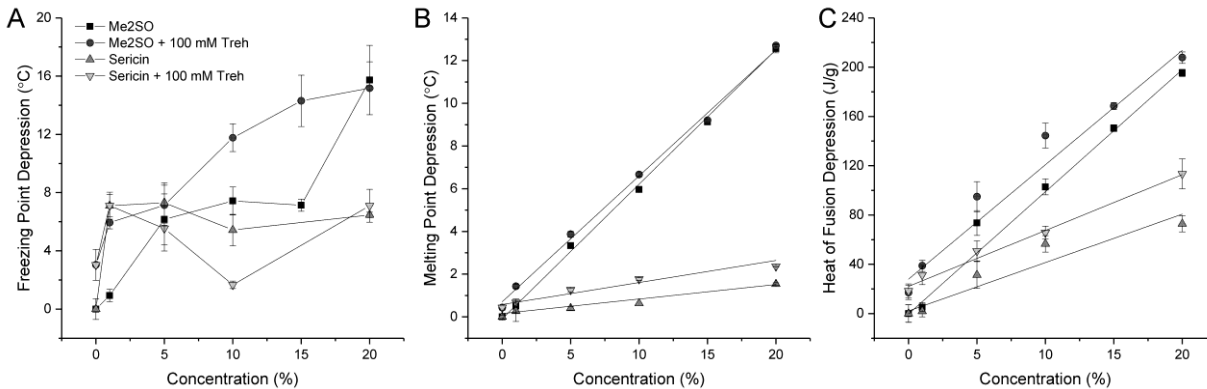
Figure-3-6 DSC analysis of individual CPA constituents: Thermodynamic parameters were acquired for solutions with varied CPA compositions. Solutions were created with concentrations of 0-20% of DMSO (v/v) or sericin (w/v) with or without the addition of 100 mM trehalose. (A) Freezing point depression had large immediate increases for all conditions, DMSO had more significant effects at the highest concentrations. (B) All solutions had increasing melting point depression with increased CPA concentration. (C) Heat of fusion depression had similar trends as melting point depression, but with DMSO and sericin solutions having closer m values. Error bars indicate ±SEM, n=3.

Figure 3-6B indicates the trends in melting point depression in CPA formulations. Unlike the freezing point, melting point depression followed a linear trend for all solutions tested. The DMSO solutions also containing 100 mM trehalose had a stronger effect on melting point depression at low concentrations of DMSO, but the trend disappears as the concentration of DMSO is increased. Sericin had significantly less effect on the melting point depression, however, the addition of 100 mM trehalose further reduced the melting point depression in these solutions.

The heat of fusion depression follows similar trends to melting point depression. DMSO solutions have a stronger effect on depressing the heat of fusion, although high sericin concentration solutions (10%-20%) also significantly decrease the heat of fusion. The addition of 100 mM trehalose has opposite effects on heat of fusion depression when added to DMSO and sericin, respectively. Addition of trehalose to DMSO solutions increased the heat of fusion depression across all concentrations, while it decreased the heat of fusion depression when added

56

to sericin solutions. This behavior indicates a different form of molecular interaction between DMSO-trehalose and sericin-trehalose.
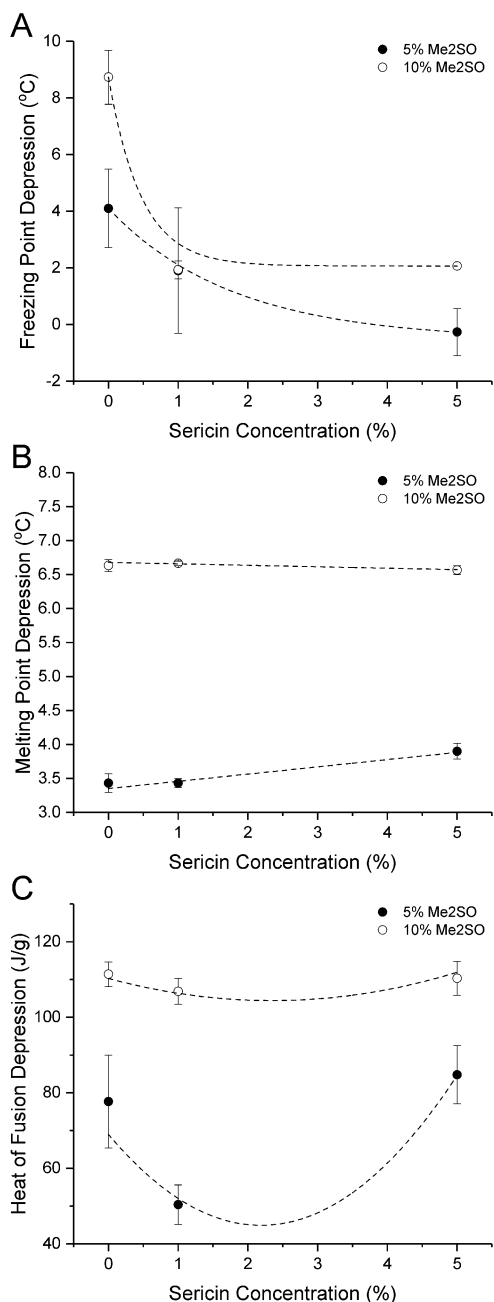
Figure 3-7 DSC analysis of CPA solutions: (A) CPA solutions are made with pure water and contain 100 mM trehalose, either 5% or 10% DMSO, various concentrations of sericin (0-5% w/v) Freezing point depression is plotted using an exponential decay function, which decreases with increasing sericin concentration (w/v). (B) Change in sericin concentration has small effect on the change in melting point. (C) A drop in heat of fusion depression at 1% sericin is highly pronounced with 5% DMSO. Error bars indicate ±SEM, n=3.

As a synergistic effect between trehalose and sericin was observed in DSC thermograms described above. CPA formulations containing DMSO (5% and 10%) with varying amounts of sericin and 100 mM trehalose were studies using DSC. When sericin concentration is increased from 1 – 5%, a significant increase in freezing point can be observed in CPA formulations containing both 5% and 10% DMSO (Figure 3-7A). Progressive addition of sericin results in marginal but linear increase in melting point for CPA formulations containing 10% DMSO, whereas in formulations containing 5% DMSO an opposite trend is observed (Figure 3-7B). Heat of fusion values in 5% DMSO based CPA formulations show a significant reduction initially with increase in sericin concentration. However, the trend is reversed on further addition of sericin. A similar trend with lower heat of fusion values is observed in CPA formulations containing 10% DMSO (Figure 3-7C).

Figure 3-8A indicates the post-thaw membrane integrity of the HepG2 cells cryo-processed using different CPA formulations. Membrane integrity for cells frozen in 5% and 10% DMSO were 46% and 73% respectively. The addition of trehalose to both 5% and 10% DMSO solutions resulted in increase in membrane integrity. The addition of 1% sericin to CPA solutions without trehalose resulted in an increase in a 20% increase membrane integrity with no additional gain in membrane integrity achieved by increasing the concentration of sericin. Adding 100 mM trehalose to CPA formulations containing 1% and 5% sericin in 10% DMSO resulted in a decrease of membrane integrity. The same trend is observed in CPA formulations containing 5% DMSO, with maximum loss of viability (25%) is observed in solutions containing both 5% sericin and 100 mM trehalose.

Figure 3-8B describes the post-thaw growth kinetics of HepG2 cells that were frozen in the most successful initial viability conditions. All solutions for the growth analysis contained

58

10% DMSO to ensure optimal survival and to emphasize the effect of the additives in the

solutions. 24 hours post-thaw, cell numbers of <50% of the initially counted viability were

observed. Growth then continued in an expected exponential growth pattern for all solutions. The

day 5 count begins to show a marginal separation between the cell growth from the solutions

frozen in DMSO alone and the solutions containing additives with the solution containing both

sericin and trehalose being the most effective. This trend becomes even more obvious on day 7.

The cells frozen in solutions containing additives show growth significantly higher than that of

the cells frozen in just DMSO.
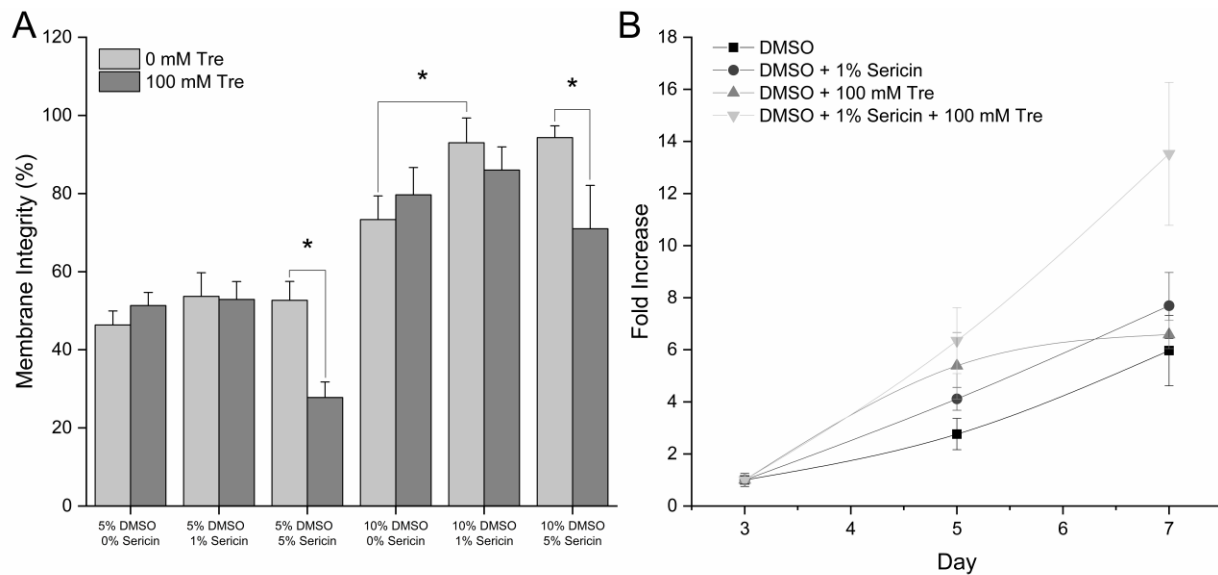
Figure 3-8 Health outcomes of mammalian cells for various CPAs A) Immediate membrane integrity for HepG2 cells after freezing for various CPA solutions with and without trehalose. Solutions containing 10% DMSO overall showed higher membrane integrity. Error bars show ±SEM, n=3. B) Growth outcomes of HepG2 cells after freezing for various CPA solutions. Counts were performed immediately post-thaw (day 0), 3 days, 5 days, and 7 days post-thaw. The solution containing both trehalose and sericin had optimal growth kinetics, while all solutions containing additives outperformed the solution containing only DMSO. Error bars show ±SEM n =4.

3.4 Discussion

Dimethyl sulfoxide (DMSO) is one of the most commonly used CPAs [4] even though

the use of DMSO at high concentrations have been frequently and closely associated with

cellular toxicity effects [5-7,35,36]. Use of additives that replaces or augments the cryoprotective

effect of DMSO have been explored as a viable strategy to reduce the need for higher concentration of DMSO in CPAs [37,38]. In this study we explored the effect of addition of sericin as an additive to DMSO and its impact on solution properties relevant to cryopreservation outcomes, including heat of fusion, freezing point, and H-bonding characteristics.

The role of H-bonding in modulating cryopreservation outcomes is well accepted [24,39,40], there have been very few studies that directly link the H-bonding characteristics with the contents of CPA formulations. While some molecular dynamic simulation studies have looked at the effect of presence of CPA components such as DMSO, ethylene glycol and glycerol on H-bonding [40,41], experimental verification of the ability of the CPA components to influence H-bonding with water molecules is lacking. In the present study, a combination of Raman microspectroscopy and DSC based analysis was undertaken to understand the ability of sericin to influence H-bonding characteristics.

A number of techniques, including Raman [42], NMR [43], X-ray [44], neutron diffraction [45], and femtosecond spectroscopy [46] have been used to study the effect of water molecules to understand associated physico-chemical effects. The Raman microspectroscopy technique used in this study is an excellent tool to characterize and quantify the effect of H-bonding at molecular level in an aqueous environment at low temperatures [13,23]. The technique was used to characterize and quantify the nature of the H-bonding network by following changes in constituent peak intensities in the OH stretching regions in the Raman spectra in presence of sericin at different temperatures (Figure 3-2). In pure water the number of symmetrically arranged water clusters having lower energy forms increases at lower temperatures causing a characteristic increase in intensity of the symmetric OH stretching peak (Figure 3-2B). The opposite trend is observed for asymmetric OH stretching peak representing

incomplete water clusters. This observation is consistent with the cluster flickering phenomena

described by Frank et al. [47] and can be quantified by comparing the rate of change of the

intensities of symmetric and asymmetric peaks (Figure 3-2C) [23,47]. It was found that presence

of sericin influences the ratio of the rate of change of the symmetric peak (m_{sym}) and rate of

change of asymmetric peak (m_{asym}). This effect was particularly noticeable at higher sericin

concentrations, decreasing the ratio significantly due to a decrease of incomplete water clusters

and increase in overall number of strongly H-bonded water clusters (Figure 3-2D). Presence of

DMSO in water-DMSO binary solutions is known to reduce the number of incomplete water

clusters at lower temperature in similar fashion [31]. Considering the relationship between the

number of symmetrically bonded water clusters and ice crystal formation [13], this indicates an

ability of sericin to modulate ice crystal formation. This is highly significant given the fact that

the number and size of ice crystal formation have been directly linked to post-thaw viability

outcomes in several studies [13,48] and indicates the possible role played by sericin as an

additive. At higher concentration of 5% sericin, there appears to be a significant increase in rate

of change in asymmetric peak intensity with temperature. In addition to the change in number of

H-bonded water clusters, the functional OH groups on sericin molecules may be a contributing

factor to the intensity variation in asymmetric peak intensity.

The effect of presence of sericin on formation of H-bonding in water clusters was

extended to quantify the thermodynamic relationships. Van't Hoff analysis was used to quantify

enthalpy of H-bond formation using the spectral data (Figure 3-3B). A similar approach was

employed by Dolenko et al. using Raman spectral data collected at different temperatures to

quantify the differences in energy of hydrogen bonding between alcohol−water solutions [31].

The results indicate that the sericin can influence both enthalpy and entropy of solution by

modulating H-bonding interactions with water. The strongest effects were observed at a sericin concentration of 1% w/v where a difference of over 60% was noticed compared to pure water. The significant reduction in enthalpy indicates weakened H-bonding while the decreased entropy indicates a more highly ordered H-bonding network in presence of 1% sericin (Figure 3-3B and 3-3C). However, with increase in sericin concentration, the trend is lost and possibly indicates an increase in incompletely formed water clusters. This is an important aspect that can be used to understand the critical parameters related to the extracellular environment at lower temperature in presence of sericin. While DMSO has a similar effect on enthalpy and H-bonding characteristics, studies indicate an absence of such trends with increasing concentrations[49,50]. The overall linear relationship between enthalpy and entropy in aqueous solutions of sericin (Figure 3-3D), despite significant depression of enthalpy at 1% w/v concentration, implies a strong trend of entropy-enthalpy compensation. This compensatory trend between entropy and enthalpy is a classic indicator of weak intermolecular interactions such as H-bonding [51,52]. he observed coordinated decrease in entropy and enthalpy at 1% sericin solution possibly indicates a decrease in entropy of activation which may indicate an increased steric hindrance. However, it is important to note that the degree of steric hindrance caused by the nature of the H-bonding network in presence of 1% sericin follow the overall reaction framework defined by the isokinetic line. Furthermore, in such an energetic framework, the reaction of forming a symmetric bond from asymmetric bond is significantly more favorable for 1% sericin solution in comparison with solutions containing higher concentration of sericin.

Along with the intensities, a shift in Raman peak positions in OH stretching region indicates the change in energy characteristics of associated water clusters [34]. A shift towards lower wavenumbers indicates lower energy transition while a shift towards higher wavenumber

is generally associated with transition to higher energy state. The dynamics related to change in the wavenumber of peak positions in the OH stretching region of liquid water is often connected to the reorganization of H-bonding in the local solvent network [53]. However, being a collective phenomenon, it is difficult to quantify the extent of reorganization in the local H-bonding network. Recent studies indicate a linear relationship between the change in wavenumbers of the peaks in OH stretching region and the charge and energy transfer through donor-acceptor water pairs in water-clusters. This linearity of a hydrogen bond can be related to the bond stretch frequency exhibited by its components. Increased hydrogen bonding strength shifts the OH stretching band toward lower wavenumbers [34]. This shift is noticeably observed during the formation of ice, when the spectra shifts from a broad OH peak to a sharp OH band at a much lower wavenumber [54]. Both the symmetric and asymmetric peaks were found to exhibit a shift towards low wavenumber as temperature decreases. The ratio of the shift with change in temperature remains approximately proportional for all solutions tested (Figure 3-5A). Interestingly, observed differences between solutions with varying concentrations of sericin only become significant at lower temperatures (Figure 3-4C and 3-4D). This possibly indicates that sericin actively reduces the energy associated with the H-bonded water clusters at lower temperatures. While further studies are required to fully understand the effect of such behavior, it can be said that the rate of energy shift associated with H-bonded structure is more prominent among the water clusters incompletely bound by H-bonding (Figure 3-4B). For solutions containing 1% sericin, the symmetric and asymmetric peak shifts to higher wavenumbers are significant compared to water, indicating an overall weakening in bonding strength at low temperatures. These results agree with the general trend observed in Van't Hoff analysis discussed above.

Spectroscopic studies were useful in developing an understanding of the fundamental effect of sericin on H-bonding in aqueous solutions. The thermodynamic parameters derived from DSC studies provide valuable insights to relate the concentrations and compositions of CPA solutions to post-thaw viability. During the slow cooling cryopreservation technique employed here, extracellular ice nucleation in supercooled condition is guided by the thermodynamic properties of the individual components of CPA formulation. A decrease in extracellular ice nucleation has been traditionally linked to the probability of incidence of generally lethal IIF in multiple studies [4,55,56]. Furthermore, increasing the concentrations of the non-permeating components of CPA formulations generally increase the tonicity of the extracellular solution and in turn causes the cell volume to decrease and intracellular osmolality to increase, which will also decrease the incidence of IIF [55]. This may be one of the contributing factors that can explain the increase in viability observed when certain additives are included in CPA formulation in addition to traditional permeating CPAs such as DMSO [18,19]. However, there is a possibility that additives such as trehalose and sericin may influence the thermodynamic properties of the extracellular solution in a unique way due to their synergistic interaction. When 100 mM trehalose is added to sericin solutions at different concentrations, a significant loss of freezing point depression trend is observed especially at the 10% w/v sericin concentration. (Figure 3-6A). A similar effect was observed when adding low concentrations of sericin (1-5% w/v) to DMSO based CPA solutions (Figure 3-7A). In addition to probabilistic decrease of IIF, such increase in freezing point may also prevent chilling injuries [57]. Sericin may also have a role to play in preventing re-crystallization injury. Studies with human oocytes indicate that post-thaw survival of cells can be maximized and incidence of IIF can be minimized by raising the freezing point close to the melting point of CPA formulation [56].

Sericin on its own has a minimal effect on melting point compared to DMSO. The addition of trehalose decreases the melting point even further, indicating the synergistic effects of trehalose and sericin (Figure 3-6B). However, this synergistic effect still has a lower impact compared to DMSO. This phenomenon is also observed by the minimal change to melting point caused by the addition of sericin to DMSO/trehalose-based CPA solutions (Figure 3-7B). Furthermore, the variation in heat of fusion value can be directly related to the difference in the nature of extracellular ice crystals formed [58]. Even though in a multi-component system, the concept of latent heat is complicated by the possible internal melting and freezing at microscale that can happen over a wide temperature range [59], a variation in heat of fusion will generally indicate a change in the overall quantity of the ice crystals formed [60]. As seen in Figure 3-6C, increasing the concentration of sericin in CPA formulation does not change the quantity of ice formation at the same freezing rate compared to DMSO. However, with an addition of 100 mM trehalose the heat of fusion increases indicating a significant change in the amount of the ice formation. This observation is supported by detailed Raman microspectroscopic study of the nature of the ice crystal formation in presence of 100 mM trehalose in DMSO solution by Solocinski et al. [13]. Addition of 100 mM trehalose in sericin solution has a similar effect and one can assume similar trends in ice crystal formation as in a DMSO solution containing 100 mM trehalose. This is another possible indication that trehalose and sericin can synergistically modulate ice formation in extracellular environments.

The membrane integrity of HepG2 cells cryopreserved using the CPA formulations described here indicate a higher viability of CPA formulations containing 10% DMSO (Figure 3-8). This observation is consistent with increased probability of intracellular damage due to formation of IIF when CPA formulations containing 5% DMSO as predicted by the calorimetry

65

studies. While the addition of 100 mM trehalose to 10% DMSO solution led to an increased membrane integrity in comparison to 10% DMSO solution, addition of 1% sericin (w/v) to 10% DMSO resulted in a considerable increase in membrane integrity. Effect of addition of 1% sericin to 10% DMSO solution was higher than the CPA formulations containing 100 mM trehalose to 10% DMSO solution. This indicates the superior nature of sericin as an additive. While the thermogravimetric studies indicate distinct synergistic advantages of using both trehalose and sericin as an additive in 10% DMSO solution, the membrane integrity data indicate a 5% decrease, possibility due to increased hyperosmotic exposure and solution effects injury [55,61]. The post-thaw growth study indicates that additives can enhance long-term viability and growth characteristics of HepG2 cells after freezing. By day 7, there was a significant difference between all of the additive-containing solutions and the solution containing just DMSO, indicating a quicker return to normal cell growth kinetics. Interestingly, the day 1 count indicated a >50% loss of cells from the initial post-thaw count for all conditions. We attribute these losses to late onset apoptosis and the semi-rigorous procedure for trypsinizing and counting cells 24 hours post-thaw. Further studies are underway to investigate the long-term impacts of the use of sericin as a CPA additive on cellular growth and health.

The study presented here provides important insight to how sericin impacts the H-bonding network and thermophysical properties of the CPA formulation during cryopreservation and provides a practical approach towards using sericin in CPA formulation as an additive to ameliorate post-thaw injuries in culture condition. While the prospect of using additives to reduce DMSO in CPAs is highly attractive, further research is required to optimize solution contents and determine what other additives can enhance preservation outcomes.

3.5 Bibliography

[1]   E. E. Benson, "Cryopreservation Theory," in *Plant Cryopreservation: A Practical Guide*, B. M. Reed, Ed. New York, NY: Springer New York, 2008, pp. 15–32.

[2]   Z. H. Chang and J. G. Baust, "Physical aging of glassy state: DSC study of vitrified glycerol systems," *Cryobiology*, vol. 28, no. 1, pp. 87–95, Feb. 1991, doi: 10.1016/0011-2240(91)90010-L.

[3]   B. C. Hancock, S. L. Shamblin, and G. Zografi, "Molecular Mobility of Amorphous Pharmaceutical Solids Below Their Glass Transition Temperatures," *Pharm. Res.*, vol. 12, no. 6, pp. 799–806, Jun. 1995, doi: 10.1023/A:1016292416526.

[4]   "Mazur P. Principles of cryobiology. InLife in the frozen state 2004 May 10 (pp. 29-92). CRC press.," .

[5]   "Effect of DMSO exposure without cryopreservation on hematopoietic progenitor cells. - Abstract - Europe PMC." https://europepmc.org/article/med/8504273 (accessed May 12, 2020).

[6]   G. M. Fahy, "The relevance of cryoprotectant 'toxicity' to cryobiology," *Cryobiology*, vol. 23, no. 1, pp. 1–13, Feb. 1986, doi: 10.1016/0011-2240(86)90013-1.

[7]   J. Galvao, B. Davis, M. Tilley, E. Normando, M. R. Duchen, and M. F. Cordeiro, "Unexpected low-dose toxicity of the universal solvent DMSO," *FASEB J.*, vol. 28, no. 3, pp. 1317–1330, Dec. 2013, doi: 10.1096/fj.13-235440.

[8]   "Molecular Basis for Dimethylsulfoxide (DMSO) Action on Lipid Membranes | Journal of the American Chemical Society." https://pubs.acs.org/doi/abs/10.1021/ja063363t (accessed May 12, 2020).

[9]   "Dimethyl Sulfoxide: An Effective Penetration Enhancer for Topical Administration of NSAIDs: The Physician and Sportsmedicine: Vol 39, No 3." https://www.tandfonline.com/doi/abs/10.3810/psm.2011.09.1923 (accessed May 12, 2020).

[10]   "DMSO triggers the generation of ROS leading to an increase in artemisinin and dihydroartemisinic acid in Artemisia annua shoot cultures | SpringerLink." https://link.springer.com/article/10.1007/s00299-009-0807-y (accessed May 12, 2020).

[11]   C. Yuan *et al.*, "Dimethyl Sulfoxide Damages Mitochondrial Integrity and Membrane Potential in Cultured Astrocytes," *PLoS ONE*, vol. 9, no. 9, Sep. 2014, doi: 10.1371/journal.pone.0107447.

[12]   "DMSO induces drastic changes in human cellular processes and epigenetic landscape in vitro | Scientific Reports." https://www.nature.com/articles/s41598-019-40660-0 (accessed May 12, 2020).

[13]   J. Solocinski, Q. Osgood, M. Wang, A. Connolly, M. A. Menze, and N. Chakraborty, "Effect of trehalose as an additive to dimethyl sulfoxide solutions on ice formation, cellular viability, and metabolism," *Cryobiology*, vol. 75, pp. 134–143, Apr. 2017, doi: 10.1016/j.cryobiol.2017.01.001.

[14]   Y.-Q. Zhang, "Applications of natural silk protein sericin in biomaterials," *Biotechnol. Adv.*, vol. 20, no. 2, pp. 91–100, May 2002, doi: 10.1016/S0734-9750(02)00003-4.

[15]   R. Dash, C. Acharya, P. C. Bindu, and S. C. Kundu, "Antioxidant potential of silk protein sericin against hydrogen peroxide-induced oxidative stress in skin fibroblasts," *BMB Rep.*, vol. 41, no. 3, pp. 236–241, Mar. 2008, doi: 10.5483/BMBRep.2008.41.3.236.

[16]   "Supplemental Silk Protein, Sericin, Suppresses Colon Tumorigenesis in 1,2-Dimethylhydrazine-Treated Mice by Reducing Oxidative Stress and Cell Proliferation: Bioscience, Biotechnology, and Biochemistry: Vol 65, No 10." https://www.tandfonline.com/doi/abs/10.1271/bbb.65.2181 (accessed May 12, 2020).

[17]   Y. Miyamoto *et al.*, "Cryopreservation of Human Adipose Tissue-Derived Stem/Progenitor Cells Using the Silk Protein Sericin," *Cell Transplant.*, vol. 21, no. 2–3, pp. 617–622, Mar. 2012, doi: 10.3727/096368911X605556.

[18]   M. Sasaki, Y. Kato, H. Yamada, and S. Terada, "Development of a novel serum-free freezing medium for mammalian cells using the silk protein sericin," *Biotechnol. Appl. Biochem.*, vol. 42, no. 2, pp. 183–188, 2005, doi: 10.1042/BA20050019.

[19]   "Cryopreservation of Adipose-Derived Mesenchymal Stem Cells - Chika Miyagi-Shiohira, Kiyoto Kurima, Naoya Kobayashi, Issei Saitoh, Masami Watanabe, Yasufumi Noguchi, Masayuki Matsushita, Hirofumi Noguchi, 2015." https://journals.sagepub.com/doi/full/10.3727/215517915X689100 (accessed May 12, 2020).

[20]   "Potential applications of silk sericin, a natural protein from textile industry by-products - Pornanong Aramwit, Tippawan Siritientong, Teerapol Srichana, 2012." https://journals.sagepub.com/doi/abs/10.1177/0734242X11404733 (accessed May 12, 2020).

[21]   J. Meneghel, P. Kilbride, J. G. Morris, and F. Fonseca, "Physical events occurring during the cryopreservation of immortalized human T cells," *PLOS ONE*, vol. 14, no. 5, p. e0217304, May 2019, doi: 10.1371/journal.pone.0217304.

[22]   R. Wang, C. Pellerin, and O. Lebel, "Role of hydrogen bonding in the formation of glasses by small molecules: a triazine case study," *J. Mater. Chem.*, vol. 19, no. 18, pp. 2747–2753, Apr. 2009, doi: 10.1039/B820294J.

[23]   Q. Sun, "The Raman OH stretching bands of liquid water," *Vib. Spectrosc.*, vol. 51, no. 2, pp. 213–217, Nov. 2009, doi: 10.1016/j.vibspec.2009.05.002.

[24]   J. L. Dashnau, N. V. Nucci, K. A. Sharp, and J. M. Vanderkooi, "Hydrogen Bonding and the Cryoprotective Properties of Glycerol/Water Mixtures," *J. Phys. Chem. B*, vol. 110, no. 27, pp. 13670–13677, Jul. 2006, doi: 10.1021/jp0618680.

[25]   "Fourier transforms in the computation of self-deconvoluted and first-order derivative spectra of overlapped band contours | Analytical Chemistry." https://pubs.acs.org/doi/abs/10.1021/ac00232a034 (accessed May 12, 2020).

[26]   M. Starzak and M. Mathlouthi, "Cluster composition of liquid water derived from laser-Raman spectra and molecular simulation data," *Food Chem.*, vol. 82, no. 1, pp. 3–22, Jul. 2003, doi: 10.1016/S0308-8146(02)00584-8.

[27]   Q. Sun, "Local statistical interpretation for water structure," *Chem. Phys. Lett.*, vol. 568–569, pp. 90–94, May 2013, doi: 10.1016/j.cplett.2013.03.065.

[28]   "Tetrahedral Ordering in Water: Raman Profiles and Their Temperature Dependence | The Journal of Physical Chemistry A." https://pubs.acs.org/doi/abs/10.1021/jp9052083 (accessed May 12, 2020).

[29]   J. D. Smith, C. D. Cappa, K. R. Wilson, R. C. Cohen, P. L. Geissler, and R. J. Saykally, "Unified description of temperature-dependent hydrogen-bond rearrangements in liquid water," *Proc. Natl. Acad. Sci.*, vol. 102, no. 40, pp. 14171–14174, Oct. 2005, doi: 10.1073/pnas.0506899102.

[30]   D. M. Carey and G. M. Korenowski, "Measurement of the Raman spectrum of liquid water," *J. Chem. Phys.*, vol. 108, no. 7, pp. 2669–2675, Feb. 1998, doi: 10.1063/1.475659.

[31]   T. A. Dolenko *et al.*, "Raman Spectroscopy of Water–Ethanol Solutions: The Estimation of Hydrogen Bonding Energy and the Appearance of Clathrate-like Structures in Solutions," *J. Phys. Chem. A*, vol. 119, no. 44, pp. 10806–10815, Nov. 2015, doi: 10.1021/acs.jpca.5b06678.

[32]   E37 Committee, "Practice for Heat Flow Calibration of Differential Scanning Calorimeters," ASTM International. doi: 10.1520/E0968-02R14.

[33]   L. Zhao, K. Ma, and Z. Yang, "Changes of Water Hydrogen Bond Network with Different Externalities," *Int. J. Mol. Sci.*, vol. 16, no. 4, pp. 8454–8489, Apr. 2015, doi: 10.3390/ijms16048454.

[34]   K. M. Hunter, F. A. Shakib, and F. Paesani, "Disentangling Coupling Effects in the Infrared Spectra of Liquid Water," preprint, Oct. 2018. doi: 10.26434/chemrxiv.7189562.v1.

[35]   "The viability of cryopreserved PBPC depends on the DMSO concentration and the concentration of nucleated cells in the graft: Cytotherapy: Vol 7, No 4." https://www.tandfonline.com/doi/abs/10.1080/14653240500238251 (accessed May 22, 2020).

[36]   T. Suzuki, H. Komada, R. Takai, K. Arii, and T. T. Kozima, "Relation between Toxicity of Cryoprotectant DMSO and Its Concentration in Several Fish Embryos," *Fish Sci*, vol. 61, pp. 193–197, Jan. 1995, doi: 10.2331/fishsci.61.193.

[37]   J. M. Baust, R. Van Buskirk, and J. G. Baust, "Modulation of the cryopreservation cap: elevated survival with reduced dimethyl sulfoxide concentration," *Cryobiology*, vol. 45, no. 2, pp. 97–108, Oct. 2002, doi: 10.1016/S0011-2240(02)00100-1.

[38]   L. M. Currie, S. A. Livesey, J. R. Harper, and J. Connor, "Cryopreservation of single-donor platelets with a reduced dimethyl sulfoxide concentration by the addition of second-messenger effectors: enhanced retention of in vitro functional activity," *Transfusion (Paris)*, vol. 38, no. 2, pp. 160–167, 1998, doi: 10.1046/j.1537-2995.1998.38298193098.x.

[39]   F. Franks, "Solute—Water interactions: Do polyhydroxy compounds alter the properties of water?," *Cryobiology*, vol. 20, no. 3, pp. 335–345, Jun. 1983, doi: 10.1016/0011-2240(83)90022-6.

[40]   L. Weng, C. Chen, J. Zuo, and W. Li, "Molecular Dynamics Study of Effects of Temperature and Concentration on Hydrogen-Bond Abilities of Ethylene Glycol and Glycerol: Implications for Cryopreservation," *J. Phys. Chem. A*, vol. 115, no. 18, pp. 4729–4737, May 2011, doi: 10.1021/jp111162w.

[41]   A. Luzar and D. Chandler, "Structure and hydrogen bond dynamics of water–dimethyl sulfoxide mixtures by computer simulations," *J. Chem. Phys.*, vol. 98, no. 10, pp. 8160–8173, May 1993, doi: 10.1063/1.464521.

[42]   L. Zhou, T. P. Mernagh, and C. Le Losq, "Observation of the Chemical Structure of Water up to the Critical Point by Raman Spectroscopic Analysis of Fluid Inclusions," *J. Phys. Chem. B*, vol. 123, no. 27, pp. 5841–5847, Jul. 2019, doi: 10.1021/acs.jpcb.9b02129.

[43]   J. Rönnols, O. Engström, U. Schnupf, E. Säwén, J. W. Brady, and G. Widmalm, "Inter-residual Hydrogen Bonding in Carbohydrates Unraveled by NMR Spectroscopy and Molecular Dynamics Simulations," *ChemBioChem*, vol. 20, no. 19, pp. 2519–2528, Oct. 2019, doi: 10.1002/cbic.201900301.

[44]   J. Niskanen *et al.*, "Compatibility of quantitative X-ray spectroscopy with continuous distribution models of water at ambient conditions," *Proc. Natl. Acad. Sci.*, vol. 116, no. 10, pp. 4058–4063, Mar. 2019, doi: 10.1073/pnas.1815701116.

[45]   A. K. Soper and A. Luzar, "A neutron diffraction study of dimethyl sulphoxide–water mixtures," *J. Chem. Phys.*, vol. 97, no. 2, pp. 1320–1331, Jul. 1992, doi: 10.1063/1.463259.

[46]   S. Woutersen, U. Emmerichs, and H. J. Bakker, "Femtosecond Mid-IR Pump-Probe Spectroscopy of Liquid Water: Evidence for a Two-Component Structure," *Science*, vol. 278, no. 5338, pp. 658–660, Oct. 1997, doi: 10.1126/science.278.5338.658.

[47]   H. S. Frank and W.-Y. Wen, "Ion-solvent interaction. Structural aspects of ion-solvent interaction in aqueous solutions: a suggested picture of water structure," *Discuss. Faraday Soc.*, vol. 24, no. 0, pp. 133–140, Jan. 1957, doi: 10.1039/DF9572400133.

[48]   C. J. Capicciotti, J. S. Poisson, C. N. Boddy, and R. N. Ben, "Modulation of antifreeze activity and the effect upon post-thaw HepG2 cell viability after cryopreservation," *Cryobiology*, vol. 70, no. 2, pp. 79–89, Apr. 2015, doi: 10.1016/j.cryobiol.2015.01.002.

[49]   T. Matsui, L. G. Hepler, and D. V. Fenby, "Thermodynamic investigation of complex formation by hydrogen bonding in binary liquid systems. Chloroform with triethylamine, dimethyl sulfoxide, and acetone," May 01, 2002. https://pubs.acs.org/doi/pdf/10.1021/j100639a006 (accessed Jun. 08, 2020).

[50]   C. V. Krishnan and H. L. Friedman, "Solvation enthalpies of various nonelectrolytes in water, propylene carbonate, and dimethyl sulfoxide," May 01, 2002. https://pubs.acs.org/doi/pdf/10.1021/j100725a066 (accessed Jun. 08, 2020).

[51]   J. D. Dunitz, "Win some, lose some: enthalpy-entropy compensation in weak intermolecular interactions," *Chem. Biol.*, vol. 2, no. 11, pp. 709–712, Nov. 1995, doi: 10.1016/1074-5521(95)90097-7.

[52]   J. E. LEFFLER, "THE ENTHALPY-ENTROPY RELATIONSHIP AND ITS IMPLICATIONS FOR ORGANIC CHEMISTRY," *J. Org. Chem.*, vol. 20, no. 9, pp. 1202–1231, Sep. 1955, doi: 10.1021/jo01126a009.

[53]   D. Ojha, A. Henao, and T. D. Kühne, "Nuclear Quantum Effects on the Vibrational Dynamics of Liquid Water," *J. Chem. Phys.*, vol. 148, no. 10, p. 102328, Mar. 2018, doi: 10.1063/1.5005500.

[54]   T. C. Sivakumar, S. A. Rice, and M. G. Sceats, "Raman spectroscopic studies of the OH stretching region of low density amorphous solid water and of polycrystalline ice Ih," *J. Chem. Phys.*, vol. 69, no. 8, pp. 3468–3476, Oct. 1978, doi: 10.1063/1.437079.

[55]   K. Muldrew, J. P. Acker, J. A. W. Elliott, and and L. E. McGann, "The Water to Ice Transition: Implications for Living Cells," *Life in the Frozen State*, May 10, 2004. https://www.taylorfrancis.com/ (accessed Jun. 08, 2020).

[56]   F. S. Trad, M. Toner, and J. D. Biggers, "Effects of cryoprotectants and ice-seeding temperature on intracellular freezing and survival of human oocytes," *Hum. Reprod.*, vol. 14, no. 6, pp. 1569–1577, Jun. 1999, doi: 10.1093/humrep/14.6.1569.

[57]   J. J. Lemasters and C. Oliver, *Cell Biology of Trauma*. CRC Press, 1995.

[58]   P. M. Mehl, "Nucleation and Crystal Growth in a Vitrification Solution Tested for Organ Cryopreservation by Vitrification," *Cryobiology*, vol. 30, no. 5, pp. 509–518, Oct. 1993, doi: 10.1006/cryo.1993.1051.

[59]   G. A. Maykut and N. Untersteiner, "Some results from a time-dependent thermodynamic model of sea ice," *J. Geophys. Res. 1896-1977*, vol. 76, no. 6, pp. 1550–1575, 1971, doi: 10.1029/JC076i006p01550.

[60]   A. A. Flores and H. D. Goff, "Ice Crystal Size Distributions in Dynamically Frozen Model Solutions and Ice Cream as Affected by Stabilizers," *J. Dairy Sci.*, vol. 82, no. 7, pp. 1399–1407, Jul. 1999, doi: 10.3168/jds.S0022-0302(99)75366-X.

[61]   H. T. Meryman, R. J. Williams, and M. St. J. Douglas, "Freezing injury from 'solution effects' and its prevention by natural or artificial cryoprotection," *Cryobiology*, vol. 14, no. 3, pp. 287–302, Jun. 1977, doi: 10.1016/0011-2240(77)90177-8.

Chapter 4 Optimization and Cellular Evaluation of Cryopreservable Hydrogel

4.1 Introduction

The cells that make up tissues and organs in our bodies function and interact in a three-dimensional (3D) environment. However even today, most cells are cultured virtually in two dimensions (2D). Forcing cells to adapt to an in vitro 2D extracellular matrix (ECM) can cause changes to the metabolism and typical functionality. In a research scenario, these changes manifest as results that do not properly model the parallel in vivo system [1], [2]. Major phenotypic differences in cell survival, differentiation, signaling, and migration have been illuminated when comparing cells in different geometric environments [3], [4]. Clearly, there is a need for more biologically relevant and controllable 3D cell culture systems where cells can grow, differentiate, and function similarly to how they would in a physiological system.

An example of the potential of in vitro 3D cell culture systems is in drug discovery and testing. A study shows that only 12% of drugs which make it to clinical trials are approved for use in humans [5]. This statistic indicates the need for more reliable cell and tissue models that can reveal a drugs lack of efficacy in biologically relevant systems to improve the failure rate of clinical trials. In addition, appropriate cell models would reduce the application of animal testing, especially for toxicity studies that have a high risk of being harmful [6], [7]. In fact, Atkins et. al. show that animal models are actually poor predictors of human toxicity in phase I oncology trials [8]. So, by developing improved 3D cancer cell models which are directly cultured from patients,

we can better predict the clinical outcome of treatments such as chemotherapy without the use of animal testing [9].

Nearly all cells that make up tissue are surrounded and attached to an extracellular matrix (ECM). The ECM is made up of some 300 different proteins. Some of the major components include collagens, proteoglycans, elastin, and cell-binding glycoproteins, each with distinct physical and biochemical properties and functions [10]. There are several materials that have demonstrated applicability to provide a pseudo-ECM that can mimic several mechanical and biological properties. Polymer hydrogels are similar in structure to mammalian ECM [11] and are commonly used for cell entrapment which involves suspending the cells in a gel precursor and then initiating the gelation process either covalently or ionically [12]. Some examples of synthetic polymers that can form hydrogels are polyethylene glycol (PEG) [13], poly(hydroxyethyl methacrylate) (polyHEMA) [14], Polyvinyl Alcohol (PVA) [15], and polycaprolactone (PCL) [16]. Natural polymers (and polymeric proteins) able to form hydrogels are alginate [17], chitosan [18], hyaluronan [19], dextran [20], collagen [21], and fibrin [22].

There are many factors to consider when selecting a material for hydrogel cell encapsulation. Synthetic polymers possess more reproducible mechanical and physical properties than natural polymers, however, many are avoided due to harsh cross-linking conditions [23]. With that being said, some synthetic polymers, such as PEG-acrylates [24], have been proven suitable for cell based hydrogel formation. Natural polymers of animal origin have strong biocompatibility, although using these results in a loss of experimental control due to high batch to batch variability. In addition, there are immunological and xenogeneic exposure concerns with these materials, especially in a clinical setting [25].

Non-animal origin nature polymers have less harsh gelation properties, while still maintaining strong biocompatibility. Alginate hydrogels have proven highly applicable for cell encapsulation due to its ability to crosslink in physiological conditions. Other properties that make alginate hydrogels desirable are gentle dissolution for cell retrieval, a pore network that allows the diffusion of nutrient and waste products, relative inertness, and easy manipulation of mechanical properties. Since alginate was first used to encapsulate pancreatic islets in 1980 [26], it has been heavily characterized for 3D cell culture of a multitude of cellular systems [27]–[31]. Clinical translation of novel 3D cell encapsulation-based technologies requires the development of efficient preservation techniques that allow long-term storage and acceptable viability/functionality post-preservation. Cryopreservation is the best option for long-term storage of cellular material and has been extensively used for banking of cell lines. However, there is a minimal amount of research regarding cryopreservation of hydrogel encapsulated cells. Pradvyuk et. al. compared the efficacy of different cooling techniques on alginate encapsulated mesenchymal stem cells (MSCs) and found that the MSCs slow cooled with controlled ice nucleation were able to achieve multilineage differentiation following thawing [32]. Another group compared conventional freezing and vitrification of myoblast cells encapsulated in RGD-alginate hydrogels and concluded that conventional freezing was ideal due to simplicity of procedure and slightly superior post-thaw outcome [33]. Malpique et. al. determined using alginate encapsulation to cryopreserve neurospheres resulted in reduced recovery time and fragmentation post-thaw [34]. These studies confirm the efficacy of alginate encapsulated for cryopreservation, however, to the best of our knowledge no one has optimized the specific procedure and cryoprotective formulations used for alginate encapsulated cryopreservation.

In this study, a metabolic assay is used to assess and optimize each step of the slow-cooling cryopreservation process of alginate encapsulated hepatocytes. Following process optimization, several post-thaw metabolic comparisons were performed to determine the optimal cryoprotective solution the hydrogels are frozen in. The results indicate incubating the cells for 24 hours after encapsulation is the most significant step to improve post-thaw viability. In addition, solute injury appears to play a more significant role for encapsulated cryopreservation. This was indicated by a reduction in post-thaw metabolism of cells preserved in solutions containing additional additives that are typically used to improve cell suspension preservation. The optimal CPA formula was subsequently adjusted considering these findings.

Following optimization studies, viability, growth, and metabolic studies were performed on cryopreserved hydrogels containing three cell types of different tissue origin – HepG2, Neuro 2A, and RAW 264.7 cells. Because the optimization studies were performed using HepG2 cells, it is not surprising that these cells displayed the highest initial survivability (68%), followed by Neuro 2A cells (46%), and RAW cells (31%). In addition, each cell type displayed different growth and metabolic characteristics following thawing. These results suggest the suggested cryopreservation protocol and CPA formulation is acceptable for a multitude of cell types; however, to maximize post-thaw application, each cell type would require its own ECM, cryopreservation protocol, and CPA optimization study. This research is a good starting point for the creation of novel cryopreservation protocols of hydrogel encapsulated cells and other 3D pseudo-ECM applications.

4.2 Materials and Methods

4.2.1 Cell Culture

Human hepatocellular carcinoma (HepG2), mouse neuroblastoma (Neuro 2A), and mouse macrophage (RAW 264.7) cells were obtained from the American Type Culture Collection (Manassas, VA) and grown in 25 cm^2 culture flasks (Corning Inc. Corning, NY). HepG2 cells were cultured in Opti-MEM (Gibco) culture media supplemented with 5% fetal bovine serum (FBS) (Gibco) and penicillin-streptomycin to yield final 100 units/mL penicillin G and 100 µg/mL streptomycin sulfate (Hyclone-Thermo Scientific, Logan, UT). Neuro 2A and RAW 264.7 cells were cultured in Dulbecco's Modified Eagle Medium (DMEM) supplemented with 10% FBS and penicillin-streptomycin (same concentration as Opti-MEM). All cells were incubated in an atmosphere of 5% CO_2 and 95% air.

4.2.2 Alginate Preparation and Cryopreservation

Sodium alginate powder was procured from Sigma Aldrich (St. Louis, MO). Alginate powder was dissolved in deionized and distilled 18 MΩ water (Gibco) to reach desired concentration. The cells were detached and collected from culture flasks using trypsinization followed by centrifugation and resuspension in growth media. Typical experimentation used an initial alginate concentration of 2.5% (w/w) and was mixed 4:1 concentration with the cell solution. The final concentration of alginate in pre-gel solution becomes 2% (w/w) and the concentration of cells used targeted $1x10^5$ cells per hydrogel. 100 µL of pre-gel solution was pipetted into each well of a 96-well plate, followed by 200 µL of a 100 mM calcium chloride ($CaCl_2$) solution. The plate was then placed inside of cell incubator for 1 hour for the alginate hydrogels to form. Afterward, hydrogels are removed from wells and undergo several wash

cycles in phosphate buffered saline to remove excess $CaCl_2$ solution. Several hydrogels are then placed in each 20 mm culture dish containing appropriate cell culture medium.

Before cryopreservation, hydrogels are typically allowed to equilibrate in culture for 24 hours. The cryopreservation protocol begins with removing 3 hydrogels from culture and immediately placing in the cryovial containing cryopreservation solution (CPA). A passive freezing container that can hold up to 12 cryovials and capable of controlling the cooling rate at 1°C/min (Cool Cell LX, 137 Biocision, Menlo Park, CA) was used to store samples at cryogenic temperatures. Hydrogels were stored at -80°C for a minimum of 24 hours. The thawing procedure consists of quickly thawing each cryovial in a 37°C water bath until both the CPA and hydrogels are completely unfrozen. The hydrogels are removed from the cryovial and immediately washed in culture media several times to remove lingering CPA that could be toxic to the cells. The gels are then moved into culture dishes with media and placed in incubator until further processing is necessary. Figure 4-1 provides a general schematic for the formation and preservation of HepG2 encapsulated hydrogels.
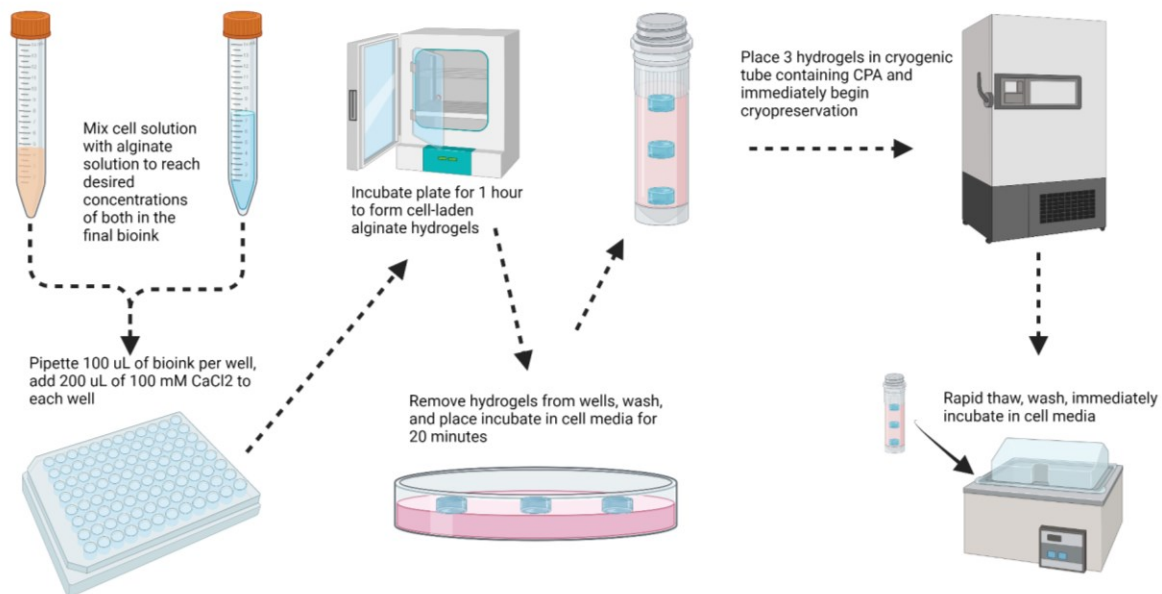
Figure 4-1 Visual schematic of cell encapsulated hydrogels and their subsequent cryopreservation

4.2.3 Resazurin Based Metabolic Assay

The metabolic activity of the cells in each hydrogel was directly assessed using a resazurin-based in vitro toxicology assay kit (TOX8, Sigma Aldrich). Each hydrogel was placed into a well of a 48-well plate containing 300 µL of solution that was 90% PBS and 10% resazurin solution (v/v). After incubation for a specified time, hydrogels are stirred in well and resazurin solution is collected. Two end point absorbance readings are collected at 600 nm and 690 nm for each sample. Final Absorbance = Absorbance (600 nm)-Absorbance (690 nm).

4.2.4 Dissolution of Alginate Hydrogels and Cell Quantification

Cell-laden alginate hydrogels were incubated for 30 minutes in 50 mM sodium citrate solution to dissolve gelled alginate. Post-dissolution, 5 mL of cell culture medium was added cell-containing solution to reduce viscosity and chelator concentration. The solution is then centrifuged and removed, followed by resuspension of the cells in growth media. Cell numbers were then quantified using hemacytometer (Hausser Scientific, Horsham, PA) counts and membrane integrity was assessed using trypan blue exclusion.

4.2.5 Fluorescence Based Assessment of Viability and Growth

Cells were identified inside of post-cryopreserved hydrogels using the nucleic acid stain SYTO13 (ThermoFisher Scientific, Waltham MA). Dead cells were identified using Ethidium Bromide (EtBr) dye. A SYTO-EtBr stain was formed using final concentrations of 125 µM SYTO13 and 250 µM EtBr. Hydrogels were incubated in a solution containing 10% stain and 90% PBS for 20 minutes. Gels were then washed several times in PBS to diffuse out as much of the remaining stain as possible. Fluorescence images were collected with an IX73 microscope (Olympus Corp, Tokyo, Japan) containing a custom band filter with FITC/DAPI (Semrock, West

Henrietta NY), and a QImaging (BC, Canada) microscope camera. Analysis of fluorescent images was performed using ImageJ particle analysis tool. A chemical and spectroscopic schematic are visualized in figure 4-2.
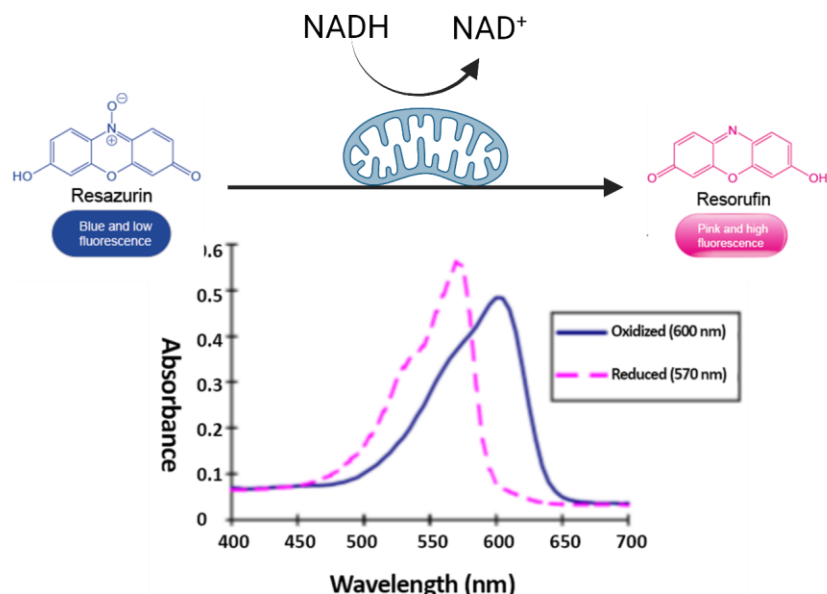
Figure 4-2 Resazurin Schematic: Chemical reaction responsible for the reduction of the resazurin molecule. Absorbance peaks shift to lower wavelength with the molecule's reduction to resorufin.

4.3 Results and Discussion - Optimization of Cryopreservation for HepG2 Encapsulated Alginate Hydrogels

4.3.1 Alginate Precursor Formulation

The optimization of alginate hydrogel cryopreservation can be broken down into three major objectives: Bio-ink optimization, protocol optimization, and CPA optimization with the latter two objectives being of primary focus. Figure 4-3 compares the recovered metabolic activity of HepG2 cells encapsulated in different alginate concentrations (1, 2, and 3% w/v).
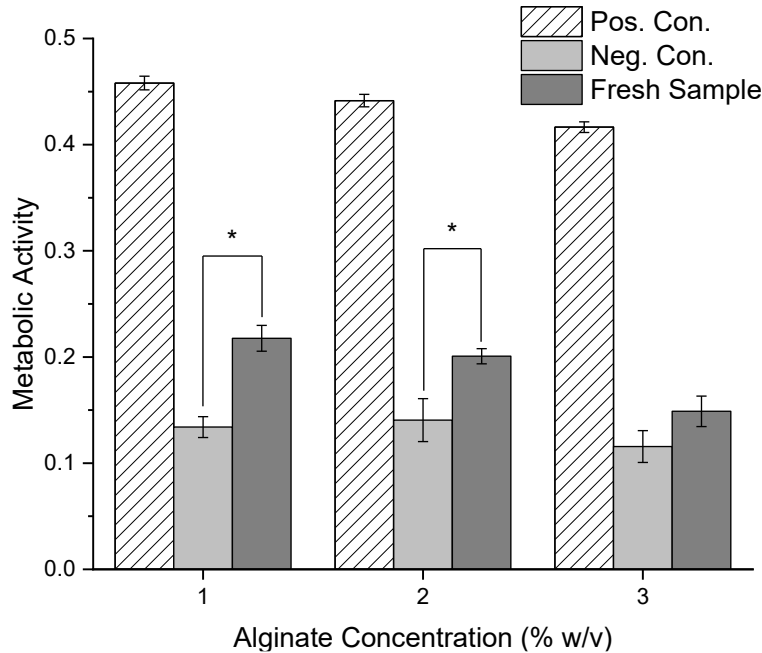
Figure 4-3 Post-Thaw Metabolic Activity of Alginate Formulations: Alginate hydrogels contain sodium alginate concentration between 1-3%. The cryopreserved samples are compared to non-frozen cells (positive control) and cryopreserved hydrogels without cells (negative control). Error bars represent ±SEM, n = 3.

Under standard conditions (positive control), all three concentrations of hydrogel promote high viability and metabolic activity, but lower alginate concentrations are moderately superior. Similarly, the 1% and 2% alginate concentrations resulted in significantly higher metabolic activity post-cryopreservation compared to the negative controls. Again, the lowest concentration appears to have moderately stronger metabolic activity, although there are degradation and workability concerns at this lower concentration. For these reasons, further studies were performed using 2% alginate hydrogels.

4.3.2 Protocol Optimization

Further optimization was performed to the cryopreservation protocol itself. The slow-cooling protocol for alginate hydrogel cryopreservation is similar to that of standard cellular suspension freezing with some other considerations due to the 3D encapsulation structure. If the hydrogels are not exposed to CPA diffusion for an ample period to reach the inner encapsulation

structure, the cells experience intracellular ice formation (IIF) injury. In addition, there are cytotoxic injuries at longer CPA exposure times [35], [36]. Therefore, it is important to determine whether CPA incubation is required or detrimental protocol for the cells.
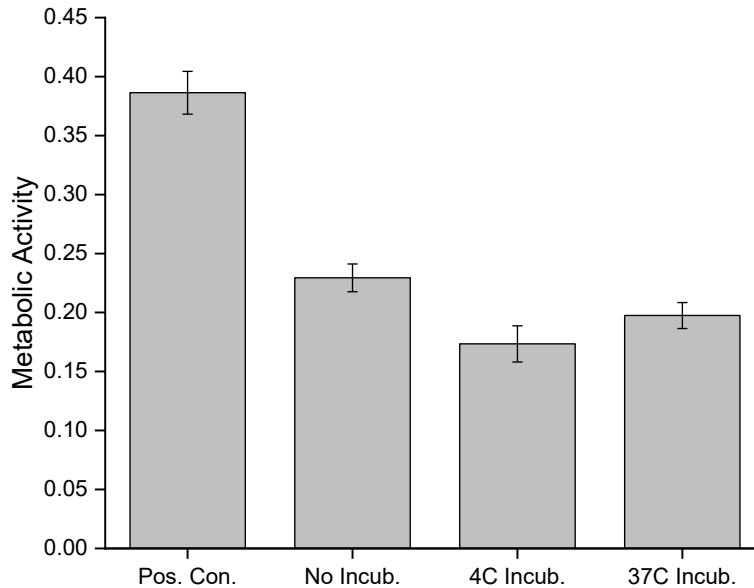
Figure 4-4 Post-Thaw Metabolic Activity of Hydrogels Subject to Differing CPA Incubation Conditions: The hydrogels subject to no CPA incubation were immediately cryopreserved following gelation. The other two conditions sustained 30-minute CPA incubation periods at 4°C and 37°C respectively. Positive control represents cells that did not undergo cryopreservation. Error bars represent ±SEM, n = 3.

Figure 4-4 compares immediate post-thaw metabolic activity of encapsulated HepG2 cells subject to three different CPA incubation protocols. No incubation describes placing the freshly created hydrogels into the CPA solution and immediately starting standard cryopreservation protocol. The other two incubation conditions comprise of a 30-minute incubation in the CPA either at 4°C or 37°C. The hydrogels that were not subject to a CPA incubation display moderately higher metabolic activity following cryopreservation, while the 30-minute incubation at low temperatures resulted in the lowest metabolic activity. Because these experiments were performed using slow-cooling cryopreservation, it is likely the encapsulated cells are exposed long enough during the 1°C/min cooling process to prevent IIF. CPA incubation would become more prominent for hydrogels of larger volume, less porosity, or

using cryopreservation protocols that involve less inherent incubation times (vitrification). Interestingly, the 30-minute incubation at 4°C resulted in lower metabolic activity than the 30-minute incubation at 37°C. This result disagrees with other studies that conclude DMSO and other membrane-penetrating CPAs are more toxic at higher temperatures [37], [38]. However, it is difficult to conclude whether this is a discernible difference for hydrogel freezing or if "cold-shock" reduction of metabolic activity [39] is outweighing cytotoxicity of DMSO for short incubation times. We can conclude that CPA incubation is unnecessary and even detrimental to post-thaw HepG2 metabolism and will therefore not be included in slow-cooling protocol.

3D structure also needs to be considered when thawing slow-cooled hydrogels back to ambient temperatures. Figure 4-5 compares the immediate post-thaw metabolic activity of HepG2 encapsulated hydrogels for thaw times ranging between 60 and 120 seconds.
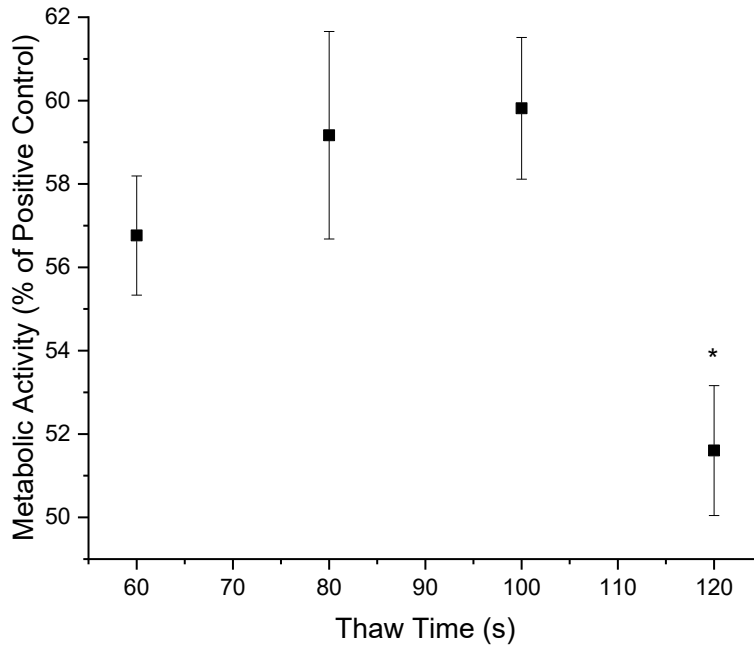
Figure 4-5 Comparison of Post-Thaw Metabolic Activity for Differing Thaw Times: Thaw times ranged between 60 seconds and 120 seconds. Hydrogels thawed at low end of time spectrum do not undergo full thawing until later in protocol. In comparison gels thawed at high end of time spectrum have been thawed and undergo shear stress due to thawing procedure. Error Bars represent ±SEM, n = 3." *" represent ANOVA with p value < 0.05.

The metabolic activity is measured as a percentage of the positive control cells that did not undergo cryopreservation. There was no significant metabolic difference between the 60, 80, and 100 second thaw time conditions; however, there appears to be a moderate linear improvement up until 100 seconds. We hypothesize that this is due to incomplete hydrogel thawing for the 60 and 80 second conditions. The metabolic activity then steeply drops off at the 120 second condition. This is likely due to sheer stress from thawing procedure injuring the encapsulated cells that have already been fully thawed. The results indicate there is an optimal thawing time of approximately 100 seconds for these hydrogels as there are cell injury considerations on both sides of the non-optimal spectrum. It is also important to note that optimal thaw times will likely change if the CPA or bio-ink formulation is changed.

The final protocol-based optimization performed tested the importance of pre-cryopreservation alginate incubation and the addition of 5 mM L-glutamine to the bio-ink formula. L-glutamine is an essential amino acid that is commonly included in mammalian cell culture media to promote growth and metabolism [40]. In addition, L-glutamine has been used as been shown to improve cryopreservation outcome of mammalian spermatozoa cells [41]. Figure4-6 displays these post-thaw metabolic activities as percentages of respective positive controls (not frozen) to remove metabolic contribution from growth; however, it is important to note that due to potential maximum reduction of resazurin to resorufin this normalization could be unreliable.
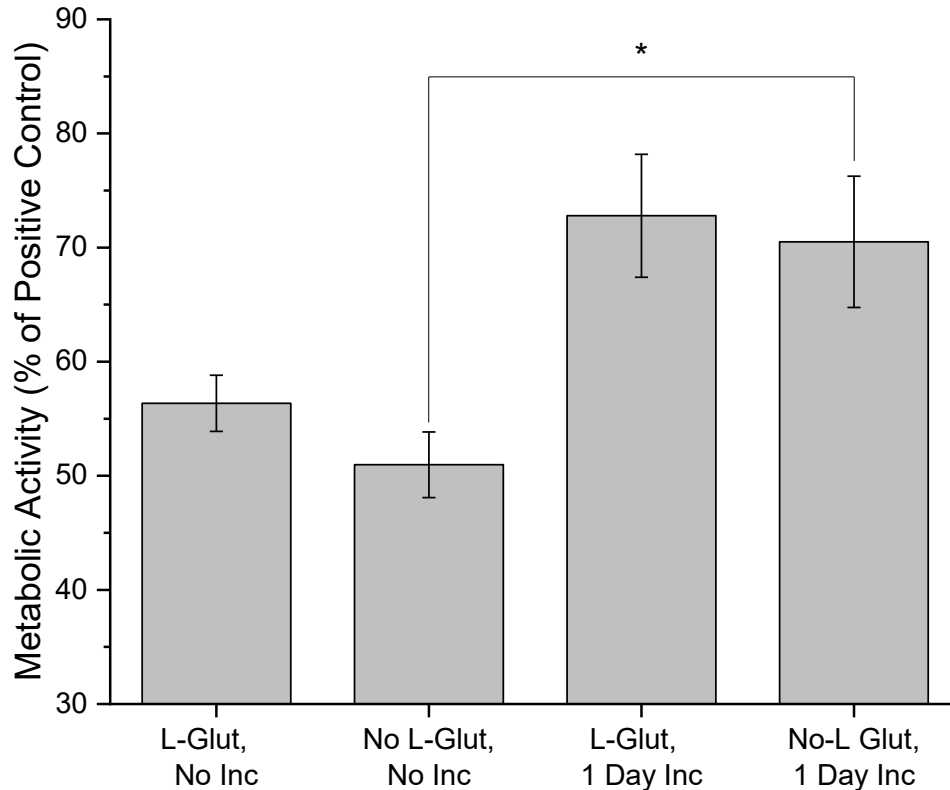
Figure 4-6 Post-Thaw Metabolic Activity Comparison of Equilibration and L-Glutamine in Alginate Precursor: Cells without incubation were immediately frozen after gelation, while other condition is frozen 24 hours after gelation. The L-glut condition contained an additional 5 mM L-glutamine in the alginate precursor solution. . Error Bars represent ±SEM, n = 3."*" represent ANOVA with p value < 0.05.

The addition of L-glutamine resulted in a moderate increase in post-thaw metabolic activity for both incubation conditions. More significant differences were observed when comparing the incubation conditions of the hydrogels. Gels that were incubated for 24 hours before cryopreservation had a 18% and 20% increase in metabolic activity for the added L-glutamine and no added L-glutamine conditions. These results would suggest that allowing the cells to equilibrate for 24 hours in the hydrogel pre-cryopreservation is beneficial to post-thaw metabolic activity and that the addition of L-glutamine to the bio-ink is most-likely is not beneficial enough to incentivize further use.

4.3.3 CPA Formulation

The remaining optimization studies are focused on characterizing and improving post-thaw metabolic activity of encapsulated HepG2 cells by adjusting the CPA formulation. The base CPA that is commonly used for HepG2 suspension freezing consists of 90% Opti-MEM media that is supplemented with 5% (v/v) serum and 10% DMSO. Previous studies have shown the benefit of using CPA additives such as trehalose and sericin to improve post-thaw biological outcome. Therefore, these studies begin by assessing previously optimal additive formulations (100 mM trehalose and 1% w/v sericin) to determine whether they have the same beneficial effect on hydrogel cryopreservation.
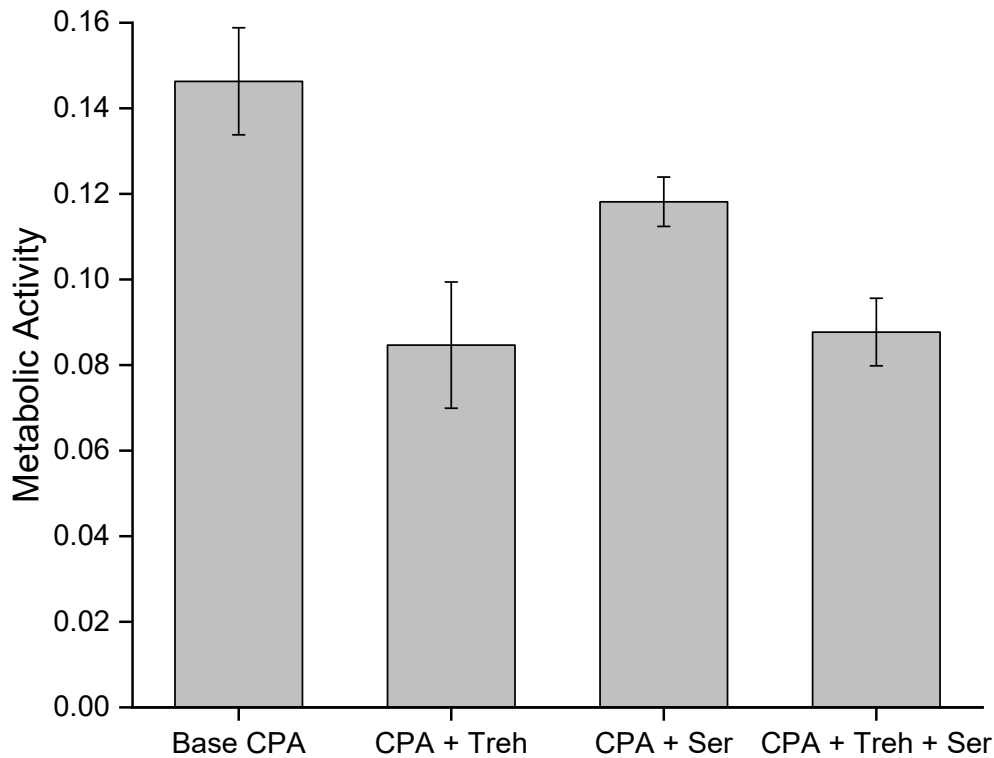
Figure 4-7 Additive Comparison Post-Thaw Metabolic Activity: Base CPA contained Opti-MEM media complimented with 5% FBS and 10% DMSO. Further CPA additives are 100 mM trehalose, 1% (w/v) sericin or both. Error Bars represent ±SEM, n = 3.

Figure 4-7 compares the post-thaw metabolic activity of hydrogels that were cryopreserved in the base CPA, base CPA with 100 mM trehalose, base CPA with 1% sericin,

and base CPA with both concentrations of additives. Surprisingly, the addition of any additive to the base CPA solution resulted in a negative impact on the post-thaw metabolic activity. In particular, the conditions including 100 mM trehalose had significantly lower metabolic activity and there was no observable color change of the resazurin solution during the assay. Other studies have highlighted the potential risk of osmotic injury when using trehalose in CPA formulations at a concentration higher than 100 mM [42]. It is possible that osmotic stress injury is enhanced in the 3D hydrogel cryopreservation and further studies were performed to study this phenomenon.

It is possible that the osmolarity of the base CPA is already cryogenic injury in the alginate encapsulated environment. Typical Opti-MEM media has an average osmolality of 272.7 mOsmol/kg [43] and the added FBS typically has an osmolality between 280-340 mOsmol/kg [44] depending on the batch. So, a 5% v/v FBS supplemented Opti-MEM media should have an estimated osmolality of ~275 mOsmol/kg or osmolarity of 275 mOsmol/L.
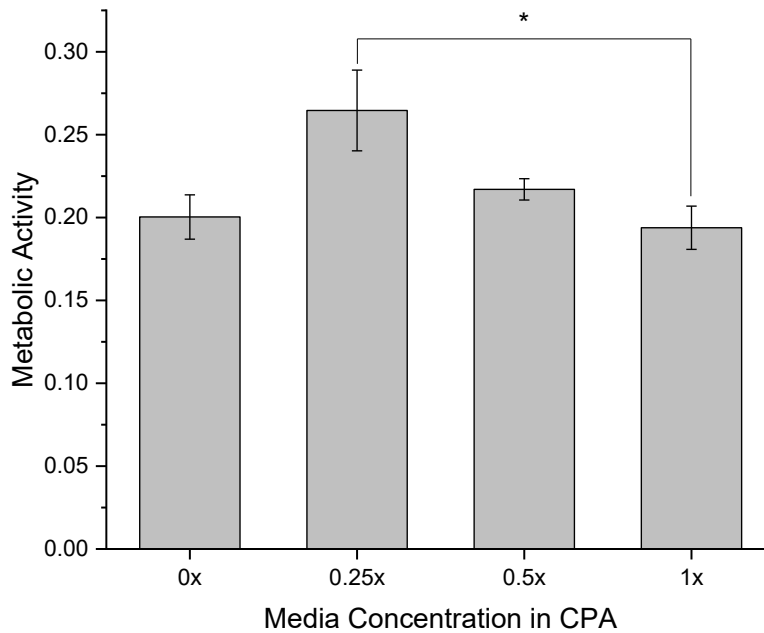
Figure 4-8 Metabolic Activity of CPA Solutions Containing Different Concentrations of Media: Media concentration differs between 0x (pure water solvent) and normal 1x media. Error Bars represent ±SEM, n = 3."*" represent ANOVA with p value < 0.05.

Figure 4-8 compares the post-thaw metabolic activity of HepG2 encapsulated cells that were frozen in CPA solutions that are made up of different concentrations of media + 10% v/v of DMSO. The 1x is our base CPA. The 0.5x and 0.25x media concentrations are base media that is diluted with pure water and the 0x CPA contains pure water with DMSO. The data shows that cell hydrogels frozen in CPA solutions containing full concentration of media and no media had the lowest metabolic profile after cryopreservation. Diluting the media concentration by half resulted in a moderate uptick of metabolic activity post-thaw, but the cells frozen in CPA solution containing a quarter of the typical osmolarity from the media had significantly higher metabolic activity. These results suggest reducing the osmolarity via media dilution is an effective technique to improve post-thaw cellular outcome. In addition, it appears that the alginate encapsulation of the cells itself is adding to the osmolarity of the cells during cryopreservation. This could be one explanation for why the cells frozen in lower concentration alginate encapsulations had higher metabolic activity post-thaw. This is a potential opening for a large breadth of research moving forward in encapsulation freezing; however, this research continues using the same alginate encapsulation characteristics and attempts to improve post-thaw outcome by improving CPA formulation.

The next study determines whether trehalose can be added at lower concentrations by reducing osmolarity of the CPA through media dilution.
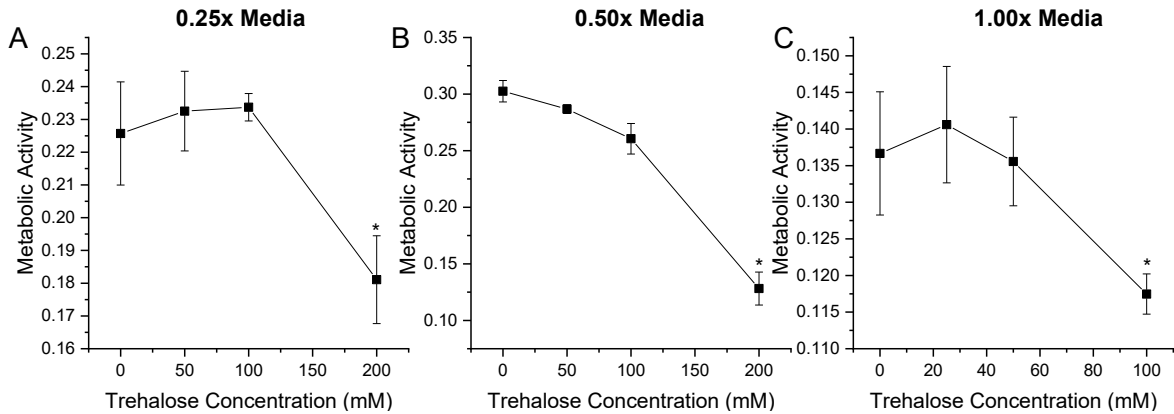
Figure 4-9 Comparison of CPA Formulations with Differing Media and Trehalose Concentration: Reduction of media concentration appears to allow slight increase in trehalose concentration without negative impact. Error Bars represent ±SEM, n = 3." *" represent ANOVA with p value < 0.05.

Figure 4-9 compares the post-thaw metabolic activity of encapsulated HepG2 cells that are frozen in varying media and trehalose concentrations. The data from Figure 4-9C agrees with previous data from Figure 4-7 that the encapsulated cells frozen in non-diluted media with 100 mM trehalose have significantly lower metabolic activity post-thaw. This data also suggests that lower concentrations of trehalose (25-50 mM) can be used without the negative effect; however, no positive impact can be statistically differentiated. In addition, diluting the media concentration appears to allow a higher concentration of trehalose to be added into the CPA without major negative cellular outcome. The cells frozen in 0.5x diluted media were able to withstand up to 100 mM trehalose with a minimal impact on the post-thaw metabolic activity. Further dilution allowed a positive impact on the post-thaw metabolic activity of the cells up to 100 mM trehalose, but still see major decline in metabolic activity at the 200 mM condition. This data supports the osmolarity injury hypothesize proposed previously. If it is assumed that media osmolarity is approximately 275 mOsmol/L, then a 50:50 dilution reduces the osmolarity by 137.5 mOsmol/L and a 25:75 dilution reduces osmolarity by 207 mOsmol/L. Data from Figure 4-9C suggests that the osmolarity of the CPA solution can be potentially raised to ~300 mOsmol/L before significant negative impacts are observed. A 0.5x media dilution CPA with an

additional 100 mM trehalose is still well under that 300 mOsmol/L limit, while an additional 200 mM trehalose goes over the limit. Interestingly, the CPA containing 0.25x diluted media and 200 mM trehalose would still be under the supposed osmolarity limit, however a significantly negative cellular metabolism is still recorded. This data suggests that membrane damage caused by an increase in solutes may be more significantly connected to tonicity instead of osmolarity alone. Tonicity is considered effective osmolarity and is affected by solutes that are restricted to one side of the membrane [45]. There are several dissolved molecules in media that add to the osmolarity; however, they do not add to tonicity because they are able to cross the plasma membrane freely. Therefore, a direct reduction in media osmolarity does not allow 100% replacement by an effective osmol such as trehalose.

A CPA formulation study would not be complete without examining arguably the most important component DMSO. DMSO is considered a membrane penetrating cryoprotectant that is used in most standard CPA formulations. At higher concentrations, DMSO is toxic to cells within a relatively short period of time; therefore, it is important to determine optimal DMSO concentrations within different CPA formulations.
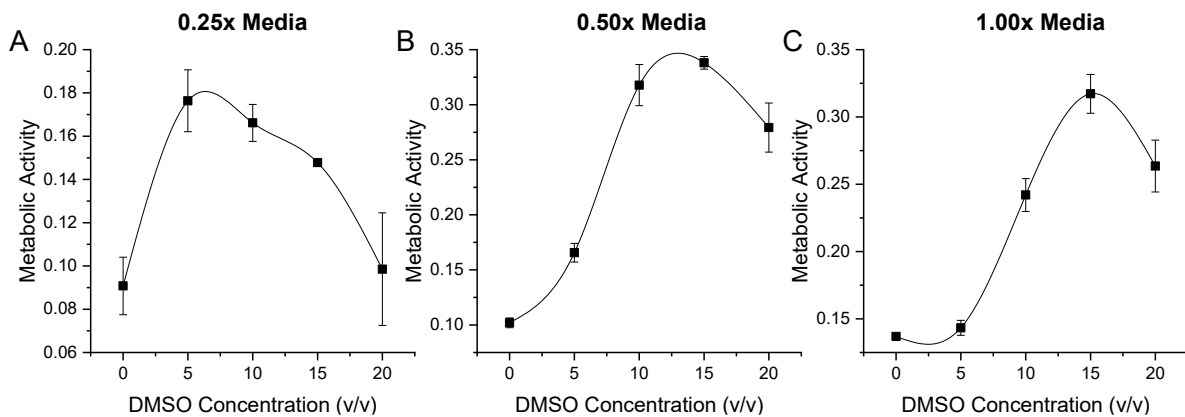
Figure 4-10 Comparison of CPA Containing Differing Concentrations of Media and DMSO: Decreasing media concentration shifts the optimal DMSO concentration for hydrogel cryopreservation. . Error Bars represent ±SEM, n = 3.

Figure 4-10 compares the post-thaw metabolic activity of encapsulated HepG2 cells frozen in CPAs consisting of different concentrations of media and DMSO. Interestingly, the is an observable shift in the optimal DMSO concentration as the media concentration of the CPA is diluted. At normal media concentrations, immediate post-thaw metabolic activity is measured highest for the 15% DMSO concentration. Interestingly, the cells frozen in 5% DMSO for this media condition performed equally as the cells frozen without any DMSO. In addition, there is a significant drop-off of metabolic activity at the highest DMSO concentration (20%) due to the toxicity issues for the cells. As the media concentration is dropped, the optimal DMSO concentration shifts and the 5% DMSO condition performs equal to (0.5x) or higher than the other conditions (0.25x). This data suggests that the addition of DMSO to the CPA helps to mitigate solute injury sustained during cryopreservation. This is most likely explained by DMSO's ability to increase membrane porosity, allowing water and other larger dissolved molecules to flow through the membrane more freely, this decreasing the osmotic pressure [46], [47].

These results have potential implications for the reduction of toxic DMSO in CPA formulations. A similar study was performed on cells cryopreserved using the suspension freezing method to determine whether these findings are limited to hydrogel freezing.
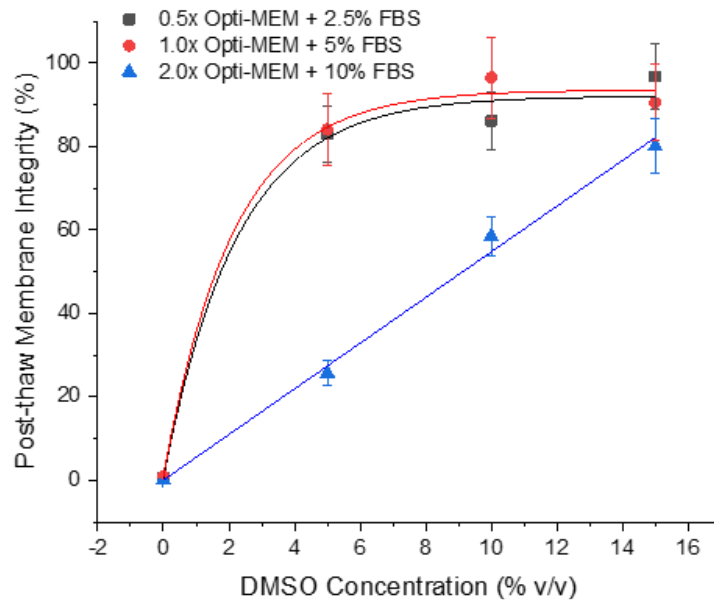
Figure 4-11 Comparison of Media and DMSO Change in CPA for Suspension Freezing: Cells were frozen in suspension instead of encapsulation. At higher media concentrations, addition of DMSO results in linear increase of membrane integrity. At lower media concentration, DMSO has plateauing beneficial effect at higher concentrations. Error Bars represent ±SEM, n = 3.

Figure 4-11 compares immediate post-thaw membrane integrity counts of HepG2 cells suspension cryopreserved using the slow-cooling method in differing concentrations of media (0.5x, 1.0x, and 2.0x) and DMSO (0-15% v/v). Cells frozen in the lower media concentrations (0.5x and 1.0x) had higher overall viabilities for all DMSO concentrations. Similarly, to the hydrogel studies, the 5% DMSO CPA condition was highly ineffective at producing viable cells post-cryopreservation with the highest media concentration (2.0x). In addition, the 15% DMSO condition produced significantly higher post-thaw viability compared to the lower concentrations. With lower overall solute concentration in the CPA, there is no statistically significant difference in the post-thaw viability of the cells frozen in solutions containing 5,10, or 15% DMSO. These results closely agree with what was observed in the hydrogel freezing experiments; however, it is important to note that these studies only consider membrane integrity. The minor differences observed in the CPA effectiveness may be due to a disconnect of cell viability and cell metabolism after cryopreservation.

The final CPA formulation study focused again on the use of sericin as an additive to the CPA formula. Previous studies showed that the addition of sericin was detrimental to post-thaw metabolic activity of the cells frozen in the standard CPA formulation.
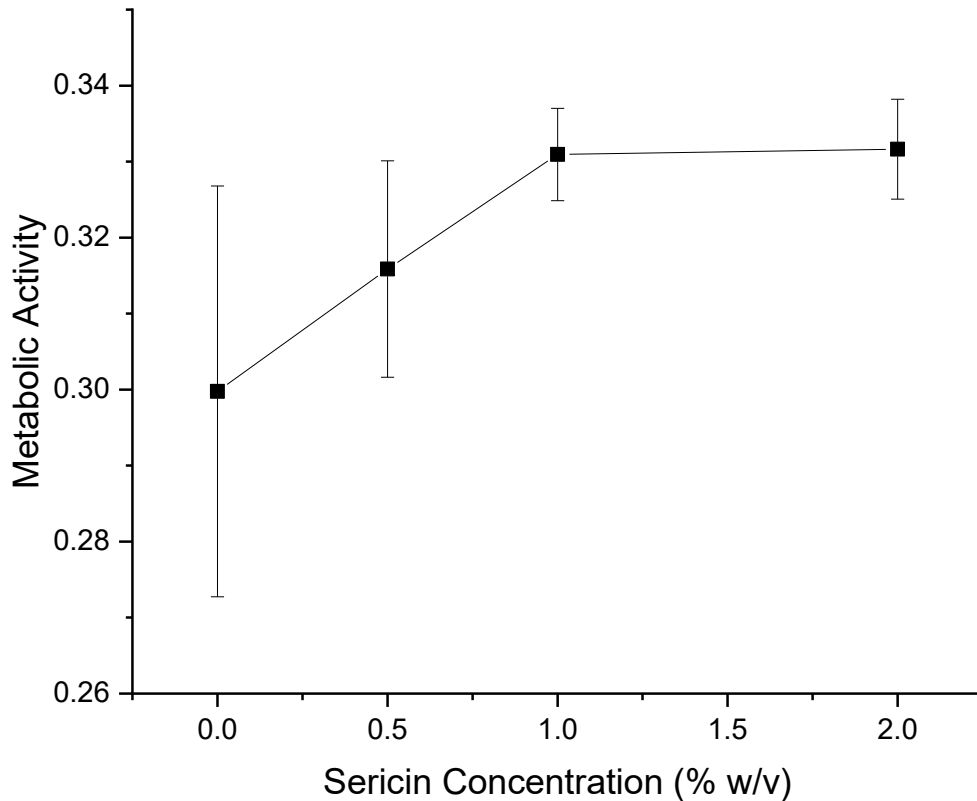
Figure 4-12 Comparison of Sericin Additive: Post-thaw metabolic activity if evaluated for gels frozen with 0.5x base CPA + 0-2% w/v sericin. Reducing media concentration to 0.5x allows minor beneficial impact on metabolic activity with sericin. Error Bars represent ±SEM, n = 3.

Figure 4-12 examines post-thaw metabolic activity of encapsulated HepG2 cells that were frozen in a CPA formulation containing the 0.5x media dilution and different concentrations of sericin (0-2% w/v). Results prove that the addition of up to 2% sericin to the CPA can have a positive impact on post-thaw metabolic activity of the cells in the lower tonicity media solutions. However, it is important to note that the potential impact is minimal and non-statistically significant.

4.3.4 Final Alginate, Protocol, and CPA Selection

The final product of the optimization studies is primarily focused on maximizing post-thaw metabolic output of encapsulated cells. Other secondary factors are considered and often account for reasoning why a more extreme parameter was not selected for use in further cryopreservation studies and will be discussed in detail. The protocol for slow-cooling hydrogel freezing is like that of typical cell suspension freezing. A 24-hour equilibration period was added to the protocol to begin forming their own ECM and start growing as they would in a normal physiological environment. This step could also potentially allow higher concentrations of $CaCl_2$ to be used for gelation as there would be ample time for the excess $CaCl_2$ molecules to diffuse out of the hydrogel. It was determined that no additional CPA incubation step was required for hydrogels with these specific geometric and porosity properties; however, it would be important to consider this step should major changes be made to these properties. Finally, a rapid thawing step using water bath agitation was again optimized for these specific bio-ink and CPA properties. Although, if the thaw-time is not the low or high extreme, there should not be a major impact on the cellular health from this step alone.

Many of the major discoveries were made in the bio-ink and CPA formulation studies. After several studies it appears that bio-ink formulation has a significant impact on the post-thaw cellular outcome. Preliminary studies suggested that using a lower concentration (1% w/v) of alginate for gelation would result in improved post-thaw metabolic activity; however, it was not significant compared to the 2% alginate concentration at the time and it was selected for further studies. CPA formulation studies suggest that the alginate encapsulation is adding to osmotic pressure applied and therefore makes the use of other additives non-beneficial. Other studies have shown that sodium alginate itself has cryoprotective abilities both in a gel and non-gel form

[48], [49], so the addition of other non-membrane penetrating additives may have higher potential for negative impact without significant CPA or bio-ink modulation. For this reason, no additional trehalose or sericin are used in the final CPA formulation for alginate hydrogel freezing. Further studies are required to determine whether lower alginate concentration would make a significant difference on metabolic activity and solute concerns. The final bio-ink for this research will utilize the 2% alginate hydrogels for workability and tested success reasons and will adjust the CPA around the bio-ink selection.

There are many factors to consider when choosing DMSO concentration in the CPA. The alginate and suspension freezing data supports the conclusion that DMSO is more necessary when the overall extracellular environment has a higher osmolarity or tonicity (including the CPA). With this is mind, the 5% DMSO condition was only effective at the lowest media concentration (0.25x) and there are time considerations to consider when using this low of a media concentration for cells that may be exposed to this environment for longer periods of time. The 10% DMSO concentration is the most commonly for suspension freezing [50] and gives the most consistently high post-thaw metabolic activity output other than the 15% concentration. Ultimately the 10% DMSO concentration was chosen for the final CPA selection due to toxicity concerns of the 15% DMSO condition. In addition, the use of a 0.5x diluted media was chosen as this is the concentration where the 10% DMSO condition was the most optimal. Further studies will test viability, growth, and metabolism characteristics of multiple cell types frozen using these specifically chosen parameters.

4.4 Results and Discussion – Evaluation of Optimized Cryopreservation System

Previously, a broad optimization study was performed to adjust the hydrogel properties, cryopreservation protocol, and CPA formulation to optimize the immediate post-

cryopreservation metabolic activity of HepG2 cells. The remaining research was focused on evaluating whether this cryopreservation methodology is effective long-term health and growth of HepG2 cells. In addition, identical studies were performed on two other cell types of neurological and immunological origin to determine whether this exact methodology can be applied to a multitude of cells or whether further optimization is required for each cell type.

4.4.1 HepG2 Cells

To begin, the metabolic activity of encapsulated HepG2 cells was evaluated across 7 days under both frozen and non-frozen conditions. Figure 4-13 plots the metabolic activity of non-frozen encapsulated HepG2 cells. The data points represent absorption readings performed the day of encapsulation (day 0), 1-, 4-, and 7-days following encapsulation.
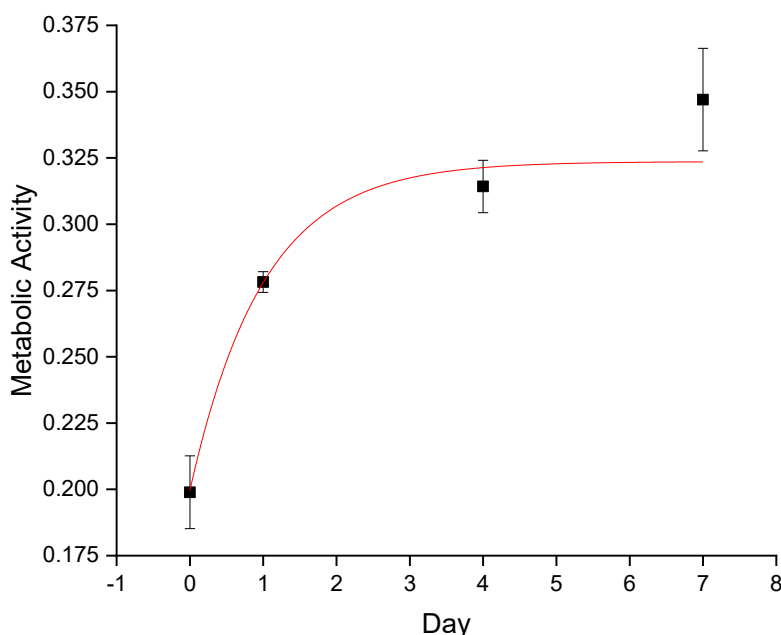
Figure 4-13 Metabolic Grow-out of Non-Frozen HepG2 Hydrogels: Grow-out data collected from 0-7 days. Data fitted with exponential decay model. Error Bars represent ±SEM, n = 3.

The plotted data is fitted with an exponential decay model. This data suggests that there is no lag period of growth or metabolism for HepG2 cells following encapsulation. In addition, there appears to be a plateau phase to the metabolism at later days in the experiment; however, it

is likely this plateau is due to the limited reduction capacity of the resazurin molecule. Figure 4-14 plots the same grow-out metabolic activity for encapsulated HepG2 cells following cryopreservation.

These data points are fitted with a sigmoidal model due to the 1–2-day metabolic growth lag experienced by cells. Following this lag period, the cells enter an exponential growth phase, and a reach a similar plateau observed for the non-frozen cells.
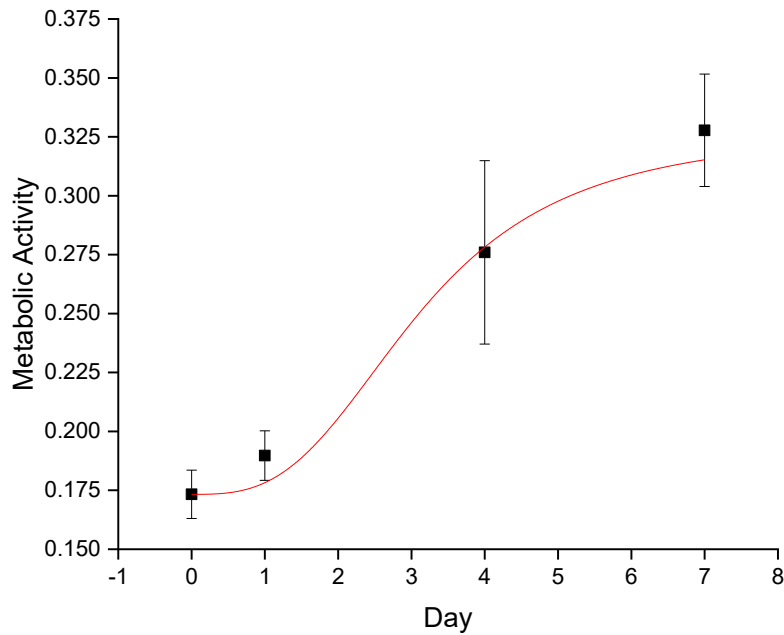
Figure 4-14 Metabolic Growth Profile of Cryopreserved HepG2 Hydrogels: Metabolic activity follows sigmoidal model from day 0 to day 7. Error Bars represent ±SEM, n = 3.

A grow-out cell quantification study was performed on frozen encapsulated HepG2 cells to confirm that most metabolic activity change was due to cellular growth inside of the hydrogel. Hydrogels were dissolved using a calcium chelator and counted using standard trypan blue exclusion technique.
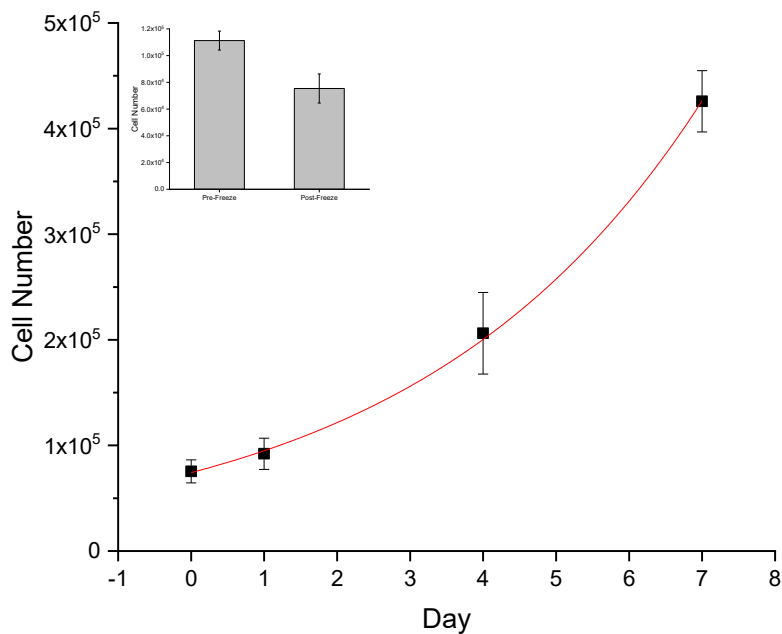
Figure 4-15 Cell Quantification of Cryopreserved HepG2 Hydrogels: Cells maintain exponential growth following a short lag period at day 1. Inset figure plots pre-freeze viability to post-freeze viability. Error Bars represent ±SEM, n = 3.

Figure 4-15 plots the subsequent cell counts following cryopreservation. The inset figure plots the comparison of live cells within the hydrogels immediately pre-freeze and post-freeze. The immediate post-thaw viability was calculated to be 66.8% ± 10.7%. Growth following cryopreservation is characterized by a minor lag period and continual exponential growth throughout the 7-day period. Cell number is plotted against cell metabolic activity for the parallel growth days (0, 1, 4) in figure 4-16 and a linear regression is fitted with an r value greater that 0.99; indicating increase in metabolic activity for the HepG2 cells is due to an increase in cell number.
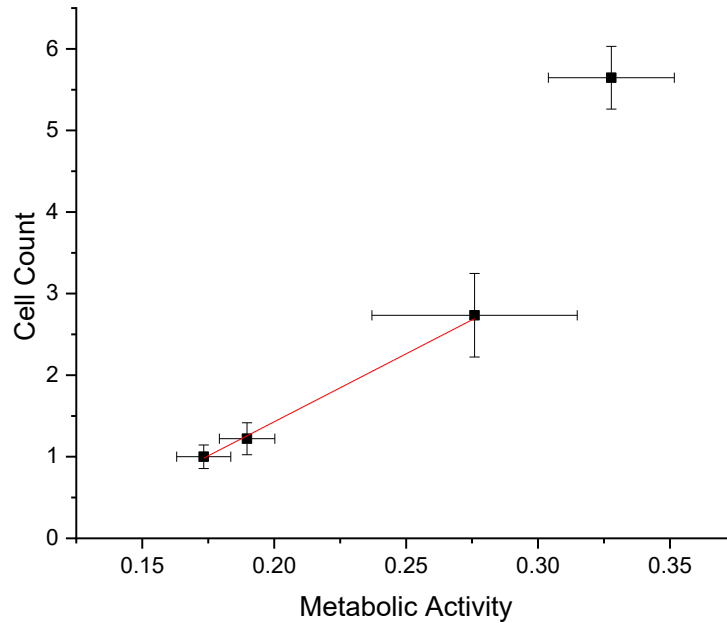
Figure 4-16 Growth and Metabolic Comparison of Cryopreserved HepG2 Hydrogels: Growth and Metabolic activity fit a linear regression model with R > 0.99. Growth continues while metabolic assay reaches upper limit at day 7. Error Bars represent ±SEM, n = 3.

A live-dead assay employing fluorescence microscopy was used to further characterize the growth of encapsulated HepG2 cells following cryopreservation. Using image processing software, the viability of the cells on day 0 was assessed to be 66.1 ± 6.2% (data not shown), which is within 1 percentage point of the viability recorded using trypan blue exclusion. Figure 4-17 displays a set of fluorescent images for growth day 0, 1, 4, and 7.
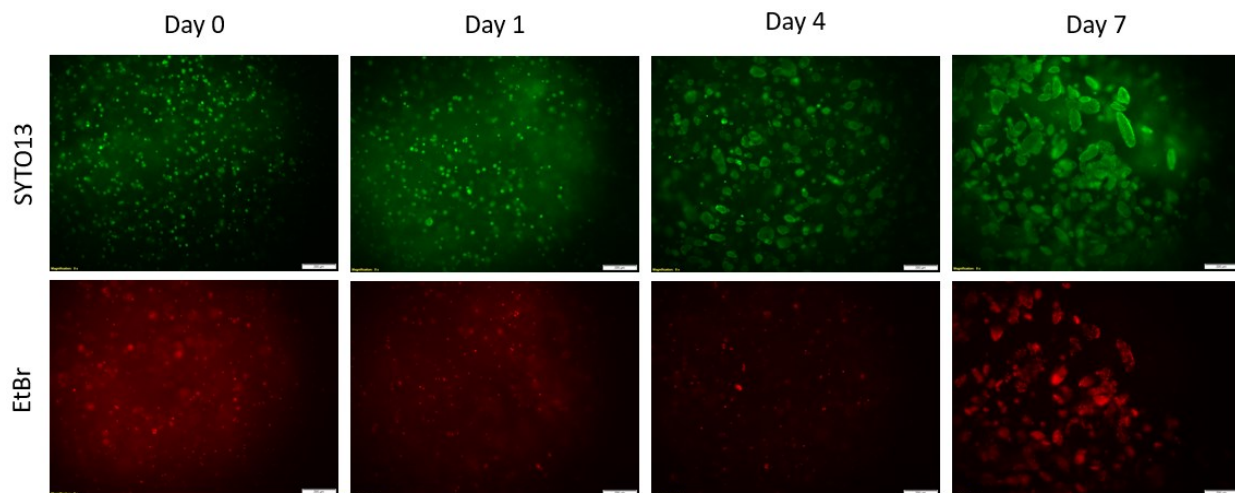
Figure 4-17 Fluorescent Evaluation of Post-Thaw HepG2 Hydrogel Growth
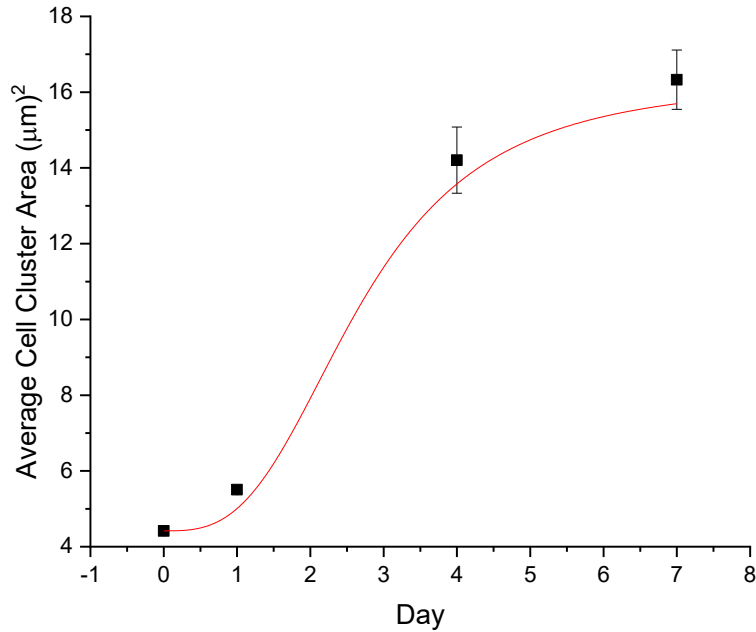
Figure 4-18 Cluster Growth of Cryopreserved HepG2 Hydrogels: Cluster size growth follow sigmoidal model. Error Bars represent ±SEM, n = 3.

Each growth day has a set of two images showing the total number of cells (SYTO13) and the dead-cells (EtBr). Cells appear to be growing in clusters that are increasing overall size at each progressive day. The average cell cluster size was assessed using an image particle analysis (Figure 4-18). Average cell cluster size grew from 4.42±.045 µM on day 0 to 16.33±0.78 µM with a maximum cluster size of 307 µM observed.

4.4.2 Neuro 2A Cells

Neuro 2A cells are a mouse neural crest-derived cell line that is extensively used to study neuronal differentiation, growth, and signaling pathways because of their ability to quickly differentiate into neurons within a few days [55]. Therefore, these cells are a good candidate for studying the growth and metabolic effects that the newly developed hydrogel cryopreservation system has on neural origin cells.

Figure 4-19 shows the increase in recorded metabolic activity of encapsulated Neuro2A cells cultured under physiological conditions.
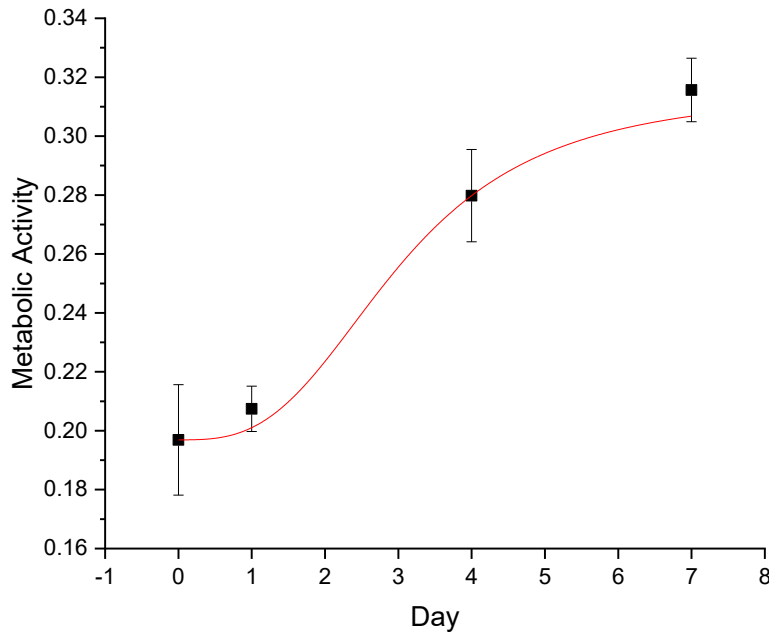
Figure 4-19 Metabolic Growth of Non-Frozen Neuro 2A Hydrogels: Data fitted with sigmoidal model. Error Bars represent ±SEM, n = 3.

As expected, there is a minor lag period immediately after exposing the cells to the new encapsulated environment followed by typical exponential growth period and a plateau likely due to a previously mentioned assay limitation. Studies have shown that neuronal interaction with their environment have implications on growth, morphology, and functionality [56]. In alginate hydrogels specifically, a study showed that hydrogel systems that had an elastic modulus like that of brain tissue best promoted neuronal growth. They found that neuronal stem cells grown in alginate hydrogels consisting of 0.25% w/v alginate and cured with 10 mM $CaCl_2$ resulted in the highest growth potential over a 7 day period [57]. Interestingly, the hydrogels used in this study would potentially have elastic moduli over 100-fold greater than the optimal growth hydrogels used in other studies. This suggests neuronal growth and function could be improved by reducing the moduli of the hydrogels; however, there are potential mechanical

issues related to cryopreservation of these constructs that may impose a limitation on the moduli reduction.
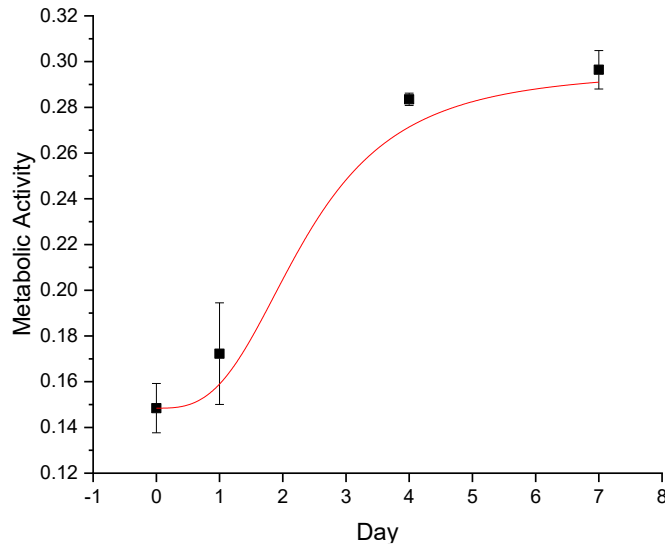
Figure 4-20 Metabolic Growth of Neuro 2A Hydrogels Following Cryopreservation: The data is fitted with sigmoidal model and is similar to that of non-frozen cells. Error Bars represent ±SEM, n = 3.

Figure 4-20 plots the post-thaw metabolic activity of Neuro 2A hydrogels that were cryopreserved. The fitted metabolic data follows a similar trend to that of the non-frozen hydrogels with a minor lag phase, exponential growth, and assay limit plateau. This data suggests that the cells can recover from cryopreservation stress quickly and resume similar activity. However, there appears to be a disconnect between cellular metabolism and cell growth if we compare the cell quantification data displayed in Figure 4-21 to the metabolic activity.
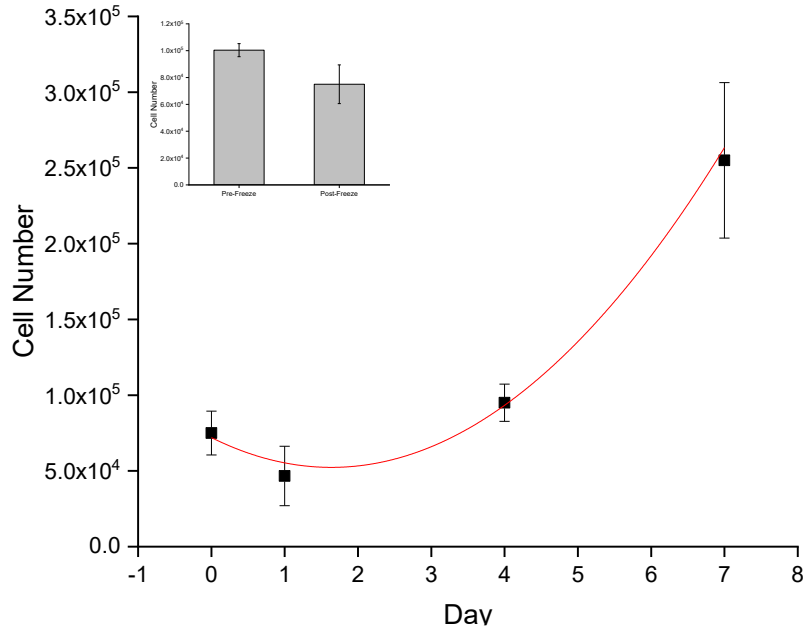
Figure 4-21 Cell Quantification of Cryopreserved Neuro 2A Hydrogels: Results point to delay-onset of Neuro 2A cells in hydrogels post-thaw. This delayed cell death is followed by exponential growth of surviving cells. Error Bars represent ±SEM, n = 3.

This is primarily characterized by 30% reduction in the number of cells recorded 24 hours after thawing compared to the initial count. To the best of our knowledge, this is the first indication of delayed-onset apoptosis of cryopreserved Neuro 2A cells in an encapsulated environment. Following this delayed cell death, the cells enter an exponential growth phase and there is a 3.4-fold increase in cell number by the 7th day of growth compared to pre-freeze quantification.
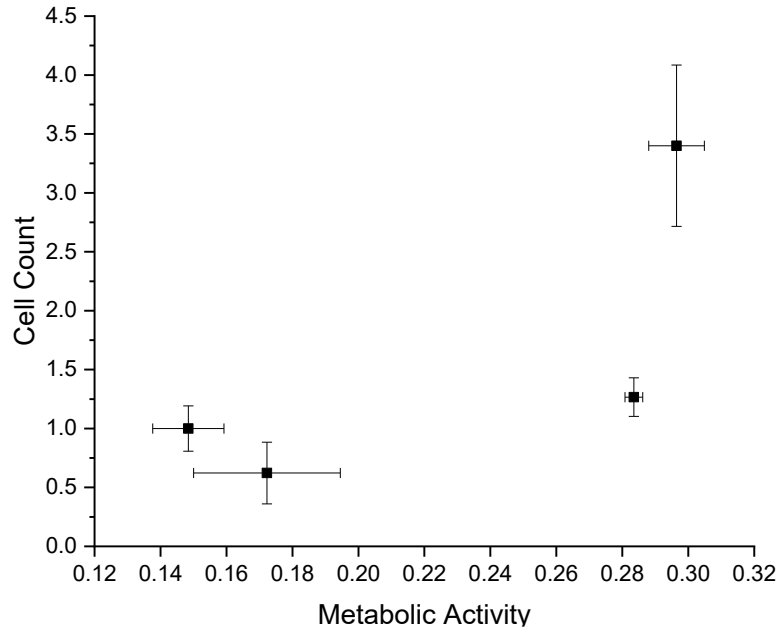
Figure 4-22 Growth and Metabolic Comparison of Frozen Neuro 2A Hydrogels: There is a disconnect of cell count and metabolic activity for day 1. Even though cells appear to be dying, there is an increase in overall metabolic activity due to increased cellular metabolism. Error Bars represent ±SEM, n = 3.

Figure 4-22 illustrates this disconnect between cell number and cell metabolism recorded for the neuro 2A cells following preservation. Even though there is a reduction in the cell number 24-hours post-thaw there is still a recorded increase in the overall metabolic activity, indicating an enhanced stress response. However, this response appears to reduce by the fourth day of incubation in growth media. Overall, this data suggests there is a delayed period for the Neuro 2A cells to return to normal metabolic and growth activity compared to the HepG2 cells. This indicates a potential for improvement to the alginate matrix to improve neurological cell outcome following cryopreservation. The fluorescent images for a grow-out following cryopreservation of encapsulated Neuro 2A cells agree with the metabolic and growth data (Figure 4-23).
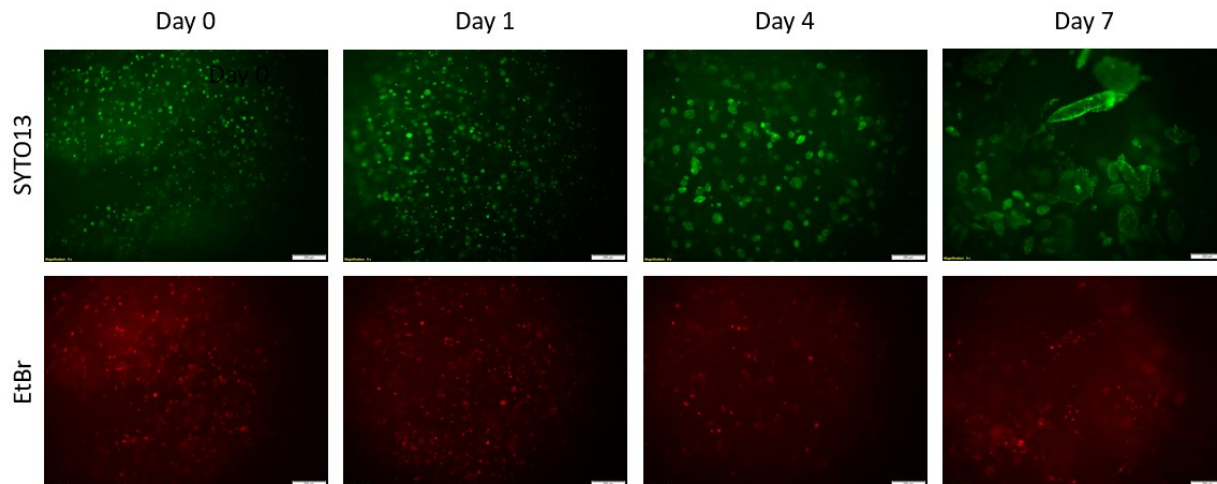
Figure 4-23 Fluorescent Evaluation of Frozen Neuro 2A Hydrogels

Interestingly, the initial viability calculated from the day 0 images indicates a viability similar to the day 1 record from the cell quantification. This suggests that the fluorescent images are better able to detect delayed onset apoptosis of the neuro 2A cells than the standard trypan blue exclusion assay. In addition, Neuro 2A cells are growing in similar spherical clusters that characterize the HepG2 growth. Again, this growth pattern is a result of limited attachment to the alginate matrix and the clustered growth is detected across multiple cell origins. The average size of these cell clustered were recorded in Figure 4-24.
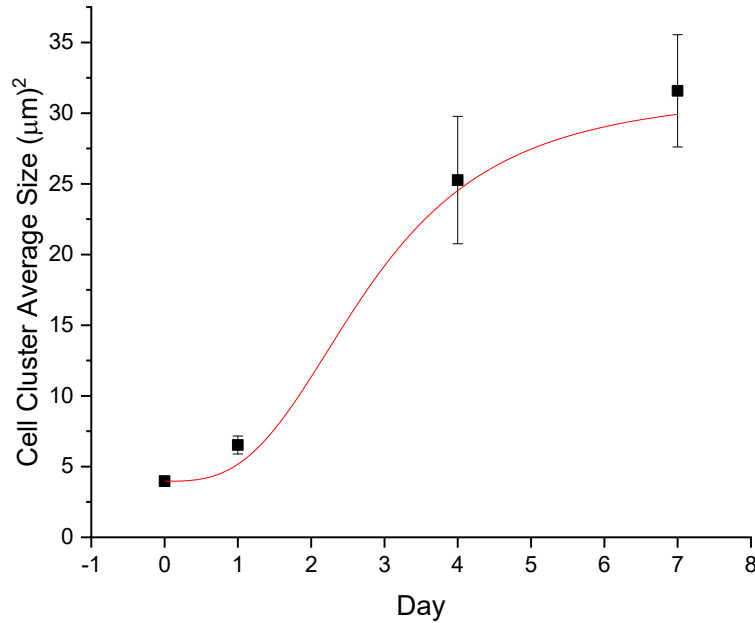
Figure 4-24 Cluster Growth of Cryopreserved Neuro 2A Hydrogels: Cluster growth of Neuro 2A cells follows similar pattern to that of HepG2 cells indicating an attachment dependent growth mechanism. Data fitted with sigmoidal model and error bars represent ±SEM, n = 3.

The increase in size of the average cluster size follows a similar logistic curve as the metabolic data. There is a minor increase in the cell cluster size 1 day after thawing; indicating that even though some cells experience delayed onset apoptosis, there is still growth occurring in less injured cells. There is a large spike in average crystal size 4- and 7-days following cryopreservation indicating exponential cell growth, Interestingly, the Neuro 2A cells had larger average cell cluster sizes than the HepG2 cells. This result could be explained by smaller number of viable cells following cryopreservation and excess growth materials are absorbed by the smaller number of surviving cells.

4.4.3 RAW 264.7 Cells

RAW 264.7 cells are a monocyte/macrophage transformed cell line cell originating from Abelson leukemia virus of mice. These cells are described as an appropriate model of macrophages and can perform pino- and phagocytosis [58]. In addition, these cells can kill target

cells via antibody dependent cytotoxicity [59]. RAW 264.7 cells were used in this study to evaluate the effectiveness of the developed cryopreservation system on encapsulated immune cells and study their response following cryopreservation. Figure 4-25 plots metabolic activity of RAW 264.7 cells immediately (day 0), 1-, 4-, and 7-days following hydrogel crosslinking.
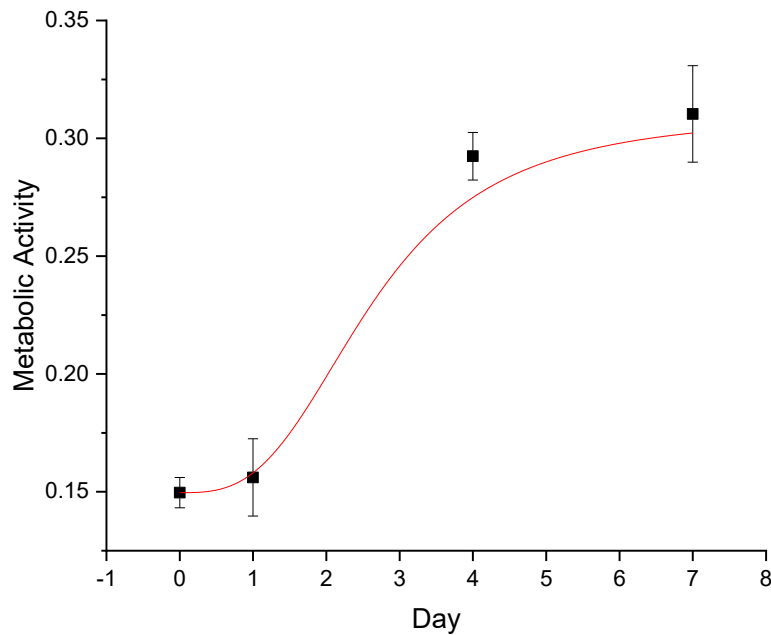
Figure 4-25 Metabolic Activity of Non-Frozen RAW 264.7 Hydrogels: RAW 264.7 cells follow typical growth characteristics in the hydrogel. Error bars represent ±SEM, n = 3.

Observed metabolic increased follow similar trends to those of Neuro 2A cells where there an approximate 1-day lag period before exponential metabolic growth and an assay plateau. Figure 4-26 then plots the post-thaw metabolic activity of these encapsulated cells 0-, 1-, 4-, and 7-days following cryopreservation. Interestingly, the metabolic response following cryopreservation is significantly different compared to normal growth conditions.
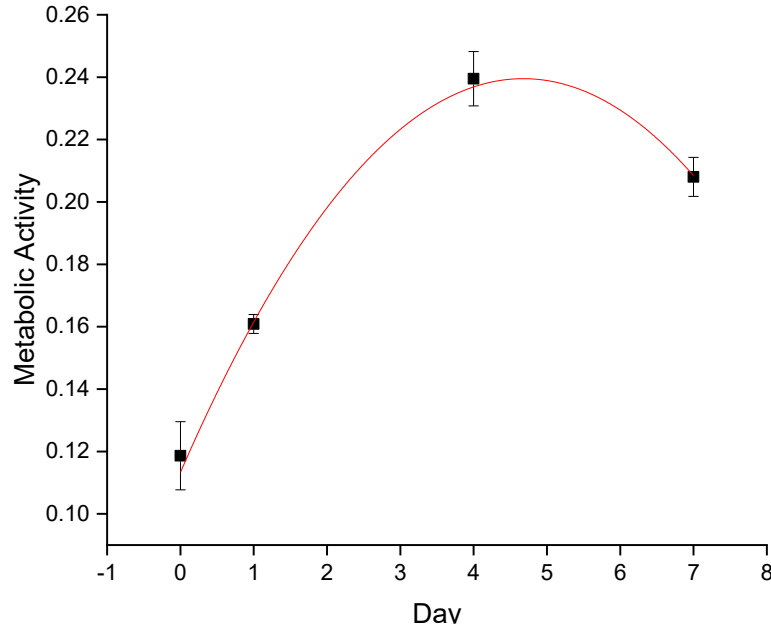
Figure 4-26 Metabolic Activity of Cryopreserved RAW 264.7 Hydrogels: Cryopreserved RAW 264.7 cells follow different metabolism characteristics vs. non-frozen cells. There is an immediate growth phase following thawing followed by a decrease in metabolic activity at day 7 lower than the typical assay limit. error bars represent ±SEM, n = 3.

The increase in metabolic activity is immediately in the exponential phase. Interestingly, this metabolic increase tapers off and even decreases on day 7 at much lower levels that the expected assay limitation. Therefore, we can draw the conclusion that the metabolic decrease here is a function of the cell response itself. There is a lack of literature corresponding to macrophage response to cryopreservation; however, we hypothesize that their innate stress response characteristics results in an atypical metabolic activity response following cryopreservation. The cell quantification growth results pictured in Figure 4-27 follow similar trends to that observed in the metabolic cryopreservation response.
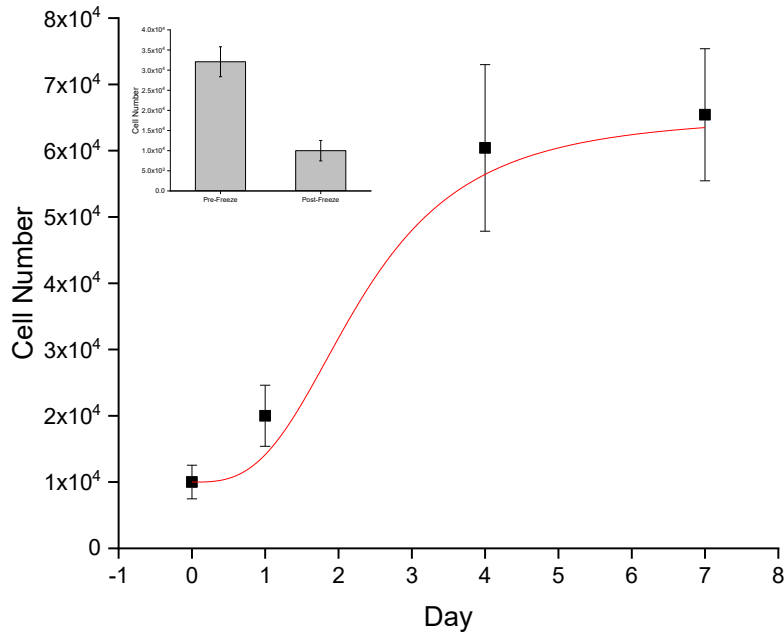
Figure 4-27 Cell Quantification of Cryopreserved RAW 264.7 cells: Cell quantification results align well with metabolism data. There appears to be immediate growth followed by a plateau after day 4. error bars represent ±SEM, n = 3.

The immediate viability was calculated to be $31.2 \pm 8.7\%$, which is much lower than that calculated for the other tested cell types. It is important to note, however, that these hydrogels contained a significantly lower cell number than what would be typically used (~32,000 cells/ gel). The growth inside of these hydrogels appears to be immediate with a doubling of the cell number from day-0 to day-1. Interestingly, the cell growth appears to stagnate following day 4, which corresponds to the metabolic plateau observed in Figure 4-26. The comparison of growth and metabolic activity can be observed in Figure 4-28.
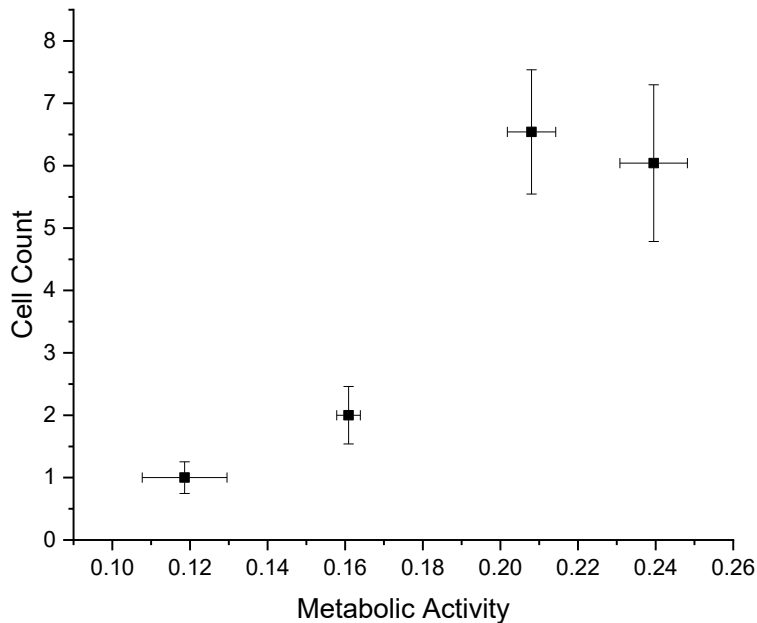
Figure 4-28 Comparison of Growth and Metabolism for Cryopreserved RAW 264.7 Hydrogels

From day 0 to day 4 the growth and metabolism almost correspond with a linear coefficient; however, there is a slight disconnect on day 1. We observe the effect of the growth and metabolic plateau on day 7, suggesting a relaxation of stress response a few days following cryopreservation. RAW 264.7 growth following cryopreservation was further evaluated using a green/red fluorescence assay (Figure 4-29).
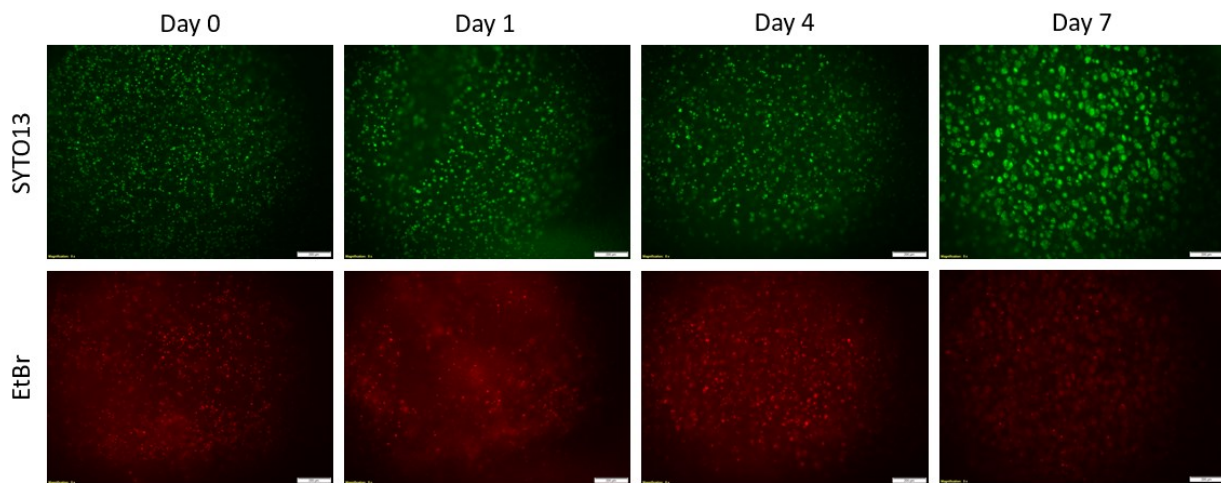
Figure 4-29 Fluorescent Evaluation of Cryopreserved RAW 264.7 Hydrogels: Growth appears to be more uniform compared to HepG2 and Neuro 2A cells across 7 days. This is likely due to RAW 264.7 cells being able to grow in suspended or lightly attached environment.

Interestingly, the immediate post-thaw viability calculated using this method was 62.4 ± 7.4% (data not shown). This result is significantly different from that calculated using the other method. This could suggest that hydrogel cell density is an important factor to the viability and growth response of RAW 264.7 cells following cryopreservation. In addition, the average cluster growth characteristics are significantly different than what was recorded for HepG2 and Neuro 2A cells. The increase in cluster size recorded from day 0 to day 7 follows a linear trend increasing from 2.97 µM in average size to 8.37 µM.
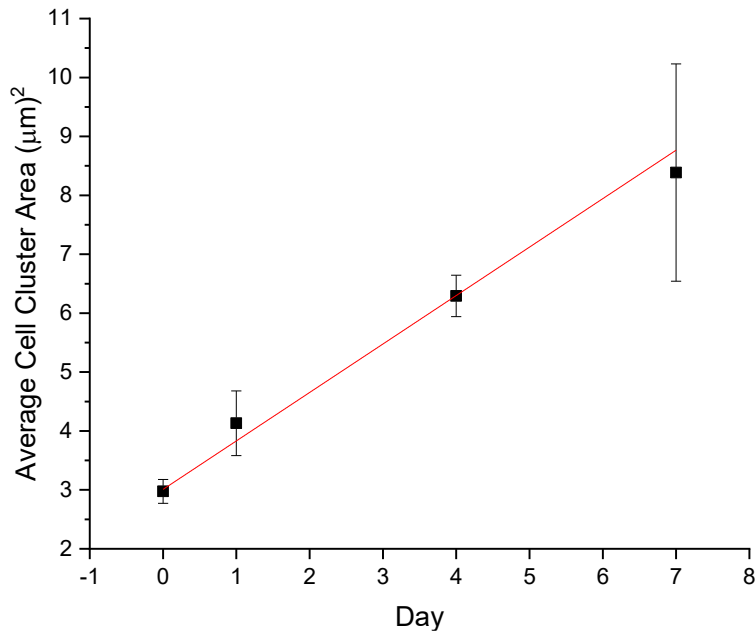
Figure 4-30 Cluster Size of Cryopreserved RAW 264.7 Hydrogels: Cluster growth follows a linear growth model, indicating uniform growth in RAW 264.7 cells and less clustering. error bars represent ±SEM, n = 3.

The overall smaller increase in cluster size suggests that either the cells are not growing as quickly in the hydrogels, or the cells are growing more evenly. RAW 264.7 cells are considered semi-adherent and are able to grow without strong ECM attachment and even in suspension, which would explain why the growth cluster are more homogeneous in hydrogels compared to cells which are heavily attachment dependent.

4.5 Bibliography

[1]   J. Lee, M. J. Cuddihy, and N. A. Kotov, "Three-dimensional cell culture matrices: state of the art," *Tissue Eng. Part B. Rev.*, vol. 14, no. 1, pp. 61–86, Mar. 2008, doi: 10.1089/TEB.2007.0150.

[2]   C. M. Moysidou, C. Barberio, and R. M. Owens, "Advances in Engineering Human Tissue Models," *Front. Bioeng. Biotechnol.*, vol. 8, p. 1566, Jan. 2021, doi: 10.3389/FBIOE.2020.620962/BIBTEX.

[3]   M. G. Rubashkin, G. Ou, and V. M. Weaver, "Deconstructing Signaling in Three Dimensions," *Biochemistry*, vol. 53, no. 13, p. 2078, Apr. 2014, doi: 10.1021/BI401710D.

[4]   P. A. Kenny *et al.*, "The morphologies of breast cancer cell lines in three-dimensional assays correlate with their profiles of gene expression," *Mol. Oncol.*, vol. 1, no. 1, p. 84, Jun. 2007, doi: 10.1016/J.MOLONC.2007.02.004.

[5]   J. H. Crowe, J. S. Clegg, and L. M. Crowe, "Anhydrobiosis: the water replacement hypothesis," *Prop. Water Foods ISOPOW 6*, pp. 440–455, 1998, doi: 10.1007/978-1-4613-0311-4_20.

[6]   N. C. Maiti, M. M. Apetri, M. G. Zagorski, P. R. Carey, and V. E. Anderson, "Raman Spectroscopic Characterization of Secondary Structure in Natively Unfolded Proteins: r-Synuclein," 2004, doi: 10.1021/ja0356176.

[7]   G. D. Prestwich, "Evaluating drug efficacy and toxicology in three dimensions: using synthetic extracellular matrices in drug discovery," *Acc. Chem. Res.*, vol. 41, no. 1, pp. 139–148, Jan. 2008, doi: 10.1021/AR7000827.

[8]   J. T. Atkins *et al.*, "Pre-clinical animal models are poor predictors of human toxicities in phase 1 oncology clinical trials," *Br. J. Cancer 2020 12310*, vol. 123, no. 10, pp. 1496–1501, Sep. 2020, doi: 10.1038/s41416-020-01033-x.

[9]   T. Andersen, P. Auk-Emblem, and M. Dornish, "3D Cell Culture in Alginate Hydrogels," *Microarrays 2015, Vol. 4, Pages 133-161*, vol. 4, no. 2, pp. 133–161, Mar. 2015, doi: 10.3390/MICROARRAYS4020133.

[10]   B. Yue, "Biology of the Extracellular Matrix: An Overview," *J. Glaucoma*, vol. 23, no. 8, p. S20, Dec. 2014, doi: 10.1097/IJG.0000000000000108.

[11]   E. C. González-Díaz and S. Varghese, "Hydrogels as Extracellular Matrix Analogs," *Gels*, vol. 2, no. 3, Sep. 2016, doi: 10.3390/GELS2030020.

[12]   J. L. Drury and D. J. Mooney, "Hydrogels for tissue engineering: scaffold design variables and applications," *Biomaterials*, vol. 24, no. 24, pp. 4337–4351, Nov. 2003, doi: 10.1016/S0142-9612(03)00340-5.

[13]   C. C. Lin and K. S. Anseth, "PEG hydrogels for the controlled release of biomolecules in regenerative medicine," *Pharm. Res.*, vol. 26, no. 3, pp. 631–643, Mar. 2009, doi: 10.1007/S11095-008-9801-2.

[14]   H. Studenovská, M. Šlouf, and F. Rypáček, "Poly(HEMA) hydrogels with controlled pore architecture for tissue regeneration applications," *J. Mater. Sci. Mater. Med.*, vol. 19, no. 2, pp. 615–621, Feb. 2008, doi: 10.1007/S10856-007-3217-0.

[15]   S. Jiang, S. Liu, and W. Feng, "PVA hydrogel properties for biomedical application," *J. Mech. Behav. Biomed. Mater.*, vol. 4, no. 7, pp. 1228–1233, Oct. 2011, doi: 10.1016/J.JMBBM.2011.04.005.

[16]   I. Hernandez, A. Kumar, and B. Joddar, "A Bioactive Hydrogel and 3D Printed Polycaprolactone System for Bone Tissue Engineering," *Gels*, vol. 3, no. 3, Sep. 2017, doi: 10.3390/GELS3030026.

[17]   F. Abasalizadeh *et al.*, "Alginate-based hydrogels as drug delivery vehicles in cancer treatment and their applications in wound dressing and 3D bioprinting," *Journal of Biological Engineering*, vol. 14, no. 1. BioMed Central Ltd, pp. 1–22, Mar. 13, 2020, doi: 10.1186/s13036-020-0227-7.

[18]   F. Ahmadi, Z. Oveisi, M. Samani, and Z. Amoozgar, "Chitosan based hydrogels: characteristics and pharmaceutical applications," *Res. Pharm. Sci.*, vol. 10, no. 1, p. 1, Feb. 2015.

[19]   X. Xu, A. K. Jha, D. A. Harrington, M. C. Farach-Carson, and X. Jia, "Hyaluronic Acid-Based Hydrogels: from a Natural Polysaccharide to Complex Networks," *Soft Matter*, vol. 8, no. 12, p. 3280, Mar. 2012, doi: 10.1039/C2SM06463D.

[20]   S. R. Van Tomme and W. E. Hennink, "Biodegradable dextran hydrogels for protein delivery applications," *Expert Rev. Med. Devices*, vol. 4, no. 2, pp. 147–164, Mar. 2007, doi: 10.1586/17434440.4.2.147.

[21]   E. E. Antoine, P. P. Vlachos, and M. N. Rylander, "Review of Collagen I Hydrogels for Bioengineered Tissue Microenvironments: Characterization of Mechanics, Structure, and Transport," *Tissue Eng. Part B. Rev.*, vol. 20, no. 6, p. 683, Dec. 2014, doi: 10.1089/TEN.TEB.2014.0086.

[22]   P. A. Janmey, J. P. Winer, and J. W. Weisel, "Fibrin gels and their clinical and bioengineering applications," *J. R. Soc. Interface*, vol. 6, no. 30, p. 1, Jan. 2009, doi: 10.1098/RSIF.2008.0327.

[23]   J. Maitra and V. K. Shukla, "Cross-linking in Hydrogels - A Review," *Am. J. Polym. Sci.*, vol. 4, no. 2, pp. 25–31, 2014, doi: 10.5923/J.AJPS.20140402.01.

[24] I. Mironi-Harpaz, D. Y. Wang, S. Venkatraman, and D. Seliktar, "Photopolymerization of cell-encapsulating hydrogels: Crosslinking efficiency versus cytotoxicity," *Acta Biomater.*, vol. 8, no. 5, pp. 1838–1848, May 2012, doi: 10.1016/J.ACTBIO.2011.12.034.

[25] E. A. Aisenbrey and W. L. Murphy, "Synthetic alternatives to Matrigel," *Nat. Rev. Mater.*, vol. 5, no. 7, p. 539, Jul. 2020, doi: 10.1038/S41578-020-0199-8.

[26] F. Lim and A. M. Sun, "Microencapsulated islets as bioartificial endocrine pancreas," *Science*, vol. 210, no. 4472, pp. 908–910, 1980, doi: 10.1126/SCIENCE.6776628.

[27] S. J. Bidarra, C. C. Barrias, and P. L. Granja, "Injectable alginate hydrogels for cell delivery in tissue engineering," *Acta Biomater.*, vol. 10, no. 4, pp. 1646–1662, Apr. 2014, doi: 10.1016/J.ACTBIO.2013.12.006.

[28] H. J. Kong, M. K. Smith, and D. J. Mooney, "Designing alginate hydrogels to maintain viability of immobilized cells," *Biomaterials*, vol. 24, no. 22, pp. 4023–4029, Oct. 2003, doi: 10.1016/S0142-9612(03)00295-3.

[29] A. Kaczmarek-Pawelska, "Alginate-Based Hydrogels in Regenerative Medicine," *Alginates - Recent Uses This Nat. Polym.*, Jul. 2019, doi: 10.5772/INTECHOPEN.88258.

[30] M. I. Neves, L. Moroni, and C. C. Barrias, "Modulating Alginate Hydrogels for Improved Biological Performance as Cellular 3D Microenvironments," *Front. Bioeng. Biotechnol.*, vol. 8, p. 665, Jun. 2020, doi: 10.3389/FBIOE.2020.00665/BIBTEX.

[31] A. C. Hernández-González, L. Téllez-Jurado, and L. M. Rodríguez-Lorenzo, "Alginate hydrogels for bone tissue engineering, from injectables to bioprinting: A review," *Carbohydr. Polym.*, vol. 229, p. 115514, Feb. 2020, doi: 10.1016/J.CARBPOL.2019.115514.

[32] A. I. Pravdyuk, Y. A. Petrenko, B. J. Fuller, and A. Y. Petrenko, "Cryopreservation of alginate encapsulated mesenchymal stromal cells," *Cryobiology*, vol. 66, no. 3, pp. 215–222, Jun. 2013, doi: 10.1016/J.CRYOBIOL.2013.02.002.

[33] H. F. Ahmad and A. Sambanis, "Cryopreservation effects on recombinant myoblasts encapsulated in adhesive alginate hydrogels," *Acta Biomater.*, vol. 9, no. 6, pp. 6814–6822, Jun. 2013, doi: 10.1016/J.ACTBIO.2013.03.002.

[34] R. Malpique *et al.*, "Alginate encapsulation as a novel strategy for the cryopreservation of neurospheres," *Tissue Eng. - Part C Methods*, vol. 16, no. 5, pp. 965–977, Oct. 2010, doi: 10.1089/TEN.TEC.2009.0660/ASSET/IMAGES/LARGE/FIGURE7.JPEG.

[35] J. J. Jaskiewicz, R. D. Sandlin, A. A. Swei, G. Widmer, M. Toner, and S. Tzipori, "Cryopreservation of infectious Cryptosporidiumparvum oocysts," *Nat. Commun.*, vol. 9, no. 1, Dec. 2018, doi: 10.1038/S41467-018-05240-2.

[36] N. Nikolaou, C. J. Green, P. J. Gunn, L. Hodson, and J. W. Tomlinson, "Optimizing human hepatocyte models for metabolic phenotype and function: effects of treatment with dimethyl sulfoxide (DMSO)," *Physiol. Rep.*, vol. 4, no. 21, Nov. 2016, doi: 10.14814/PHY2.12944.

[37] B. P. Best, "Cryoprotectant Toxicity: Facts, Issues, and Questions," *Rejuvenation Res.*, vol. 18, no. 5, p. 422, Oct. 2015, doi: 10.1089/REJ.2014.1656.

[38] A. Lawson, H. Ahmad, and A. Sambanis, "CYTOTOXICITY EFFECTS OF CRYOPROTECTANTS AS SINGLE-COMPONENT AND COCKTAIL VITRIFICATION SOLUTIONS," *Cryobiology*, vol. 62, no. 2, p. 115, Apr. 2011, doi: 10.1016/J.CRYOBIOL.2011.01.012.

[39] A. Roobol, M. J. Carden, R. J. Newsam, and C. M. Smales, "Biochemical insights into the mechanisms central to the response of mammalian cells to cold stress and subsequent rewarming," *FEBS J.*, vol. 276, no. 1, pp. 286–302, Jan. 2009, doi: 10.1111/j.1742-4658.2008.06781.x.

[40] "L-Glutamine in Cell Culture." https://www.sigmaaldrich.com/US/en/technical-documents/technical-article/cell-culture-and-cell-culture-analysis/mammalian-cell-culture/glutamine (accessed Dec. 08, 2021).

[41] E. de Mercado *et al.*, "Evaluation of l-glutamine for cryopreservation of boar spermatozoa," *Anim. Reprod. Sci.*, vol. 115, no. 1–4, pp. 149–157, Oct. 2009, doi: 10.1016/J.ANIREPROSCI.2008.11.014.

[42] J. Solocinski, Q. Osgood, M. Wang, A. Connolly, M. A. Menze, and N. Chakraborty, "Effect of trehalose as an additive to dimethyl sulfoxide solutions on ice formation, cellular viability, and metabolism," *Cryobiology*, 2017, doi: 10.1016/j.cryobiol.2017.01.001.

[43] A. K. Kolonko, N. Bangel-Ruland, F. M. Goycoolea, and W.-M. Weber, "Chitosan Nanocomplexes for the Delivery of ENaC Antisense Oligonucleotides to Airway Epithelial Cells," doi: 10.3390/biom10040553.

[44] "Value FBS | Thermo Fisher Scientific - US." https://www.thermofisher.com/us/en/home/life-science/cell-culture/mammalian-cell-culture/fbs/value-fbs.html (accessed Dec. 08, 2021).

[45] L. R. Sanders, "Water Metabolism," *Endocr. Secrets*, pp. 205–226, 2009, doi: 10.1016/B978-0-323-05885-8.00024-6.

[46] M. Bouquet, J. Selva, and M. Auroux, "Effects of cooling and equilibration in DMSO, and cryopreservation of mouse oocytes, on the rates of in vitro fertilization, development, and chromosomal abnormalities," *Mol. Reprod. Dev.*, vol. 40, no. 1, pp. 110–115, 1995, doi: 10.1002/MRD.1080400114.

[47]   S. A. Ock and G. J. Rho, "Effect of dimethyl sulfoxide (DMSO) on cryopreservation of porcine mesenchymal stem cells (pMSCs)," *Cell Transplant.*, vol. 20, no. 8, pp. 1231–1239, 2011, doi: 10.3727/096368910X552835.

[48]   X. Xiang, Z. Liu, and G. Zhao, "Sodium Alginate as a Novel Cryoprotective Agent for Cryopreservation of Endothelial Cells in a Closed Polytetrafluoroethylene Loop," *https://home.liebertpub.com/bio*, vol. 18, no. 4, pp. 321–328, Aug. 2020, doi: 10.1089/BIO.2020.0020.

[49]   P. Kumar *et al.*, "Sodium alginate potentiates antioxidants, cryoprotection and antibacterial activities of egg yolk extender during semen cryopreservation in buffalo.," *undefined*, vol. 209, Oct. 2019, doi: 10.1016/J.ANIREPROSCI.2019.106166.

[50]   J. Meneghel, P. Kilbride, J. G. Morris, and F. Fonseca, "Physical events occurring during the cryopreservation of immortalized human T cells," *PLoS One*, 2019, doi: 10.1371/journal.pone.0217304.

[51]   S. Surapaneni, T. Pryor, M. D. Klein, and H. W. T. Matthew, "Rapid hepatocyte spheroid formation: optimization and long-term function in perfused microcapsules.," *ASAIO J.*, vol. 43, no. 5, pp. M848-53, Sep. 1997, doi: 10.1097/00002480-199709000-00104.

[52]   S. F. Lan, B. Safiejko-Mroczka, and B. Starly, "Long-term cultivation of HepG2 liver cells encapsulated in alginate hydrogels: A study of cell viability, morphology and drug metabolism," *Toxicol. Vitr.*, vol. 24, no. 4, pp. 1314–1323, Jun. 2010, doi: 10.1016/J.TIV.2010.02.015.

[53]   X. Huang, X. Zhang, X. Wang, C. Wang, and B. Tang, "Microenvironment of alginate-based microcapsules for cell culture and tissue engineering," *J. Biosci. Bioeng.*, vol. 114, no. 1, pp. 1–8, Jul. 2012, doi: 10.1016/J.JBIOSC.2012.02.024.

[54]   S. M. Coward, C. Selden, A. Mantalaris, and H. J. F. Hodgson, "Proliferation rates of HepG2 cells encapsulated in alginate are increased in a microgravity environment compared with static cultures," *Artif. Organs*, vol. 29, no. 2, pp. 152–158, Feb. 2005, doi: 10.1111/J.1525-1594.2005.29026.X.

[55]   R. G. Tremblay, M. Sikorska, J. K. Sandhu, P. Lanthier, M. Ribecco-Lutkiewicz, and M. Bani-Yaghoub, "Differentiation of mouse Neuro 2A cells into dopamine neurons," *J. Neurosci. Methods*, vol. 186, no. 1, pp. 60–67, Jan. 2010, doi: 10.1016/J.JNEUMETH.2009.11.004.

[56]   P. Madhusudanan, G. Raju, and S. Shankarappa, "Hydrogel systems and their role in neural tissue engineering," *J. R. Soc. Interface*, vol. 17, no. 162, Jan. 2020, doi: 10.1098/RSIF.2019.0505.

[57]   A. Banerjee *et al.*, "The influence of hydrogel modulus on the proliferation and

differentiation of encapsulated neural stem cells," *Biomaterials*, vol. 30, no. 27, pp. 4695–4699, Sep. 2009, doi: 10.1016/J.BIOMATERIALS.2009.05.050.

[58]   B. Taciak *et al.*, "Evaluation of phenotypic and functional stability of RAW 264.7 cell line through serial passages," *PLoS One*, vol. 13, no. 6, Jun. 2018, doi: 10.1371/JOURNAL.PONE.0198943.

[59]   A. L. Fuentes, L. Millis, J. Vapenik, and L. Sigola, "Lipopolysaccharide-mediated enhancement of zymosan phagocytosis by RAW 264.7 macrophages is independent of opsonins, laminarin, mannan, and complement receptor 3," *J. Surg. Res.*, vol. 189, no. 2, pp. 304–312, Jun. 2014, doi: 10.1016/J.JSS.2014.03.024.

Chapter 5 Concluding Remarks and Future Studies

Using knowledge gleaned from CPA formulation and characterization, a cryopreservation methodology was successfully developed for alginate-based hydrogels encapsulating cells. HepG2 cells were used as the model cell type for the optimization of this system across various aspects of alginate precursor formulation, cryopreservation protocol, and CPA formulation. In addition, this system was used to cryopreserve hydrogels containing Neuro 2A cells and RAW 264.7 cells with acceptable post-that viability and metabolism recovery. This work is an important step towards understanding and developing a much-desired preservation system for 3D biosystems. This work proves that traditional slow-cooling cryopreservation methods can be effective for the preservation of small 3D encapsulation systems; however, there are several limitations and factors that must be considering as research in this area continues

5.1 ECM Selection

In this work, alginate was chosen as the primary ECM for the cells to be encapsulated in. Alginate was selected for its biocompatibility and tunable properties, which make it ideal for creating biomimetic ECM conditions and cryopreservation optimization. However, there are some disadvantages of using alginate. While alginate is a biocompatible, it does not have typical attachment sites for cellular adhesion. In some cases, this aspect is desirable; however, for the advancement of this research into more biologically relevant areas, knowing the effect ECM-adhesion has on cryopreservation outcome will be necessary. One way around this problem is to introduce extracellular proteins such a collagen to the precursor solution. In addition, alginate

molecules can be modified to include peptide motifs for cell adhesion (most commonly arginylglycylaspartic acid (RGD)) which promote cell adhesion to the alginate molecules themselves. Either of these cell-adhesion-promoting methods introduces another level of complexity to the 3D system which could drastically effect cryopreservation outcome and would require in-depth study for reconciliation.

5.2 Preservation Methodology

The work performed in this study, including suspension freezing, preserved cellular material using a slow-cooling cryopreservation method. However, there are other long-term preservation methods that have proven effective, vitrification is the most common. Vitrification involves the solidification of the aqueous cell material into a non-crystalline glassy phase. Vitrification is an attractive technique because it completely avoids ice formation and the coinciding injury [1]. Reproductive cells are particularly susceptible to ice crystal injury and vitrification is the most commonly use method for cryogenic storage [2]. These cellular differences emphasize a potential need for different preservation techniques depending on the cell/tissue type. In addition, studies have shown vitrification is a viable option for the preservation of hepatocyte spheroids [3]. Future studies should include a comparison of slow-cooling cryopreservation, vitrification, and potentially other techniques to ensure optimal procedure for each specific case.

5.3 Volumetric Diffusion Concerns

Hydrogels created for this study are made using 100 µL of alginate-cell precursor solution and are less than 10 mm in diameter. Certain cryopreservation-based diffusion concerns were concluded to not be an issue with hydrogels of this size. However, as the volume of

hydrogel and the complexity of these systems increases, so will the likelihood of diffusion concerns. In terms of cryopreservation itself, there are concerns with diffusion-based removal of the divalent cation solution used to cross-link the alginate precursor. It was shown that unsuccessful removal of excess concentrations of this solution will result in cell injury from osmotic injury. With increased volume of construct, the time scale of this removal could potentially become very high. Additionally, there are diffusion concerns with the CPA formula. It is vital that the membrane-penetrating molecules (DMSO) are given enough time to penetrate throughout the hydrogel; however, it is unlikely this will become a major concern until 100x fold increase in volume. The final and likely most important diffusion concern is thermal diffusion. As the size of the construct becomes larger, so will the non-homogeneous nature of heat flow throughout the construct. This can potentially affect the overall post-thaw outcome and will affect the homogeneous outcome through the entirety of the construct.

5.4 Functionality Assays

This research utilized viability, growth, and metabolism quantification to determine the post-thaw cellular health. While these assays prove some level of normal cellular activity, additional functionality assays will be necessary to verify proper protein expression and phenotypical results mimic what should be seen in vivo. Ideally, the cell/tissue construct will come out of cryopreservation almost entirely intact with a minimal time scale for recovery time for normal activity.

5.5 Bibliography

[1]   A. Bagchi, E. J. Woods, and J. K. Critser, "Cryopreservation and vitrification: recent advances in fertility preservation technologies," *Expert Rev. Med. Devices*, vol. 5, no. 3, pp. 359–370, 2008, doi: 10.1586/17434440.5.3.359.

[2]   J. Liebermann, "Vitrification: a simple and successful method for cryostorage of human blastocysts," *Methods Mol. Biol.*, vol. 1257, pp. 305–319, 2015, doi: 10.1007/978-1-4939-2193-5_12.

[3]   R. Magalhães *et al.*, "Vitrification successfully preserves hepatocyte spheroids," *Cell Transplant.*, vol. 17, no. 7, pp. 813–828, 2008, doi: 10.3727/096368908786516765.